5-2008

The Solubility and Diffusivity of Helium in Mercury with Respect to Applications at the Spallation Neutron Source

Matthew W. Francis
University of Tennessee - Knoxville

To the Graduate Council:

I am submitting herewith a dissertation written by Matthew W. Francis entitled "The Solubility and Diffusivity of Helium in Mercury with Respect to Applications at the Spallation Neutron Source." I have examined the final electronic copy of this dissertation for form and content and recommend that it be accepted in partial fulfillment of the requirements for the degree of Doctor of Philosophy, with a major in Nuclear Engineering.

Arthur E. Ruggles, Major Professor

We have read this dissertation and recommend its acceptance:

Robert Hinde, Lawrence W. Townsend, Belle R. Upadhyaya

Accepted for the Council:
Dixie L. Thompson

Vice Provost and Dean of the Graduate School

(Original signatures are on file with official student records.)

To the Graduate Council:

I am submitting herewith a thesis written by Matthew Wesley Francis entitled "The Solubility and Diffusivity of Helium in Mercury with Respect to Applications at the Spallation Neutron Source." I have examined the final electronic copy of this thesis for form and content and recommend that it be accepted in partial fulfillment of the requirements for the degree of Doctor of Philosophy, with a major in Nuclear Engineering.

Arthur E. Ruggles, Major Professor

_____

We have read this thesis
and recommend its acceptance:

Robert Hinde

_____

Lawrence W. Townsend

_____

Belle R. Upadhyaya

_____

Accepted for the Council:

Carolyn R. Hodges, Vice Provost and
Dean of the Graduate School

_____

(Original signatures are on file with official student records.)

The Solubility and Diffusivity of Helium in Mercury with Respect to Applications at the Spallation Neutron Source

A Dissertation
Presented for the
Doctor of Philosophy
Degree
The University of Tennessee, Knoxville

Matthew Wesley Francis
May 2008

Acknowledgement

First, I would like to express my utmost thanks to my research advisor, Dr. Arthur E. Ruggles, for his excellent guidance, patience, and financial support during my Ph.D. research and dissertation work. I am also indebted to the High Power Target sponsors at Oak Ridge National Laboratory for their ongoing support. Special thanks go to Bernie Riemer, Mark W. Wendel, and David Felde. I must thank fellow graduate student, Bo Lu, for all of his preliminary work done in this area, and experiments would have been nearly impossible without the help of Lee Hosack and Stuart Walker.

I would also like to thank my committee members—Dr. Lawrence Townsend, Dr. Belle Upadhyaya, and Dr. Robert Hinde—for their support and assistance. I am grateful for the long-time support from the Department of Nuclear Engineering at the University of Tennessee under the leadership of Dr. H.L. Dodds. I express my sincere gratitude to all my professors, and I am grateful to the UTNE staff, notably Kristin England and Gary Graves.

Finally, the greatest thanks go to my family, especially my mom and dad, who have supported me from the very beginning.

ΜΟΝΩ ΘΕΩ ΣΩΤΗΡΙ ΗΜΩΝ ΔΙΑ ΙΗΣΟΥ ΧΡΙΣΤΟΥ ΤΟΥ ΚΥΡΙΟΥ ΗΜΩΝ ΔΟΞΑ ΜΕΓΑΛΩΣΥΝΗ ΚΡΑΤΟΣ ΚΑΙ ΕΞΟΥΣΙΑ ΠΡΟ ΠΑΝΤΟΣ ΤΟΥ ΑΙΩΝΟΣ ΚΑΙ ΕΙΣ ΠΑΝΤΑΣ ΤΟΥΣ ΑΙΩΝΑΣ, αμεν

Abstract

Models for solubility of noble gases in liquid metals are reviewed in detail and evaluated for the combination of mercury and helium for applications at the Spallation Nuetron Source (SNS) at Oak Ridge National Laboratory (ORNL). Gas solubility in mercury is acknowledged to be very low; therefore, mercury has been used in ASTM standard methods as a blocking media for gas solubility studies in organic fluids and water. Models from physical chemistry predict a Henry coefficient for helium in mercury near 3.9×10^{15} Pa-molHg/molHe, but the models have large uncertainties and are not verified with data. An experiment is designed that bounds the solubility of helium in mercury to values below 1.0×10^{-8} molHe/molHg at 101.3 kPa, which is below values previously measurable. The engineering application that motivated this study was the desire to inject 10 to 15 micron-radius helium bubbles in the mercury target of the SNS to reduce pressure spikes that accompany the beam energy deposition. While the experiment bounds the solubility to values low enough to support system engineering for the SNS application, it does not allow confirmation of the theoretical solubility with low uncertainty. However, methods to measure the solubility value may be derived from the techniques employed in this study.

Executive Summary

The Spallation Neutron Source (SNS) is one of the largest science projects in the United States, with total cost near 1.7 Billion Dollars. The limiting factor of the facility had always been assumed to be the lifetime of the target window due to radiation damage. After further investigation, the lifetime of the target was determined not to be limited by radiation damage but by cavitation damage.

The cavitation damage derives from pressure waves caused by the beam energy deposition. Vapor bubbles form when low to negative pressures occur in the mercury near the stainless steel target window due to wave interaction with the structure. Collapse of these bubbles can focus wave energy in small liquid jets that erode the window surface. Compressibility of the mercury can be enhanced to reduce the amplitude of the pressure wave caused by the beam energy deposition. Two methods to enhance compressibility have been devised—small (10 to 30 μm diameter) gas bubble injection into the bulk mercury through out the target and a gas layer injected near the window in the region most vulnerable to damage. Solubility and diffusivity parameters of inert gas in mercury are required for a complete mechanical simulation and engineering of these strategies. This effort establishes the solubility and diffusivity parameters within uncertainties adequate to support design.

Only a few experimental values exist for inert gas solubility in liquid metals. The experimental values ranged several orders of magnitude. Likewise, the various theoretical models give a wide spectrum of values. In a very dilute solution where the solute is a gas and the solvent is a liquid, the solute obeys Henry's law. Henry's law states that the cover gas pressure over a solution is directly proportional to the solubility

of the gas in the solution. The constant of proportionality is called Henry's coefficient and has units of Pa-molSolvent/molSolute.

Using the hard sphere radius for helium and mercury, one obtains a theoretical Henry coefficient of helium in mercury on the order of 3.9×10^{15} Pa-molHg/molHe at 300 K. With this value and the theoretical diffusion coefficient of 4.64×10^{-9} m^2/s, a 15 μm radius helium bubble in mercury is expected to last a considerable amount of time. With this low solubility and the desired 0.5% void fraction needed to mitigate cavitation damage, a micro-bubble population within the SNS should be possible.

This low solubility was confirmed by a direct experimental method. Mercury was charged with helium and any pressure change was recorded. Any pressure change was attributed to gas going into solution. However, no pressure change was detected. Therefore, with the sensitivity of the experiment, a lower limit could be placed on the mercury-helium system. The Henry coefficient is expected to have a value above 9×10^{12} Pa-molHg/molHe, which is above values previously measurable.

A second experiment was designed that captured a 400 μm radius helium bubble on a horizontal surface penetrating into the bulk of the mercury. Using a laboratory microscope, the rate of bubble radius change was recorded. Unlike the helium bubble initially captured in water that disappeared in earlier validation of this method, the helium bubble in mercury did not disappear. This lack of helium dissolution further validates the high Henry coefficient for helium in mercury which corresponds to a low solubility.

The work related here is the first time the solubility of an inert gas in mercury has been thoroughly investigated. A compilation of experimental data has been made using a highly controlled experimental technique. The data confirms the low solubility

predicted by the theoretical models. A complete compilation of various other theories as well as other solubility experiments in liquid metals has been performed as well. All of this work is in support of the cavitation mitigation strageties at Oak Ridge National Laboratory's Spallation Neutron Source.

Table of Contents

List of Figures

List of Tables

Notation and Symbol Definitions

A	=	Avogadro's constant	6.02214×10^{23} mol^{-1}
a	=	diameter of rigid sphere	[m]
a(q)	=	structure factor	
B	=	Hildebrand's fluidity parameter	
C	=	concentration	[kg/m^3]
c	=	sound speed	[m/s]
C_D	=	drag coefficient	
C_p	=	heat capacity	[J mol^{-1} K^{-1}]
D	=	diffusion coefficient	[m^2/s]
D_o	=	diffusion frequency factor	[m^2/s]
d	=	distance from the center of neighboring atoms	[m]
e	=	charge of an electron	1.602×10^{-19} C
F	=	Helmholtz free energy	[J]
f	=	correlation coefficient	
G	=	Gibbs free energy	[J]
g	=	acceleration due to gravity	9.807 m/s^2
g(r)	=	average radial distribution function	
H	=	enthalpy	[J]
h	=	Planck's constant	6.626×10^{-34} J·s
I	=	ionization potential	[J]
J	=	atom "jump" distance	[m]

K	=	expansion coefficient [see equation (3-48)]	
K_H	=	Henry coefficient	[Pa/mole fraction]
k_B	=	Boltzmann constant	1.381×10^{-23} J/K
k	=	thermal conductivity	W m^{-1} K^{-1}
M	=	molar mass	[g/mol]
m	=	mass	[kg]
N	=	number of molecules	
n	=	number of moles	
P	=	pressure	[Pa]
p	=	vapor pressure	[Pa]
Q	=	activation energy	[J]
q	=	screening potential	
R	=	gas constant	8.314 J K^{-1} mol^{-1}
r	=	radius	[m]
Re	=	Reynolds number	
S	=	entropy	[J/K]
Sh	=	Sherwood number	
T	=	temperature	[K or °C]
T_m	=	melting temperature	[K or °C]
t	=	time	[s]
U	=	internal energy	[J]
U_∞	=	terminal rise velocity	[m/s]
u(q)	=	Fourier transform of interionic potential	

V	=	volume	[m^3]
v	=	free volume	[m^3]
v(q)	=	Fourier transform of electron-ion pseudopotential	
W	=	configurational potential energy	[J]
w	=	mixing energy	[J]
We	=	Weber number	
x	=	solubility	[mole fraction]
Z	=	partition function	
z	=	number of nearest neighbors	
z_e	=	effective number of outer electrons	
α	=	thermal expansion coefficient	[K^{-1}]
	=	polarizability	[m^3]
	=	mass transfer coefficient	[m/s]
	=	curvature of the atomic potential energy	[$\overset{O}{A}^{-1}$]
	=	screening potential factor	
β	=	$1/k_BT$	[J^{-1}]
	=	isothermal compressibility	[Pa^{-1}]
β_2	=	second viral coefficient	
γ	=	activity coefficient	
	=	geometric factor	
δ	=	solubility parameter	[$(J/m^3)^{1/2}$]

$\varepsilon(q)$	=	dialectric screening function	
η	=	dynamic viscosity	[mPa-s]
Θ_{vib}	=	characteristic vibrational temperature	[K or °C]
θ	=	angle	[radians]
μ	=	chemical potential	[J]
ν	=	vibrational frequency	[rad/s]
π	=	pi	3.14159…
ρ	=	density	[kg/m^3]
σ	=	surface tension	[N/m]
$\sigma(r)$	=	radial distribution of surface tension	
σ^*	=	area occupied by a solvent atom on hole surface	[m^2]
ϕ	=	internal energy partition function	
χ	=	atomic separation potential energy	[J]
	=	aspect ratio	
Ω	=	potential energy partition function	

SUBSCRIPTS

e	=	electron
G	=	gas
L	=	liquid
LG	=	liquid/gas solution
∞	=	bulk property
o	=	initial

SUPERSCRIPTS

(G)	=	in gas phase
(L)	=	in liquid phase
int	=	interaction term
vib	=	vibrational term
o	=	standard state
$\bar{\ldots}$	=	molar, per mole
$\dot{\ldots}$	=	time derivative, per second

1. Introduction

A great interest in producing a large flux of neutrons has led to a variety of neutron sources. Fission reactors have been the primary source of large neutron fluxes in the past. However, with the desire to produce higher neutron fluxes, the technology began to focus on accelerators with targets—for example, spallation neutron sources. Due to its large ratio of neutrons to protons, solid uranium was the most common material chosen for a target [1]. Other solid target materials include tungsten, tungsten alloys, tantalum, bismuth, and lead. However, heat generated within the solid can only be dissipated by conduction. To prevent melting, cooling the target with water has been a solution. But to reach higher beam power, water coolant is not sufficient. Furthermore, solid targets have limited lifetime in pulsed beam applications due to mechanical damage caused by stress waves induced by the beam energy deposition. Therefore, using liquid metals like sodium or the sodium/potassium alloy as the coolant has been suggested.

Liquid metals like mercury or lead/bismuth can be used as the coolant as well as the target. Mercury is liquid from -38.8°C to 356.6°C at 1 atmosphere and has the benefit of not needing additional heating to prevent solidification [2]. Not only is mercury advantageous for cooling, but because of its high number of neutrons, it is also a good spallation material [1]. Mercury is easy to purify to a high degree and does not experience mechanical degradation due to radiation exposure. However, spallation products activate mercury to a very high degree.

Three facilities are planned to implement the mercury target and coolant design. The Spallation Neutron Source (SNS) at Oak Ridge National Laboratory (ORNL) is

currently undergoing power upgrade [3]. The major construction was finished in 2006 with the beam activated on the target on April 28, 2006. A similar neutron source exists in Japan. The Japan Spallation Neutron Source (JSNS) is part of the large Japan Proton Accelerator Research Complex (J-PARC) and is still in construction [4]. The third facility—the European Spallation Source (ESS)—is still in the design phase [5].

Current research has revealed the issue of cavitation within the mercury at a high beam power [6, 7]. All the current solutions to the cavitation issue involve gas injection. However, the solubility of various gases in mercury is not known with adequate certainty to support system design. This dissertation experimentally evaluates the solubility of helium in mercury and assembles the theoretical models used in predicting solubility in liquid metals. The history of experimental solubility evaluations for gases in liquid metals is also developed, and a thorough investigation on past theories for gas solubility from statistical mechanics and physical chemistry is provided.

2. Spallation Neutron Source Cavitation Issue

2.1 Spallation Neutron Source Parameters and Motivation

The SNS is one of the largest science projects in the United States, with total cost near 1.7 Billion Dollars [3]. The SNS is an accelerator based neutron source that of January 29, 2008 once again broke a world record with its beam power of 310 kW. The designed goal is to reach a beam power of 1.4 MW. The beam consists of high energy protons that deposit their energy with a frequency of 60 Hz in a mercury flow loop. The SNS Hg target operates at relatively low pressure, 0.3 MPa (45 psig), and temperature, 90°C at target exit [8, 9]. However, the limiting factor of the facility had always been assumed to be the lifetime of the target window due to radiation damage [1]. The atomic displacements and nuclear reactions that take place within the window reduce the strength of the material.

After further investigation, the limiting lifetime of the target was determined not to be radiation damage but cavitation damage. The large amount of energy deposited in the mercury during a single proton pulse of near 1 μs leads to near constant volume heating of the mercury. While the peak temperature rise is only on the order of 10 Kelvin, the rate of rise is 14×10^6 K/s [1]. This rapid heating is a constant volume process because the energy deposited in an amount of time much less than the time required for mercury to expand. Therefore, the rapid heating induces a local pressure rise on the order of 30 MPa. The resulting pressure wave propagates through the system and causes stress on the target container [10]. Furthermore, after the pressure wave reflects off the interior target wall, a large tensile pressure develops between the receding wave front and target

wall. The mercury then cavitates. The newly created vapor bubbles quickly collapse toward the wall. The collapse of the bubbles leads to local surface damage called pitting. Damage due to pitting is believed to be proportional to the power density in the target raised to the 4^{th} power [1]. Currently, a target service life is limited by pitting erosion rather than radiation damage at 1.4 MW. Mitigation of the pressure wave effect is a prime concern in the ongoing development of high power liquid metal targets.

To mitigate pitting erosion two primary strategies have been devised. The first method involves injecting small gas bubbles (SGB) into the bulk flow of the mercury [11-14] which elevates mercury compressibility and lowers beam induced pressure amplitude. To eliminate any chemical issues that might arise, the bubbles should be composed of inert gas. A small amount of bubbles of the right size can attenuate a traveling pressure wave [1]. Furthermore, a sufficiently large volume fraction of bubbles can substantially reduce the peak pressure. Current design basis prescribes a production of a gas void fraction on the order of 0.5% with small bubbles ranging from 10 to 100 microns. However, recent investigates have shown that slightly larger bubbles might work as well [11].

While the SGB method approaches the cavitiation issue by attenuating the pressure wave, the second method introduces a gas wall between the mercury and the window to eliminate effects from cavitation bubbles [15]. Theoretically, the presence of a gas layer near a cavitation bubble reverses the bubble collapse dynamics such that the liquid jet is directed away from the wall and into the bulk of the mercury [16]. Therefore, wall damage should be eliminated.

Both methods have their advantages and disadvantages. However, the lack of solubility parameters of inert gas in mercury does not allow for a complete theoretical prediction or validation of either method. For example, bubble lifetimes or gas dissolution from the gas wall cannot be predicted without knowledge of solubility of the inert gas in the mercury.

2.2 General Solubility Definitions

Before going any further, it would be beneficial to define the parameters of solubility. In chemical terms, a system is made up of components or variables to define the system. However, in physical terms, a system is composed of phases, homogeneous portions of a system with uniform intensive variables [17]. The terms mixture and solution help describe any phase that contains more than one component. While both terms are commonly used interchangeably, Guggenheim made a distinction between them [18]. To him, a mixture describes a gaseous, liquid, or solid phase containing more than one substance, where the substances are treated uniformly. However, he defined a solution as a liquid or solid phase containing more than one substance, where the substances are treated differently. Nevertheless, some authors classify mixtures as heterogeneous and homogeneous. Therefore, to them, a homogeneous mixture is also known as a solution. Keeping with the most familiar terminology, the word solution will be preferred here.

In a solution, the solute is the substance in smaller quantity. The solvent is the substance in greater quantity. The quantity is commonly expressed in terms of mass or moles. The content of a solute in a solvent is often expressed in terms of solubility. The

solubility is defined as the proportion of one substance to the whole solution. The proportion can relate mass, number of moles, or a combination of the two. Because many systems are initially modeled with the number of molecules or atoms, the mole fraction is usually more suitable. The mole fraction, x_i, is the ratio of moles of one component to the total number of moles in the solution.

$$x_i = \frac{n_i}{n_i + \sum_{j \neq i} n_j}. \tag{2-1}$$

In a binary system, equation (2-1) is simply

$$x_A = \frac{n_A}{n_A + n_B}. \tag{2-2}$$

If the amount of solute is much less than the amount of solvent, the solution is called dilute, and the solubility of the solute can be expressed as

$$x_{solute} \approx \frac{n_{solute}}{n_{solvent}}. \tag{2-3}$$

A solution is called ideal if the interaction of the molecules is the same for alike as well as different molecules. This terminology is slightly different from the concept of ideal gases, where we assume the molecules do not interact with each other at all. Ideal solutions obey Raoult's law, which states that the individual vapor pressure for each component is equal to the vapor pressure of the pure component times the mole fraction of that component in the solution [17]. In other words,

$$p_i = p_i^{(pure)} x_i. \tag{2-4}$$

However, ideal solutions do not exist. Nevertheless, if deviations from ideality are not to large, Raoult's law will be valid in a narrow concentration range. For example, in a very

dilute solution where the solute is a gas and the solvent is a liquid, the solvent obeys Raoult's law because liquids frequently have strong interactions where gases do not. In this scenario, the solute does not obey Raoult's law but Henry's law:

$$p_i = K_H x_i, \tag{2-5}$$

where K_H is called Henry's constant. Henry's constant various from system to system.

Equation (2-5) is one of many variants of Henry's law. Henry's law can also be stated as

$$p_i = K_H c_i, \tag{2-6}$$

where c_i is the concentration of the solute in the solution given by moles of solute per liter of solution (sometimes called molarity). Or Henry's law can be

$$c_i = K_H c_{gas}, \tag{2-7}$$

where c_{gas} is the number of moles of solute per liter of solute. Adding to the ambiguity is the fact that the Henry's constant can be given as the inverse of any of the forms given above. For instance, equation (2-5) can be also written as

$$x_i = \tilde{K}_H p_i, \tag{2-8}$$

where $\tilde{K}_H = \frac{1}{K_H}$. All following analysis will keep with Henry's law as defined in equation (2-5).

2.3 Prior Theoretical Bubble lifetime work of Bo Lu

In his master's thesis, Lu [19] determined the theoretical Henry coefficients and diffusion coefficients for various inert gases in mercury. Corrections to his work will be discussed in section 3.3. However, Lu was instrumental in showing the need to

understand the solubility of inert gases in mercury and its effect on gas bubble evolution. From Lu's work, the change in radius of helium and argon gas bubbles in mercury as a function of time can be seen in Figures 2.1 through 2.4. The helium bubble trends are based on a theoretical Henry coefficient of 1.20×10^{9} Pa-molHg/molHe at 300 K. However, the xenon bubble trends are based on a theoretical Henry coefficient of 1.03×10^{15} Pa-molHg/molXe at 300 K.

The bubble lifetime trends are based on the theory of Epstein and Plesset [see section 6.1] [20]. Lu improved the model by including a time-dependent gas concentration due to bubble dissolution within the bulk of the mercury. He then solved the simultaneous differential equations using a classical 4^{th} order Runge-Kutta method. Figure 2.1 shows the scaled results for helium. As a first approximation, he assumed all bubbles in the mercury had an initial radius of 15 μm. Assuming the bubbles are all spherical and the system has a 0.5%-volume fraction, the bubble number density is on the order of 3.5×10^{11} bubbles/m^3. If the bubbles are evenly distributed, this number density indicated the bubbles are widely separated from each other at a distance of more than 100 times the bubble radius. Lu showed that a helium bubble with an initial radius of 15 μm would disappear is approximately 0.6 seconds. He predicts a very high solubility as a result of having chosen an inappropriately small helium atomic diameter in the simulation. For a lower soluble element like xenon, Figure 2.2 shows that the bulk gas concentration in the mercury levels off and prevents further bubble shrinkage.

To account for a slightly more realistic bubble size distribution, Lu re-calculated the bubble lifetimes of two bubble sizes—10 and 15 μm radii—within the mercury. His results can be seen in Figures 2.3 and 2.4. He notes that the dominant effect is still the

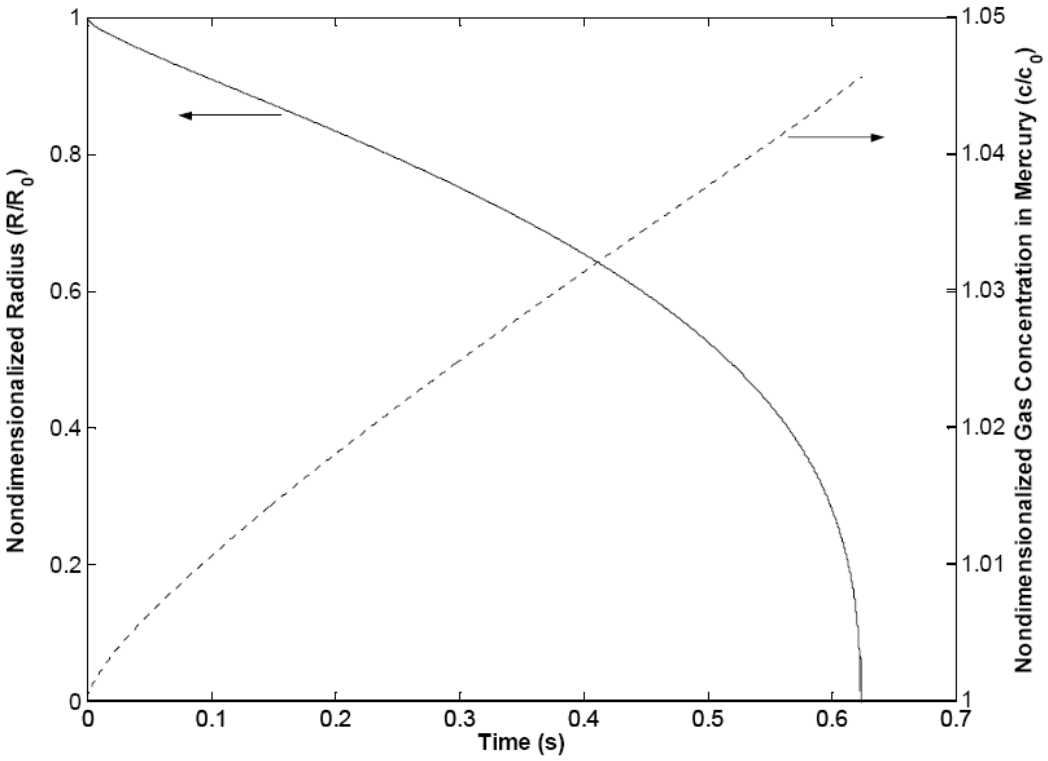

Figure 2.1: Time-Dependent Helium Bubble Radius and Gas Concentration in Mercury [Lu's *masters thesis*, used with permission]

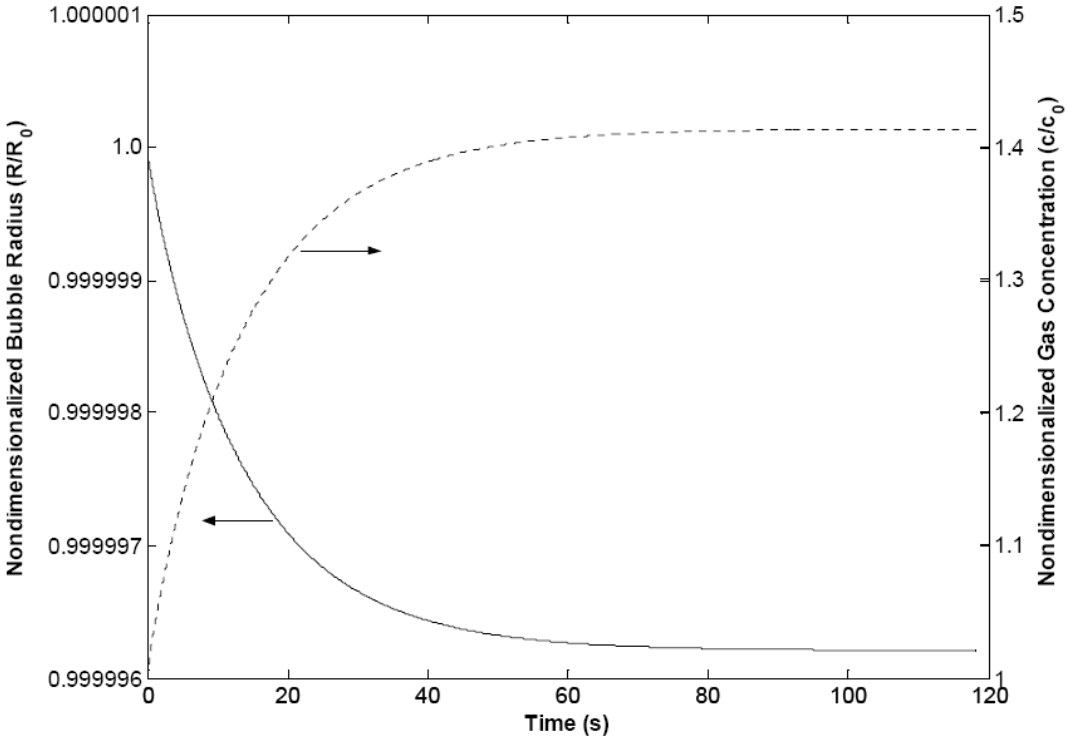

Figure 2.2: Time-Dependent Xenon Bubble Radius and Gas Concentration in Mercury [Lu's *masters thesis*, used with permission]

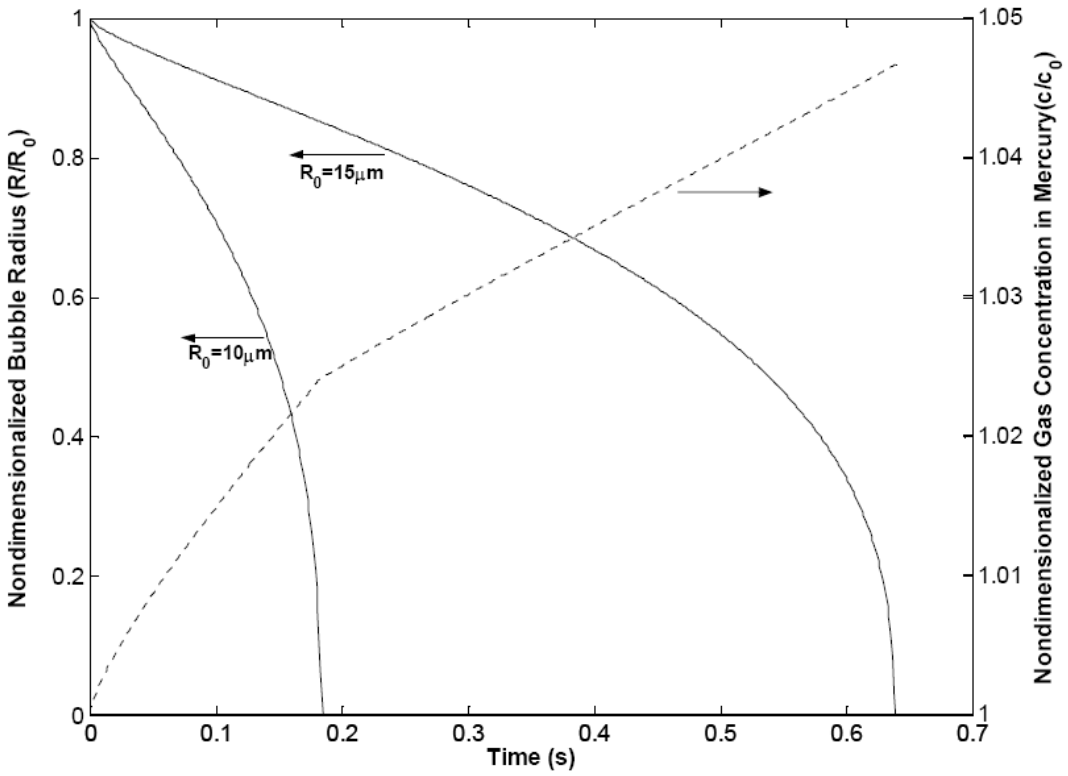

Figure 2.3: Time-Dependent Helium Bubble Radii and Gas Concentration in Mercury [Lu's *masters thesis*, used with permission]

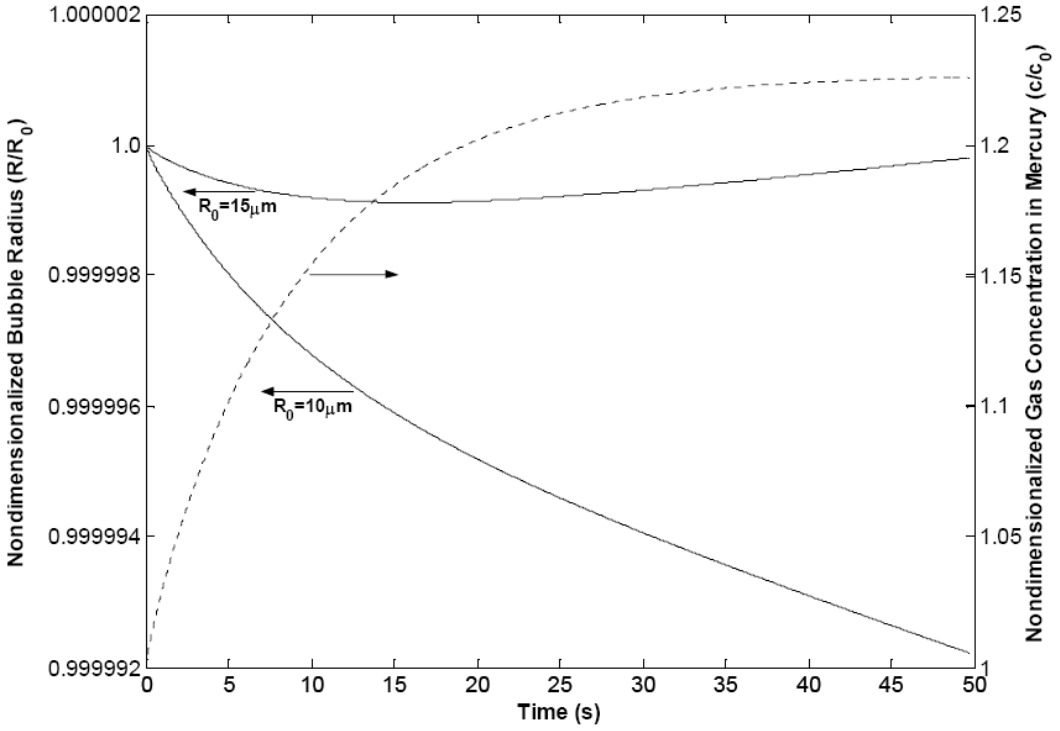

Figure 2.4: Time-Dependent Xenon Bubble Radii and Gas Concentration in Mercury [Lu's *masters thesis*, used with permission]

mass diffusion across the bubble wall. However, as can be seen in Figure 2.4, the larger xenon bubble continues to grow due to gas leaving the smaller bubble.

These simulations of bubble size evolution over time illustrated the need for basic knowledge of gas solubility and diffusivity in mercury to support engineering of gas injection systems for the SNS. A summary of past inert gas solubilities in liquid metals is needed to understand the typical order of magnitude of solubility parameters for mercury. Following the summary of liquid metal solubility will be a detailed derivation used to calculate the theoretical Henry coefficient. Using this theory, the Henry coefficient for helium in mercury will be determined and the issue of bubble lifetime is revisited.

3. Liquid Metal Solubility Values and Theory

3.1 Previous Solubility Values for Liquid Metal/Noble Gas Systems

From the 1950s to the early 1970s, the research focus on liquid metal cooled nuclear reactors supported a handful of noble gas solubility experiments in liquid metals. Gas-enriched liquid metals introduced a variety of issues. Because solubility is dependent on temperature and pressure, any change of these parameters during operation could result in gas coming out of solution and introducing gas bubbles in the flow. These bubbles could effect heat transfer or disturb reactivity within the reactor. Furthermore, gaseous fission products, like krypton and xenon, could be introduced to the liquid metal due to fuel rod damage. Understanding the solubility and how to effectively remove the gas could be instrumental in detecting fuel rod damage. Determining the solubility of xenon in liquid metals is of vital importance because (1) certain isotopes are neutron poisons and will reduce reactivity and (2) Cs-135 is a xenon decay product that could possibly attack any graphite moderators [21].

While the reasons for past research concerning liquid metal solubility is not of big importance to research with the SNS, the history of theory development and experimental results is of importance. Current theoretical results for gas solubility in liquids spread several orders of magnitude. Likewise, due to the general difficulties involved in solubility measurements of gases in ordinary liquids with relatively high solubility values, the methods for measuring solubility of gases in liquid metals often produce highly variant results. Each experimental method and the introduced errors are discussed in section 4.1. For now, the theoretical results and experimental results are just reported.

The previously published theoretical and experimental values are compiled in Tables 3.1 and 3.2, respectively. The values reported in the literature are for quite different pressure and temperature ranges. For a true comparison, the Henry's coefficient, K_H, is given at 500°C and the corresponding solubility, x, at 101.325 Pa (1 atm). The values that are enclosed in parentheses were extrapolated or calculated from the available results. Many of the extrapolations are taken from reported values from the work of Thormeier [21, 22].

As Table 3.1 shows, the theoretically values within the same liquid metal/noble gas system as well as values from system to system vary by orders of magnitude. Nevertheless, the theories all predict very low solubility values. This fact is important in context of bubble lifetime prediction as can be seen in the different bubble trends seen in Figures 2.1 through 2.4. Actually, in 1951, before any extensive liquid metal solubility experiments were performed, Barrer was unable to measure any solubility for the wide variety of liquid metal systems he examined [23].

The first experimental solubility determination in liquid metals was performed by Bonilla and his co-workers in 1955 [24]. Their technique was to saturate liquid bismuth with radio-activated xenon, freeze the melt rapidly, evacuate the chamber, melt the frozen solution, and using a detector, count the number of xenon atoms. The uncertainty of this method will be discussed in a later section. Mitra, a student of Bonilla, would lead the research sponsored by Brookhaven National Laboratory (BNL) and earn his PhD at Columbia University with his findings [25].

Table 3.1: Previous Theoretical Solubility Values for various liquid metals at 500°C and 101.3 kPa

Reference	System	$(K_H)_{500°C}$ (Pa-molMetal/molGas)	x, Solubility @ 1 atm (mole fraction)
Epstein [58]	Na/He	(7.16×10^{6})	(1.42×10^{-2})
	Na/He	(4.90×10^{14})	(2.07×10^{-10})
Mandel [59]	Na/He	(7.54×10^{14})	(1.34×10^{-10})
Mitra [25, 28]	Bi/Xe	9.81×10^{14}	1.03×10^{-10}
	Bi/Xe	9.81×10^{26}	1.03×10^{-22}
	Bi/Xe	2.45×10^{27}	4.13×10^{-23}
McMillan [61]	Bi/Xe	3.38×10^{20}	3.00×10^{-16}
Kubaschewsky [62]	Bi/Xe	1.56×10^{11}	6.51×10^{-7}
	Bi/Xe	6.76×10^{17}	1.50×10^{-13}
Slotnick [36]	Li/He	(3.19×10^{10})	(3.17×10^{-6})
	Li/He	(1.53×10^{15})	(6.61×10^{-11})
	K/He	5.80×10^{6}	1.75×10^{-2}
	K/He	4.69×10^{8}	2.16×10^{-4}
Thormeier [21, 22]	Na/He	6.63×10^{11}	1.53×10^{-7}
	Na/Ar	8.31×10^{12}	1.22×10^{-8}
	Na/Kr	3.24×10^{13}	3.13×10^{-9}
	Na/Xe	2.20×10^{14}	4.61×10^{-10}
Fukase [63]	Na/He	1.04×10^{12}	9.74×10^{-8}
	Na/Ar	1.77×10^{13}	5.72×10^{-9}
	Na/Kr	3.87×10^{13}	2.62×10^{-9}
	Na/Xe	3.46×10^{14}	2.93×10^{-10}

Table 3.2: Previous Experimental Solubility Values for various liquid metals at 500°C and 101.3 kPa

Reference	System	$(K_H)_{500°C}$ (Pa-molMetal/molGas)	x, Solubility @ 1 atm (mole fraction)
Bonilla [24]	Bi/Xe	1.01×10^{11}	1.00×10^{-6}
Raseman [26]	Bi/Xe	1.32×10^{11}	7.70×10^{-7}
Mitra [25, 28]	Na/Xe Hg/Xe Bi/Xe Bi/Xe Bi/Xe	(1.75×10^{6}) (3.85×10^{8}) $\approx 10^{11}$ (1.09×10^{11}) 2.74×10^{13}	(5.79×10^{-2}) (2.63×10^{-4}) $\approx 10^{-6}$ (9.30×10^{-7}) 3.70×10^{-9}
Eshaya [29-32]	Bi/Xe Bi/Xe Bi/Xe	 4.05×10^{12}	 2.50×10^{-8}
Hewitt [33]	Bi/Xe Bi/He	$> 5.0 \times 10^{14}$ $> 5.0 \times 10^{14}$	$< 2.0 \times 10^{-10}$ $< 2.0 \times 10^{-10}$
Watson [27]	Bi/Xe Bi/He	$> 10^{15}$ $\approx 10^{14}$	$< 10^{-10}$ $\approx 10^{-9}$
Johnson [34-35]	Pb/Kr Sn/Kr Ag/Kr Cd/Kr In/Kr	(4.09×10^{18}) (1.36×10^{21}) (9.81×10^{22}) (2.88×10^{21})	(2.48×10^{-14}) (7.44×10^{-17}) (1.03×10^{-18}) (3.51×10^{-17})
Slotnick [36]	Li/He K/He	(3.06×10^{13}) 2.58×10^{10}	(3.31×10^{-9}) 3.93×10^{-6}
Dhar [37-39]	Na/Ar Na/Ar	2.97×10^{13} 1.02×10^{13}	3.41×10^{-9} 9.92×10^{-9}
Veleckis/Dhar [40, 38]	Na/Kr	(6.54×10^{13})	(1.55×10^{-9})
Thormeier [21, 22]	Na/Ar Na/He	8.17×10^{12} 9.81×10^{11}	1.24×10^{-8} 1.03×10^{-7}
Veleckis [40]	Na/He Na/Ar	7.20×10^{11} 1.10×10^{13}	1.41×10^{-7} 9.21×10^{-9}

At the same time at BNL, Raseman, Susskind and Waide [26] were able to calculate the solubility of xenon in liquid bismuth using their bismuth/uranium stream of an in-pile loop at Brookhaven.

Using a similar approach as Mitra, Watson [27] at ORNL was unable to discover the solubility value of xenon in bismuth because the solubility was thought to be below the limit of detection. Therefore, an upper limit on solubility was placed on the bismuth/xenon system. However, prior experiments by Mitra and Waide had given solubility values above this upper limit. More finely tuned experiments were performed by Bonilla and Mitra [28], which lowered the original value of 9.3×10^{-7} atom fraction to 3.7×10^{-9}. Further experiments were performed at BNL to determine solubility of xenon in bismuth by Eshaya, Hoffmann, and Kenney [29-32]. Yet despite their careful performance of tests, they, too, obtained slightly different results.

In England, at the Atomic Energy Research Establishment (AERE), Hewitt, Lacey, and Lyall [33] also performed a similar freezing method used by Mitra. However, their results agreed with Watson's results. The best they could do was establish an upper limit on solubility as well. Also from funding by the AERE, Johnson and Shuttleworth, at the University of Leeds [34, 35], performed the freezing method on different liquid metals: lead, tin, silver, cadmium, and indium. No one else has determined the solubility of inert gases in these liquid metals. Therefore, no comparative study can be performed.

With a high interest in liquid metal cooled reactors, various organizations began to experimentally find the solubility of noble gases in liquid metals. Slotnick et al. [36] from the Conneticut Advanced Nuclear Engineering Laboratory in connection with Pratt and Whitney Aircraft Division of United Aircrafts Corporation looked into helium

solubility in lithium and potassium. They utilized a method that bubbled argon through the solution to remove the helium.

Scientists at Argonne National Laboratory became interested in sodium as a coolant over bismuth or lithium. The work of Dhar, Veleckis, Cafasso, Feder, Blomquist, Yonco and Perin [37-40] contributed solubility values of noble gases in liquid sodium. They adopted a similar process to Slotnick et al.

The Institute for Reactor Development from the Karlsruhe Nuclear Research Center in West Germany became interested in solubility of noble gases in liquid metals, as well. Thormeier [21, 22] led the research in the Fast Breeder Reactor Project in Karlsruhe. The work of Thormeier was the best effort predating the work shown in this dissertation, and, therefore, was used as a basis for the experimental and theoretical work that follows in later sections.

Na-K, an alloy of sodium and potassium, also became a candidate for a coolant in a liquid metal reactor. Like mercury, Na-K is a liquid at room temperature. Due to President Nixon's comprehensive energy plan in 1971 that included Liquid Metals Fast Breeder Reactor (LMFBR), Foust published a sodium/Na-K engineering handbook that collected many of the previous experiments listed [41]. One year before President Nixon's plan, the US Atomic Energy Commission had also issued a report that summarized the solubility and diffusivity of inert gases in liquid sodium, potassium, and Na-K [42]. From the energy plan came the Clinch River Breeder Reactor Project. Unfortunately, the project was cancelled in 1983. For the most part, liquid metal reactors have had short lives around the world. Nevertheless, liquid metal reactors are still in operation today in Russia, France, and India [43].

As can be seen, various solubility experiments have taken place with liquid metals from the late 1950s to the early 1970s. Unfortunately, these experiments are the extent of the solubility research in liquid metals. Therefore, it is necessary to understand the theory of solubility, which starts with models from statistical thermodynamics.

3.2 Theoretical Investigation of Solubility

Classical thermodynamics deals with relationships concerning the macroscopic properties of matter [17]. These relationships can be derived from the laws of thermodynamics. These laws have been inferred from observations of the behavior of bulk matter and are formulated without any concern with the microscopic structure of matter. However, to understand why matter has the properties it has, one must understand the microscopic structure. Statistical thermodynamics deals with microscopic properties and connects the atomic interactions with properties of bulk matter. This connection is brought about by partition functions and their corresponding ensemble.

A canonical ensemble is defined as a thermodynamically large system that is in constant thermal contact with the environment. A canonical ensemble has both a fixed volume and a fixed number of constituent particles. The distribution of total energy amongst the possible dynamic states of the ensemble is given by a partition function. The basic partition function, Z, takes the form:

$$Z = \sum_j e^{-\beta E_j}$$

where $\beta = \frac{1}{k_B T}$ and E_j is the total energy of state j. β is inversely proportional to the temperature times Boltmann's constant, k_B. Due to the fact that classical particles'

positions and momenta vary continuously, the partition function is more correctly written as an integral over each particle's momentum and position.

Various relationships exist between the partition function and the thermodynamic parameters of the system. The internal energy, or statistically speaking, the expected energy of an ensemble is just

$$U = -\frac{\partial \ln Z}{\partial \beta} = kT^2 \frac{\partial \ln Z}{\partial T}. \tag{3-1}$$

The entropy is defined as

$$S = k_B\left(\ln Z + \beta U\right) = \frac{\partial}{\partial T}\left(k_B T \ln Z\right) = -\frac{\partial F}{dT}, \tag{3-2}$$

where F is called the Helmholtz free energy and can be shown to be equivalent to

$$F = U - TS = -k_B T \ln Z\ . \tag{3-3}$$

The Helmholtz free energy is a function of temperature and volume. A similar relationship called the Gibbs free energy, G, is a function of temperature and pressure and is given by

$$G = U + PV - TS\,, \tag{3-4}$$

where $U + PV$ is commonly referred to as enthalpy, H.

Fowler and Guggenheim [18] show that the free energy of an assembly of N imperfect gas molecules of mass m confined to a volume V is given by

$$F = -Nk_B T \ln \phi(T) - k_B T \ln \Omega(T)\,, \tag{3-5}$$

where ϕ(T) is the internal energy partition function (and hence, a function of rotational, vibrational, electronic and nuclear spin partition functions) and Ω(T) is a potential energy partition function that takes into account the configuration of the ensemble. As an aside,

in a perfect gas the molecules are assumed to not interact; therefore, the configuration of the ensemble is neglected.

A formal expression for the free energy of a binary mixture can be obtained from equation (3-5).

$$F = -N_A k_B T \ln \phi_A(T) - N_B k_B T \ln \phi_B(T) - k_B T \ln \Omega(T) \tag{3-6}$$

where $\phi_A(T)$ is the internal energy partition function for species A, and $\phi_B(T)$ is the internal energy partition function for species B. $\Omega(T)$ now accounts for the configuration of the whole mixture.

Fowler shows that the general representation of $\Omega(T)$ can be written

$$\Omega(T) = \frac{1}{N_A! N_B!} \int \cdots \int \exp\left(-\frac{W}{k_B T}\right) (d\omega_A)^{N_A} (d\omega_B)^{N_B} , \tag{3-7}$$

where W is the configurational potential energy and $d\omega_i = dx_i dy_i dz_i$. Solving equation (3-6) comes down to evaluating $\Omega(T)$. The analysis of Fowler and Guggenheim [18] is what follows.

Before proceeding, five major conditions are needed to simplify the evaluation of $\Omega(T)$.

(1.) Both individual species, A and B, must pack in the same way. Therefore, after packing, both species have equivalent neighboring particles, z.

(2.) Both species have sufficiently similar molecular volumes, V, so that the mixture of A and B packs the same as the individual species.

(3.) Next, the ratio of the free volumes, v, of the two pure fluids does not vary from unity by more than 30%. The free volume is defined as the spherical cage that a

particle can move around in. The radius of the cage is equal to the average distance between the centers of the two molecules, which are nearest neighbors.

(4.) The individual volumes, V_A and V_B, as well as the individual free volumes, v_A and v_B, remain unaltered after mixing.

(5.) Finally, in any given configuration of volume $V_{total} = N_A V_A + N_B V_B$, the potential energy W may be regarded as the sum of contributions from pairs of closest neighbors.

These five conditions will be revisited and applied later. Actually, the first three conditions will be loosened when applying the theory to our actual situation. Nevertheless, mixtures that satisfy these conditions are referred to as strictly regular solutions.

In a pure solution of only A or B type molecules, each molecule experiences a potential, χ. The molecules, therefore, move around a minimum potential energy $-\chi_0$. If we let χ_A be χ_0 for a pure solution of A, then the minimum potential energy each A molecule experiences is $-\chi_A$. Therefore, the average energy of interaction of two A molecules is $-2\chi_A/z$, where z is once again the number of nearest neighbors. Likewise, B molecules in pure solution have a minimum potential energy of $-\chi_B$; hence, the average energy of two B molecules is $-2\chi_B/z$. Under assumption (1.), the z values for A and B are equal. During mixing, one A molecule might be replaced with one B molecule. If we define w_{AB} as the mixing energy, so that by interchanging one A molecule with one B molecule the increase of potential energy is $2w_{AB}$, then the average potential energy of an AB pair is $(-\chi_A-\chi_B + w_{AB})/z$.

Let us assume a large ensemble has N_A molecules of A and N_B molecules of B. Furthermore, assume there are zX AB neighbors. Therefore, the number of neighbors to A molecules that are not B is $z(N_A - X)$. This expression is equivalent to saying there are ½ $z(N_A - X)$ AA neighbors. Likewise, in this model we have ½ $z(N_B - X)$ BB neighbors.

The total of each combination contributes to the total potential energy W by its corresponding average energy. Therefore,

$$\begin{aligned} W &= \left(\frac{1}{2}z(N_A - X)\right)\left(\frac{-2\chi_A}{z}\right) + \left(\frac{1}{2}z(N_B - X)\right)\left(\frac{-2\chi_B}{z}\right) + (zX)\left(\frac{-\chi_A - \chi_B + w_{AB}}{z}\right) \\ &= -N_A\chi_A - N_B\chi_B + Xw_{AB} \end{aligned} \tag{3-8}$$

If equation (3-8) is then inserted into equation (3-7), one gets

$$\Omega(T) = \frac{\exp\left(\frac{N_A\chi_A + N_B\chi_B}{k_BT}\right)}{N_A!N_B!}\int\cdots\int \exp\left(-\frac{Xw_{AB}}{k_BT}\right)(d\omega_A)^{N_A}(d\omega_B)^{N_B}\ . \tag{3-9}$$

Looking at the expression within the integrals, let us introduce $\widetilde{X}$ such that

$$\exp\left(-\frac{\widetilde{X}w_{AB}}{k_BT}\right)\int\cdots\int(d\omega_A)^{N_A}(d\omega_B)^{N_B} = \int\cdots\int \exp\left(-\frac{Xw_{AB}}{k_BT}\right)(d\omega_A)^{N_A}(d\omega_B)^{N_B} \tag{3-10}$$

The integral is just

$$\int\cdots\int(d\omega_A)^{N_A}(d\omega_B)^{N_B} = (N_Av_A + N_Bv_B)^{N_A+N_B}, \tag{3-11}$$

where v_i is the free volume of the i^{th} species. Using assumption (3.) above, the geometric mean of v_A and v_B will not differ from the arithmetic mean by more than 1%. Therefore, we can say they are approximately equal:

$$\text{arithmetic mean} = \frac{N_Av_A + N_Bv_B}{N_A + N_B} \approx \left(v_A^{N_A}v_B^{N_B}\right)^{1/(N_A+N_B)} = \text{geometric mean.} \tag{3-12}$$

Taking this relationship, we can rearrange terms to achieve

$$\left(N_A v_A + N_B v_B\right)^{N_A+N_B} \approx \left(N_A + N_B\right)^{N_A+N_B}\left(v_A^{N_A} v_B^{N_B}\right) \tag{3-13}$$

For large values, $x^x \approx x!\ \exp(x)$; therefore, we can write the right hand side of equation (3-13) as

$$\left(N_A v_A + N_B v_B\right)^{N_A+N_B} \approx \left(N_A + N_B\right)!\exp\left(N_A + N_B\right)\left(v_A^{N_A} v_B^{N_B}\right), \tag{3-14}$$

By replacing relationship (3-14) for relationship (3-11) in equation (3-10), the partition function (3-9) can be written

$$\begin{aligned}\Omega(T) &= \frac{\left(N_A + N_B\right)!}{N_A! N_B!} e^{N_A} e^{N_A\chi_A/k_BT} v_A^{N_A} e^{N_B} e^{N_B\chi_B/k_BT} v_B^{N_B} e^{-\tilde{X}w_{AB}/k_BT} \\ &= \frac{\left(N_A + N_B\right)!}{N_A! N_B!}\left(e v_A e^{\chi_A/k_BT}\right)^{N_A}\left(e v_B e^{\chi_B/k_BT}\right)^{N_B} e^{-\tilde{X}w_{AB}/k_BT}\end{aligned} \tag{3-15}$$

Taking equation (3-15) and inserting into equation (3-6) yields the following expression for free energy in a binary mixture:

$$\begin{aligned}F &= -N_A k_B T \ln\phi_A(T) - N_B k_B T \ln\phi_B(T) \\ &- k_B T\left[N_A \ln\left(e v_A e^{\chi_A/k_BT}\right) + N_B \ln\left(e v_B e^{\chi_B/k_BT}\right) + \ln\left(\frac{\left(N_A + N_B\right)!}{N_A! N_B!}\right) - \frac{\tilde{X}w_{AB}}{k_B T}\right]\end{aligned} \tag{3-16}$$

Since (N_A+N_B) is very large

$$\ln\left(\frac{\left(N_A + N_B\right)!}{N_A! N_B!}\right) \approx N_A \ln\left(\frac{N_A + N_B}{N_A}\right) + N_B \ln\left(\frac{N_A + N_B}{N_B}\right).$$

With this approximation and further simplification, equation (3-16) can be written as

$$\begin{aligned}F &= N_A\left(-\chi_A - k_B T \ln\left(\phi_A(T) v_A\right) - k_B T + k_B T \ln\left(\frac{N_A}{N_A + N_B}\right)\right) \\ &+ N_B\left(-\chi_B - k_B T \ln\left(\phi_B(T) v_B\right) - k_B T + k_B T \ln\left(\frac{N_B}{N_A + N_B}\right)\right) + \tilde{X}w_{AB}\end{aligned} \tag{3-17}$$

Several attempts have been made in the literature to model actual solutions. In all of these attempts $\widetilde{X}$ was approximated as

$$\widetilde{X} = \frac{N_A N_B}{N_A + N_B}.$$

For ideal dilute solutions where A is the solvent and B is the solute,

$$\frac{N_A N_B}{N_A + N_B} \approx N_B \tag{3-18}$$

With these approximations, equation (3-17) takes the form

$$\begin{aligned} F = {} & N_A\left(-\chi_A - k_B T \ln\left(\phi_A(T) v_A\right) - k_B T + k_B T \ln\left(\frac{N_A}{N_A + N_B}\right)\right) \\ & + N_B\left(-\chi_B - k_B T \ln\left(\phi_B(T) v_B\right) - k_B T + k_B T \ln\left(\frac{N_B}{N_A + N_B}\right) + w_{AB}\right) \end{aligned} \tag{3-19}$$

With the mention of ideal dilute solutions, it seems appropriate at this time to adapt a clearer notation for the specific application of the above derivation. The setup for which the above models will apply contains dilute gas atoms as the solute in a liquid mercury solvent. As already assumed in relationship (3-18), A is the solvent and B is the solute. For clarity, let us change the subscript of the solvent A to L, for liquid, and the subscript of the solute B to G, for gas. Therefore, equation (3-19) becomes

$$\begin{aligned} F = {} & N_L\left(-\chi_L - k_B T \ln\left(\phi_L(T) v_L\right) - k_B T + k_B T \ln\left(\frac{N_L}{N_L + N_G}\right)\right) \\ & + N_G\left(-\chi_G - k_B T \ln\left(\phi_G(T) v_G\right) - k_B T + k_B T \ln\left(\frac{N_G}{N_L + N_G}\right) + w_{LG}\right) \end{aligned} \tag{3-20}$$

Using the new notation, $V_{total} = N_L V_L + N_G V_G$. Therefore,

$$N_G = \frac{V_{total} - N_L V_L}{V_G}.$$

Plugging this relationship allows equation (3-20) to be written as

$$F = N_L\left(-\chi_L - k_B T\ln\left(\phi_L(T)v_L\right) - k_B T + k_B T\ln\left(\frac{N_L}{N_L + \frac{V_{total} - N_L V_L}{V_G}}\right)\right) + N_G\left(-\chi_G - k_B T\ln\left(\phi_G(T)v_G\right) - k_B T + k_B T\ln\left(\frac{N_G}{N_L + N_G}\right) + w_{LG}\right) \quad (3\text{-}21)$$

Now for ease, equation (3-21) can be written in the following abbreviated form

$$F = F_L\left(N_A, V_{total}, T\right) + N_G\left(-\chi_G - k_B T\ln\left(\phi_G(T)v_G\right) - k_B T + k_B T\ln\left(\frac{N_G}{N_L + N_G}\right) + w_{LG}\right) \quad (3\text{-}22)$$

Furthermore, $\frac{N_G}{N_L + N_G}$ is nothing more than the definition of solubility of a gas in a liquid. Therefore, let us represent this gas solubility as x_G; now equation (3-22) is simplified to

$$F = F_L\left(N_A, V_{total}, T\right) + N_G\left(-\chi_G - k_B T\ln\left(\phi_G(T)v_G\right) - k_B T + k_B T\ln\left(x_G\right) + w_{LG}\right). \quad (3\text{-}23)$$

The difference between Helmholtz free energy and Gibbs free energy is negligible at relatively low pressures. This small difference is convenient because partial chemical potentials are easily derived from Gibbs free energy. Partial chemical potential is defined as

$$\mu_i = \frac{\partial G}{\partial N_i}. \quad (3\text{-}24)$$

Therefore, if F ~ G, then the partial chemical potential of the gas in the solution is

$$\frac{\partial G}{\partial N_G} = -\frac{\partial F_L}{\partial V_{total}}\frac{\partial V_{total}}{\partial N_G} - \chi_G - k_B T \ln\left(\phi_G(T) v_G\right) - k_B T + k_B T \ln\left(x_G\right) + w_{LG} \tag{3-25}$$

The negative partial derivative of the liquid free energy with respect to the total volume can be seen in equation (3-4) to be equal to the pressure of the fluid, or approximately the pressure on the solution, P. Because $V_{total} = N_L V_L + N_G V_G$, the partial derivative of the total volume with respect to the number of gas atoms is just V_G.

$$\mu_G^{(L)} = \frac{\partial G}{\partial N_G} = PV_G - \chi_G - k_B T \ln\left(\phi_G(T) v_G\right) - k_B T + k_B T \ln\left(x_G\right) + w_{LG} \tag{3-26}$$

Up to this point, the derived properties of the solution have assumed an ideal dilute solution as a special class of a regular solution, which is a solution that meets the five conditions stated earlier. However, the first three conditions may be too restrictive for a dilute gas. Fowler and Guggenheim give an alternative derivation, starting with a different method of approximation. First, interactions of the dissolved gas atoms with one another are considered negligible. Furthermore, they assume that the solute atoms experience a constant potential energy, $-\chi_{LG}$, throughout the solution. The result of the Fowler and Guggenheim derivation is:

$$\chi_{LG} = \chi_G - w_{LG} + k_B T + k_B T \ln\left(\frac{v_G}{V_L}\right) \tag{3-27}$$

Solving for χ_G and inserting this expression into equation (3-26), yields the following partial chemical potential:

$$\mu_G^{(L)} = PV_G - \chi_{LG} - k_B T \ln\left(\phi_G(T) V_L\right) + k_B T \ln\left(x_G\right) \tag{3-28}$$

When the solution is at saturated equilibrium, the chemical potential of the gas in the liquid phase is equal to the chemical potential of the gas in the gas phase. If we assume the gas is ideal, the chemical potential is given by

$$\mu_G^{(G)} = -k_B T \ln\left(\phi_G(T)\right) + k_B T \ln\left(\frac{p_G^{(G)}}{k_B T}\right), \tag{3-29}$$

where $p_G^{(G)}$ is the partial pressure of the gaseous solute. At equilibrium, equation (3-28) equals equation (3-29). That is,

$$\mu_G^{(L)} = \mu_G^{(G)} \tag{3-30}$$

or

$$PV_G - \chi_{LG} - k_B T \ln\left(\phi_G(T) V_L\right) + k_B T \ln\left(x_G\right) = -k_B T \ln\left(\phi_G(T)\right) + k_B T \ln\left(\frac{p_G^{(G)}}{k_B T}\right)$$

Rearranging and canceling terms we get

$$k_B T \ln\left(\frac{x_G k_B T}{p_G^{(G)} V_L}\right) = -PV_G + \chi_{LG}. \tag{3-31}$$

In many incidences the above equation is more conveniently written in terms of moles, such that equation (3-31) becomes

$$RT \ln\left(\frac{x_G RT}{p_G^{(G)} \overline{V}_L}\right) = -P\overline{V}_G + \overline{\chi}_{LG}, \tag{3-32}$$

where R is the gas constant, $\overline{V}$ is the molar volume, and $\overline{\chi}_{LG}$ is the potential energy felt by the solute atoms in the solution per mole.

In pure liquids, the molar potential energy is equal to the internal vaporization energy. The internal energy is interpreted as the expected value of the microstate energy U, equation (3-1). By the definition of enthalpy we can see the following relationship

$$-\overline{\chi} \approx U = H - PV$$
$$H \approx PV - \overline{\chi} \tag{3-33}$$

By analogy, Thormeier [21] defines the molar free energy of solution as

$$\Delta\overline{F}_{LG} = P\overline{V}_G - \overline{\chi}_{LG} \tag{3-34}$$

Inserting equation (3-34) into equation (3-32) yields

$$RT\ln\left(\frac{x_G RT}{p_G^{(G)}\overline{V}_L}\right) = -\Delta F_{LG}\,, \tag{3-35}$$

or

$$\frac{x_G}{p_G^{(G)}} = \frac{\overline{V}_L}{RT}\exp\left(\frac{-\Delta\overline{F}_{LG}}{RT}\right). \tag{3-36}$$

According to equation (2-5), the left-hand side of equation (3-36) is just the inverse of the Henry constant, K_H. Therefore,

$$K_H^{-1} = \frac{\overline{V}_L}{RT}\exp\left(\frac{-\Delta\overline{F}_{LG}}{RT}\right). \tag{3-37}$$

The molar free energy of solution, $\Delta\overline{F}_{LG}$, is the reversible work required to introduce a gas atom into a solution of concentration x_G. Due to the assumption that the gas solute atoms do not interact, or the interaction is negligible, the work required for introducing a gas atom into solution is equal to the work required for introducing a gas atom into the pure solvent. The molar Helmholtz free energy of solution is defined as

$$\Delta\overline{F}_{LG} = \Delta\overline{U}_{LG} - T\Delta\overline{S}_{LG}\,. \tag{3-38}$$

Based on the definition of $\Delta\overline{F}_{LG}$, $\Delta\overline{U}_{LG}$ can be considered the total molar internal energy for introducing the gas into the liquid.

Several approaches have been taken by different individuals in deriving an expression for the molar free energy of solution. A comparison of the various theories will be discussed later. The method adopted in this paper comes from the work of Thormeier, who relied heavily on Pierotti's work. Pierotti's more sophisticated method compared to the other theories built upon the method of Reiss, et al.

Reiss et al [44, 45] derived an estimate for the reversible work needed in the production of a spherical cavity of radius r in a fluid. The radius of the cavity is equal to the hard sphere radius of the solute. The work needed to expand the spherical cavity's radius from r to $r + dr$ can be written as a sum of the volume contribution and surface contribution:

$$dF_{LG}^{hole} = 4\pi r^2 P dr + 8\pi r \sigma(r) dr , \tag{3-39}$$

where P is the pressure of the fluid and $\sigma(r)$ is the radial distribution of the surface tension. When r is large, the surface tension is approximately constant, σ_o. Using this approximation, equation (3-39) gives

$$F_{LG}^{hole} = \frac{4}{3}\pi r^3 P + 4\pi r^2 \sigma_o . \tag{3-40}$$

As the radius becomes smaller, the curvature dependence of the surface work cannot be ignored. Therefore, equation (3-40) can be slightly altered to account for the curvature:

$$F_{LG}^{hole} = \frac{4}{3}\boldsymbol{\pi r}^3 P + 4\boldsymbol{\pi r}^2 \sigma_o \left(1 - \frac{2\Delta}{r}\right) + K_o , \tag{3-41}$$

where Δ is approximately the thickness of the inhomogeneous layer near the surface and K_o is an arbitrary correction function independent of r.

As an aside, let us call $g(r)$ the average radial distribution function for solvent molecules around a solute molecule. Thus $\rho g(r)$ is the average density of solvent molecules in contact with the solute when ρ is the number density of the particles. For rigid spheres and the use of the virial theorem, we have the following relationship:

$$\frac{P}{k_B T} = \rho + \frac{2}{3}\pi a^3 \rho^2 g(a), \tag{3-42}$$

where a is just the diameter of the rigid sphere. By these definitions, Reiss et al showed the following relationship between the reversible work and the radial distribution function:

$$F_{LG}^{hole} = k_B T \rho \int_0^r 4\pi\lambda^2 g(\lambda) d\lambda . \tag{3-43}$$

or

$$g(r) = \frac{1}{4\pi r^2 k_B T \rho} \frac{\partial F_{LG}^{hole}}{\partial r} . \tag{3-44}$$

If the virial expansion of pressure, equation (3-42), is inserted into equation (3-41), and the new expression for F_{LG}^{hole} is inserted in equation (3-44), one obtains an average radial distribution function of the form

$$g(r) = A + \frac{B}{r} + \frac{C}{r^2}, \tag{3-45}$$

where A, B, and C are just expansion coefficients. From equations (3-41) and (3-42), the four unknowns of equation (3-50) are $g(a)$, σ_o, Δ, and K_o. Reiss et al established a relationship for each coefficient and inserted it into equation (3-45). Therefore, inserting

equation (3-45) into equation (3-44) and through algebraic manipulations, equation (3-41) can be written as

$$F_{LG}^{hole} = K_o + K_1 a_{LG} + K_2 a_{LG}^2 + K_3 a_{LG}^3, \tag{3-46}$$

or

$$\overline{F}_{LG}^{hole} = \overline{K}_o + \overline{K}_1 a_{LG} + \overline{K}_2 a_{LG}^2 + \overline{K}_3 a_{LG}^3, \tag{3-47}$$

where

$$\begin{aligned}
\overline{K}_o &= RT\left\{-\ln(1-y) + \frac{9}{2}\left[\frac{y}{(1-y)}\right]^2\right\} - \frac{\pi a_L^3 \mathrm{A} P}{6} \\
\overline{K}_1 &= -\frac{RT}{a_L}\left[6\left(\frac{y}{1-y}\right) + 18\left(\frac{y}{1-y}\right)^2\right] + \pi a_L^2 \mathrm{A} P \\
\overline{K}_2 &= \frac{RT}{a_L^2}\left[12\left(\frac{y}{1-y}\right) + 18\left(\frac{y}{1-y}\right)^2\right] - 2\pi a_L \mathrm{A} P \\
\overline{K}_3 &= \frac{4}{3}\pi \mathrm{A} P
\end{aligned}, \tag{3-48}$$

and

$$\begin{aligned}
a_{LG} &= r_L + r_G \\
a_L &= 2r_L \\
y &= \frac{\pi a_{LG}^3}{6}\left(\frac{\rho_L \mathrm{A}}{\overline{m}_L}\right)
\end{aligned}$$

In the above expressions, a_i is the diameter of the i^{th} species, A is Avogadro's number, and $\overline{m}_L$ is the molar mass of the liquid. The internal pressure, P, can be found by the definition [49]

$$P = T\frac{1}{V}\left(\frac{\partial V}{\partial T}\right)_P \Bigg/ \left[-\frac{1}{V}\left(\frac{\partial V}{\partial P}\right)_P\right] = T\frac{\alpha}{\beta}, \tag{3-49}$$

where α is the thermal expansion coefficient and β is the isothermal compressibility of the solution.

Up to this point, the total molar free energy for introducing the gas into the liquid has assumed the solute to be a rigid sphere. However, in any real solution the solute will have a slight attractive potential with the induced metal ions. Furthermore, interactions can occur between the solute and the electron gas of the metal. Therefore, we can consider the process of introducing the solute molecule into the solvent as consisting of two steps. Step one consists of creating a cavity in the solvent of suitable size to accommodate the solute molecule assuming the solute is a hard sphere. The molar free energy required to introduce a hard sphere of the same radius as the cavity in the solution is just given by equation (3-47). The second step consists of introducing into the cavity a solute molecule which interacts with the solvent and its constituents [46]. The free energy for this step can be represented by

$$F_{LG}^{\text{int}} = U_{LG}^{\text{int}} - TS_{LG}^{\text{int}}. \tag{3-50}$$

This free energy can be considered the reversible work required to charge the hard sphere or cavity of step one to the required potential. Pierotti [46] assumes that TS_{LG}^{int} is negligible compared to the internal energy, U_{LG}^{int}. Therefore, $F_{LG}^{\text{int}} \approx U_{LG}^{\text{int}}$. With this assumption, U_{LG}^{int} could be visualized as a correction term to the internal energy of the free energy associated with introducing a hard sphere, i.e.,

$$\begin{aligned} \Delta F_{LG} &= F_{LG}^{hole} + F_{LG}^{\text{int}} = \left(U_{LG}^{hole} - TS_{LG}^{hole}\right) + \left(U_{LG}^{\text{int}} - TS_{LG}^{\text{int}}\right) \\ &\approx \left(U_{LG}^{hole} + U_{LG}^{\text{int}}\right) - TS_{LG}^{hole} \end{aligned}. \tag{3-51}$$

Three types of interactions can exist in the solution: solute-electron interaction, solute-solvent interaction, and solvent-solvent interaction. If the electrons in the liquid metal are uniformly distributed, the induced dipole moment on the solute molecule is on average equal to zero and can be neglected.

On the other hand, the interaction of the solute molecule and the liquid metal ion cannot be neglected. As with the solute-electron interaction, the ion-induced dipole interaction is neglected. However, the interaction energy of a non-polar molecule within a non-polar solvent cannot be neglected and is described approximately by the Lennard-Jones pairwise additive potential. The molar interaction energy per solute atom is given by

$$U_{LG}^{\text{int}} = C\left\{\sum_i \left[\frac{a_{LG}^3}{r_i^{12}} - \frac{1}{r_i^6}\right]\right\}, \tag{3-52}$$

where C is the energy dispersion constant, and r_i is the distance from the center of the solute atom to the center of the i^{th} solvent atom. It is assumed that the solute atom is completely surrounded by the solvent. Furthermore, the solvent is assumed to be infinitely large and uniformly distributed according to the number density ρ around the solute atom. The number of solvent atoms contained in a spherical shell a distance r from the center of the solute molecule is equal to $4\pi\rho r^2 dr$. Placing this relationship into equation (3-52) and changing the discrete sum to an integral gives

$$U_{LG}^{\text{int}} = 4\pi\rho C\int_d^\infty \left(\frac{a_{LG}^3}{r_i^{10}} - \frac{1}{r_i^4}\right)dr, \tag{3-53}$$

where d is the distance from the center of the solute atom to the center of the nearest solvent atom. After integrating and setting $\frac{d}{a_{LG}}$ equal to d', equation (3-53) becomes

$$U_{LG}^{\text{int}} = \frac{\pi\rho C}{6a_{LG}^3}\left[\left(\frac{2}{d'}\right)^3 - \frac{8}{3}\left(\frac{1}{d'}\right)^9\right]. \tag{3-54}$$

The minimum interaction energy occurs when d' equals unity, that is, when $d = a_{LG}$. Therefore, equation (3-54) becomes

$$U_{LG}^{\text{int}} = -\frac{8\pi\rho C}{9a_{LG}^3} \tag{3-55}$$

or

$$\overline{U}_{LG}^{\text{int}} = -\frac{8\pi\rho C}{9a_{LG}^3} A. \tag{3-56}$$

According to Young et al [47], the best overall agreement of equation (3-56) for noble gases in crystals occurs when the constant C is selected according to Slater and Kirkwood,

$$C = \frac{3eh}{4\pi m_e^{1/2}} \frac{\alpha_L \alpha_G}{\left(\frac{\alpha_L}{z_{e,L}}\right) + \left(\frac{\alpha_G}{z_{e,G}}\right)}, \tag{3-57}$$

where α_i is the polarizability of the i^{th} species, h is Planck's constant, e is the charge of an electron, m_e is the mass of an electron, and $z_{e,i}$ is the effective number of outer electrons.

The final interaction term is the solvent-solvent interaction. This interaction was first pointed out by Neff and McQuarrie [51]. Prior to their discovery, this interaction term had always been neglected. However, Neff and McQuarrie believe this term to have a reasonable effect in liquid metal solutions. Just as the solute-solvent interaction can be

written in a mathematical expression like equation (3-53), the solvent-solvent interaction can also be written mathematically:

$$U_{LL}^{\text{int}} = \frac{1}{(2\pi)^3}\int\left[\frac{8\pi}{q^2}+\frac{q^2}{8\pi}\left(\frac{1}{\varepsilon(q)}-1\right)\left|v(q)\right|^2\right]\exp(i\mathbf{q}\cdot\mathbf{r})d\mathbf{q}\,, \tag{3-58}$$

where ε(q) is the dielectric screening function and v(q) is the Fourier transform of the electron-ion pseudopotential. For now, this term will be neglected; more will be said in a later section.

So far the total molar internal energy for introducing the gas into the liquid is the work needed in the production of a hard spherical cavity of radius r in the fluid plus the interaction energy of a non-polar molecule within a non-polar solvent. However, once the solute atom is within the solvent it vibrates. Therefore, we can add a third term which we will call the molar free energy of vibration of gas dissolved in the solution, $\overline{F}_{LG}^{vib}$. As with the introduction of the free energy of interaction, we can write the following relationship

$$F_{LG}^{vib} = U_{LG}^{vib} - TS_{LG}^{vib}\,. \tag{3-59}$$

For an ideal gas the molar internal energy of vibration is already known [48, 49].

$$\overline{U}_{LG}^{vib} = \frac{R\Theta_{vib}}{\exp\left(\Theta_{vib}/T\right)-1}\,. \tag{3-60}$$

Θ_{vib} is the characteristic vibrational temperature. If we assume that the gas atoms vibrate in accord with the atoms of the surrounding liquid solvent, we can relate Θ_{vib} to T_{Debye} by

$$\Theta_{vib} = T_{Debye}\sqrt{\frac{\overline{m}_L}{\overline{m}_G}}\,, \tag{3-61}$$

where T_{Debye} is Debye's temperature [50]. Debye's temperature is related to the maximum vibration frequency of an atom in a lattice and is given by

$$T_{Debye} = \frac{h\nu_m}{k_B}, \tag{3-62}$$

where ν_m is the maximum vibration frequency. Using Andrade's formula [49] for the dynamic viscosity of liquids, η_L,

$$\eta_L = \frac{4}{3}\nu_m \left(\frac{\rho M_{LG}^2}{A^2}\right)^{1/3}, \tag{3-63}$$

where M_{LG} is the molar mass of the solution, one obtains the following equation of Θ_{vib}

$$\Theta_{vib} = \frac{3h\eta_L}{4k_B}\left(\frac{A^2}{\rho M_{LG}^2}\right)^{1/3}\sqrt{\frac{\overline{m}_L}{\overline{m}_G}}. \tag{3-64}$$

Futhermore, according to Lösch [48], the vibrational entropy of the gas dissolved in a liquid can be given by

$$\overline{S}_{LG}^{vib} = R\left(\frac{\Theta_{vib}/T}{\exp(\Theta_{vib}/T)-1} - \ln(1-\exp(-\Theta_{vib}/T))\right). \tag{3-65}$$

Therefore, inserting equation (3-60) and equation (3-65) into equation (3-59) gives

$$\overline{F}_{LG}^{vib} = R\ln(1-\exp(-\Theta_{vib}/T)). \tag{3-66}$$

As a recap, if it is assumed that introducing a gas atom into solution is the contribution of the production of a hard spherical cavity, the interaction energy of a non-polar molecule within a non-polar solvent, and the vibrational energy of the solute atom, the total molar free energy for introducing the gas into the liquid can be written as

$$\Delta\overline{F}_{LG} = \overline{F}_{LG}^{hole} + \overline{U}_{LG}^{\text{int}} + \overline{F}_{LG}^{vib}, \tag{3-67}$$

where each term is defined by equation (3-47), equation (3-56), and equation (3-66), respectively.

The physical properties needed in the theory are given in Tables 3.3 and 3.4 below as well as Appendix A. Three theoretical solubility values were calculated at 300, 400, and 500 K. Final results for the theoretical solubility using the above theory can be seen in Table 3.5. As seen in Table 3.5, the Henry coefficient decreases with increasing temperature. This decrease corresponds to an increase in solubility. Of the three molar free energies of solution, the molar energy needed for forming a hole in the liquid, $\overline{F}_{LG}^{hole}$, plays the largest role in solubility. As can be seen in equations (3-46) and (3-48), temperature effects are important in hole formation. As the temperature increases, the mercury solvent density decreases. If the mercury density decrease, the mercury atom density, $\frac{\rho_L \mathrm{A}}{\overline{m}_L}$, decreases. In other words, the mean distance between mercury atoms increases. Therefore, the temperature effect on density would cause the molar energy needed to form a hole in the liquid to decrease. However, each coefficient in equation (3-46) is linearly related to temperature. So the direct temperature reliance dominates the counter effect of the temperature-dependent density.

Thormeier [21] attributes his temperature effects on the hole-formation energy on the temperature-dependent molar mass. But molar mass is independent of temperature. Therefore, I believe either his reference was wrong or he misunderstood the results of the referenced report.

Table 3.3: Physical properties for the solute helium used in the theoretical models

Property	Helium	Reference
Hard sphere radius (10^{-10} m)	1.30	[21, 46, 52]
Polarizability (10^{-30} m^3)	0.205	[21, 47]
z_e	1.7	[21, 47]
Atomic mass (amu)	4.00262	[53]

Table 3.4: Physical properties for the solvent mercury used in the theoretical models

Property	Mercury	Temperature Dependence			Reference
		300 K	400 K	500 K	
Hard sphere radius (10^{-10} m)	1.51	--	--	--	[21, 54, 55]
Polarizability (10^{-30} m^3)	5.02	--	--	--	[21]
z_e	41.76	--	--	--	[21]
Atomic mass (amu)	200.59	--	--	--	[53]
Density (kg/m^3)	--	13 529	13 291	13 058	[53, 2]
Thermal Expansion Coefficient (10^{-4} K^{-1})	1.81	--	--	--	[53, 56]
Isothermal Compressibility (10^{-10} Pa^{-1})	--	4.013E-11	4.513E-11	5.11E-11	[53]
Dynamic Viscosity (10^{-3} Pa-s)	--	0.001526	0.0011725	0.001	[53, 2]

Table 3.5: Theoretical Henry Coefficient for Hg/He compared to Na/He using Thormeier's model

System	$\overline{F}_{LG}^{hole}$ (J/mol)	$\overline{F}_{LG}^{\text{int}}$ (J/mol)	$\overline{F}_{LG}^{vib}$ (J/mol)	Temperature (K)	Theoretical K_H (Pa-molMetal/molHe)
Hg/He	$4.3x10^{4}$	$1.2x10^{-1}$	$-9.7x10^{2}$	300	$3.9x10^{15}$
	$5.4x10^{4}$	$1.2x10^{-1}$	$-2.4x10^{3}$	400	$1.1x10^{15}$
	$6.3x10^{4}$	$1.2x10^{-1}$	$-4.2x10^{3}$	500	$3.5x10^{14}$
Na/He	$5.7x10^{4}$	$3.2x10^{-2}$	$-1.2x10^{4}$	773	$2.3x10^{11}$

One draw back of the theory presented above also deals with the hole-formation molar energy expression. The radius needed to calculate $\overline{F}_{LG}^{hole}$ is the van der Waals radius for helium. The model for $\overline{F}_{LG}^{hole}$ can be seen to be very sensitive to small changes in the radius. This sensitivity is amplified in the fact that the theoretical solubility model is related to the exponential of $\overline{F}_{LG}^{hole}$. For example, if helium is assumed to have a hard sphere radius of 135 pm, not the 130 pm assumed here, the model predicts a Henry coefficient of 1.39×10^{16} Pa-molHg/molHe. However, if helium is assumed to have a hard sphere radius of 125 pm, the model predicts a Henry coefficient of 1.16×10^{15} Pa-molHg/molHe. Consequently, the validity of the model hinges on the certainty of helium's van der Waals radius. A more thorough sensitivity study of this model can be found in Appendix C following the MATLAB code shown in Appendix B.

For comparison, the Henry coefficient for the Na/He system was also calculated using the above theory. Thormeier [21] applied this theory; however, he used slightly different physical parameters. As mentioned before, he also used a mysteriously temperature-dependent molar mass. Nevertheless, the Henry coefficient calculated here, 2.3×10^{11} Pa-molNa/molHe, still corresponds well with his calculation, 6.63×10^{11} Pa-molNa/molHe, as well as with the various experimental values that can be seen in Table 3.2.

3.3 Comparison with Other Theories

Hildebrand [57] derives a model based solely on the radial distribution function, g(r), and the potential between a central atom and its surrounding atoms. He assumes a

Lennard-Jones potential. Mitra [28] gives an excellent overview of Hildebrand's theory in the appendix of his dissertation. The final relationship is as follows:

$$-\log x = \log p_G^{\circ} + \frac{\overline{V}_G(\delta_G - \delta_L)^2}{RT} + \log\frac{\overline{V}_G}{\overline{V}_L} + \left(1 - \frac{\overline{V}_G}{\overline{V}_L}\right), \tag{3-68}$$

where p_G° is the vapor pressure and for helium is given by the following expression:

$$\log p_G^{\circ}(atm) = 1.848 - 7.948T^{-1} - 0.1363T^{-2} + 4.363T^{-3}, \tag{3-69}$$

and δ is the solubility parameter defined by Hildebrand as

$$\delta = \left(\frac{\Delta\overline{H}^{v} - RT}{\overline{V}}\right)^{1/2}, \tag{3-70}$$

where $\Delta\overline{H}^{v}$ is the molar enthalpy of vaporization. The full theory is based on rather simple principles and tends to predict much lower solubility than reported experimentally. However, a comparison of various known solubility parameters found experimentally might allow us to predict an approximate solubility value for the Hg/He system. This comparison will be discussed in section 4.2.

Epstein [58] proposed a different theory. Similar to the theory derived in section 3.2, Epstein utilizes the fact that at equilibrium the chemical potential of a noble element will be the same in both phases [See equation (3-30)]. However, Epstein arrived at slightly different forms of the chemical potentials. For the chemical potential of the noble gas in the solution, he obtained

$$\mu_G^{(L)} = RT\ln(x \cdot \gamma_G) + \mu_G^{\circ}(liq), \tag{3-71}$$

where γ_G is the activity coefficient of the solute and $\mu_G^{\circ}(liq)$ is the standard state consisting of the pure, liquid noble element. For the chemical potential of the noble gas in its pure gas phase, he obtained

$$\mu_G^{(G)} = RT \ln p + \beta \cdot p + \mu_G^{\circ}(gas), \tag{3-72}$$

where β is the second viral coefficient and

$$\mu_G^{\circ}(liq) = RT \ln p_G^{\circ} + \beta \cdot p_G^{\circ} + \mu_G^{\circ}(gas), \tag{3-73}$$

Putting equations (3-71) through (3-73) together, Epstein obtained the following relationship for Henry's coefficient

$$\ln K_H = -\ln p_G^{\circ} + \frac{(p - p_G^{\circ})}{RT}(\beta - \overline{V}_G) - \ln \gamma_G, \tag{3-74}$$

where

$$\ln \gamma_G = \frac{\overline{V}_G(\delta_G - \delta_L)^2}{RT} + \log \frac{\overline{V}_G}{\overline{V}_L} + \left(1 - \frac{\overline{V}_G}{\overline{V}_L}\right), \tag{3-75}$$

from Hildebrand's solubility parameters. The Epstein model depends heavily on the value assigned to the hypothetical vapor pressure experienced by the pure, liquid noble element, p_G°. Mitra used the theory of Epstein to calculate the solubility of xenon in liquid bismuth. However, Mitra initially used his model that erroneously assumed that $\overline{V}_G = \overline{V}_L$ rather than his corrected model shown above.

As early as 1937, Uhlig [60] proposed the replacement of the quantity ($PV_G - \chi_{LG}$) in equation (3-28), or more exact the quantity ($P\overline{V}_G - \overline{\chi}_{LG}$), by the sum of two term: μ_{LG}^{hole}, the reversible work required to make a mole of internal cavities with radii as large as the solute; and μ_{LG}^{int}, the reversible work related to the interaction of the

solute with the solvent. He considered μ_{LG}^{hole} to be related to the surface area of the gas solute and the surface tension of the liquid solvent—second term on the right side of equation (3-40). Uhlig did not evaluate μ_{LG}^{int}; he obtained this value empirically from experimental solubility values. While Uhlig's final model is rather simplistic, he led the way into thinking about solubility in these two steps.

McMillan [61] would build on the work of Uhlig. He estimated the energy of hole formation to be the product of the cavity surface area and a microscopic surface energy which is related to the enthalpy of vaporization,

$$\mu_{LG}^{hole} = \frac{\pi a_{LG}^2 \Delta \overline{H}_L^v}{4\sigma^*}, \tag{3-76}$$

where σ* is the area occupied by a solvent atom on the surface. McMillan also only considered the London dispersion force as the contributor to the energy of interaction, i.e.,

$$\mu_{LG}^{\text{int}} = -\tfrac{3}{2} z_e \frac{\alpha_L \alpha_G}{a_{LG}^2} \frac{I_L I_G}{I_L + I_G}, \tag{3-77}$$

where I is the ionization potential.

Johnson and Shuttleworth [34] also built on the work of Uhlig. For the first time, the vibration energy is introduced. They estimated the vibrational contribution, μ_{LG}^{vib}, to be equal to the enthalpy of the solvent, H_L, minus the entropy term for the solvent, TS_L. Furthermore, Johnson and Shuttleworth did not assign equal values to the partition function of the solute component, ϕ_G, in pure and solution phases [see equations (3-28) and (3-29)]. For the pure gas phase, ϕ_G is represented by its translational component, and, for the solution phase, ϕ_G is represented by the number density of the solvent. Symbolically, the chemical potentials can be written

$$\mu_G^{(G)} = kT \ln\left(\frac{h^3}{(2\pi mkT)^{3/2}}\right) + kT \ln\left(\frac{p_G^{(G)}}{k_B T}\right) \tag{3-78}$$

and

$$\mu_G^{(L)} = \mu^+ + kT \ln\left(a^3 C_L\right) \tag{3-79}$$

where C_L is the number of gas atoms in unit volume of the metal, $1/a^3$ is the number of metal atoms in unit volume of the metal, and $\mu^+ = H - TS$. Johnson and Shuttleworth consider the energy H to be made up of three terms: the energy to make a hole in the liquid the size of a solute atom, the vibrational energy of the solute atom, and the negative van der Waals interaction energy between the solute and surrounding solvent atoms. The energy required to make a hole is estimated by multiplying the surface area of the cavity by the surface energy of the liquid metal extrapolated to 0 Kelvin. Slotnick adopted the theory of Johnson and Shuttleworth in his determination of helium in lithium and potassium.

Pierotti [46] eventually evaluated the hole-formation energy in a more sophisticated way. While his form is very sensitive to the solute hard-sphere radius, the results are in better agreement with experimental values. However, Pierotti did not include a vibrational energy term in his model. But Thormeier [21] and Veleckis et al. [40] did incorporate Pierotti's model with a vibrational energy term. The model used by Thormeier is the one used in this paper.

Finally, Fukase [63] points out that in all theories up to this point, the solvent-solvent interaction has been neglected. As stated earlier, Neff and McQuarrie [51] first pointed out that this term had been neglected. The interaction term was given above in equation (3-58). The term is very math intensive. Before equation (3-58) can be used the

dielectric screening function, ε(q), as well as the Fourier transform of the electron-ion pseudopotential, v(q), for mercury must be known. This method has not been used here. However, a rough calculation for helium in mercury under the assumption that we can use the helium in sodium values of Fukase, raises the Henry coefficient derived in section 3.2 from 3.92×10^{15} to almost 2.0×10^{16} Pa-molHg/molHe.

Fukase [63] also references a new proposed method to calculate solubility in liquid metals based on the work of Faber [64]. Faber's theory is derived by a two step process as well. First, the metal is expanded uniformly through one atomic volume. Secondly, the solvent ions are rearranged at constant volume so as to produce a single vacancy and to restore its original density. In this model, the free energy of equation (3-43) is just given by

$$\Delta F_{LG} = \frac{1}{12\pi^3} \int [a(\mathbf{q}) - 1]\mathbf{q} \cdot \nabla u(\mathbf{q}) d\mathbf{q}\,, \tag{3-80}$$

where a(**q**) is the structure factor and u(**q**) is the Fourier transform of the interionic potential, equation (3-58).

Except for the later work of Fukase, all the theoretical models mentioned so far have been used to calculate the Henry coefficient for helium in mercury. The results can be seen in Table 3.6. For comparison, the models were also used to calculate the Henry coefficient for helium in sodium. For the Na/He system, the first four values, Epstein through Pierotti, are based on the calculation of Veleckis et al [40]. The Na/He system calculation using the model based on Thormeier's work is the actual theoretical value he calculated [21] and not our recalculated value that is reported in Table 3.5. As a comparison, we see that Thormeier's model appears to fit the experimental results, also

tabulated in Table 3.6, quite well. For this reason and because of the relatively straight forward math, this model is the one used in this paper.

Table 3.6 reports the Henry coefficient at one temperature. However, Figure 3.1 shows how Hg/He solubility varies with temperature based on the various theoretical models.

The models of Thormeier were revitalized by Shpil'rain et al. [49, 65] because of a renewed interest in liquid metals. They applied the model used by Thormeier to determine the solubility of helium, neon, argon, krypton, and xenon in molten lithium, sodium, potassium, rubidium, and cesium for the temperature ranges from 600 to 1500 K and pressure ranges from 0.1 to10 MPa. However, Shpil'rain's calculations for solubility are much lower than the values for sodium and helium calculated here as well as those calculated by Thormeier. The major difference is the selection of the hard sphere radius of helium. Thormeier used a hard sphere radius of 1.30×10^{-10} m, while Shpil'rain used a radius of 1.35×10^{-10} m.

Likewise, Lu [19] also used the model of Thormeier to predict the solubility of helium in mercury. His master's thesis was the initial work that led to a more extensive study for the solubility of noble gases in mercury seen here. However, in Lu's theoretical work, he used a radius for the noble gases that does not correspond to the radius needed for the Thormeier model. Therefore, for helium he used a radius of 0.31×10^{-10} m and obtained noticeably higher solubility values.

The atomic radius, or size of an atom, is not a precisely defined physical quantity. Therefore, the value assigned to a radius of a particular atom will depend on the

Table 3.6: Theoretical Henry coefficient for Hg/He with comparison to Na/He using a variety of theories

Model	K_H (Pa-molMetal/molGas)	
	Na/He @ 500°C	Hg/He @ 27°C
Hildebrand	--	8.95×10^{21}
Epstein (corrected)	1.51×10^{15}	1.01×10^{26}
McMillan	2.61×10^{8}	2.26×10^{11}
Johnson and Shuttleworth	1.30×10^{9}	1.36×10^{18}
Pierotti	8.37×10^{9}	5.78×10^{15}
Thormeier	6.63×10^{11}	3.92×10^{15}
Fukase (Faber's model)	1.04×10^{12}	--
Thormeier (exp.)	9.81×10^{11}	--
Veleckis (exp.)	7.20×10^{11}	--

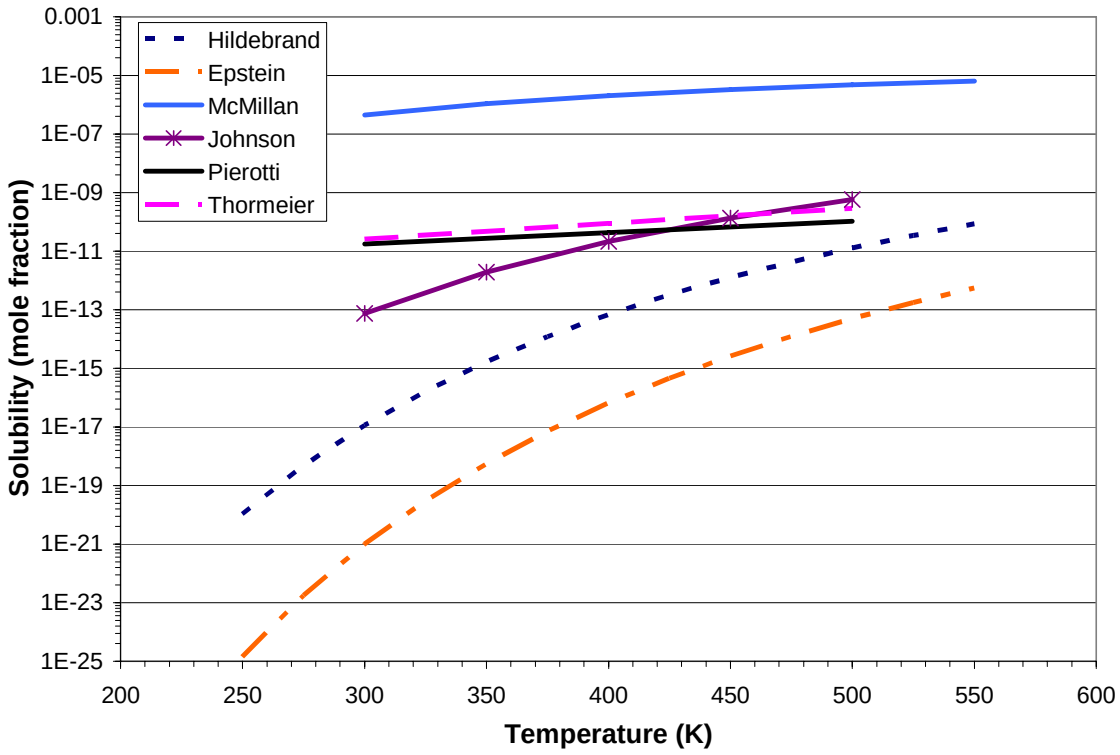

Figure 3.1: Theoretical Solubility of Helium in Mercury as a function of Temperature

definition that is chosen. The atomic radii are on the order of 30 to 300 picometers ($30x10^{-12}$ to $300x10^{-12}$ meters or 0.3 to 3.0 Angstroms) [52].

One definition for atomic radii comes from quantum mechanics. In solving the Schrödinger equation for a simple proton-electron system (the simple hydrogen atom), one obtains wavefunctions that are related to the probability of finding an electron some distance, r, from the proton. However, more complex systems like the helium atom, which includes two protons and two electrons, cannot be solved analytically using the Schrödinger equation. In dealing with these more complex systems, the wavefunctions are determined using some approximation method. Figure 3.2 below shows a typical schematic of the probability of finding an electron at a distance between r and r + dr from the nucleus for various quantum states. The peaks correspond to high probabilities of finding an electron; therefore, it is possible to define an atom's radius by the location at which one of these peaks exists. It is this method that was used by Clementi and Raimondi [73] to determine a radius for helium on the order of 31 pm. This value was used by Lu [19].

A second definition for atomic radii arrives from the interactions of atoms. When two non-polar molecules interact there are long-range forces of attraction between them. At any instant the electrons in molecule A are in some configuration which results in an instantaneous dipole moment. This instantaneous dipole moment induces a dipole in molecule B. Therefore, an instantaneous attraction is created between the two molecules. It has been shown that this induced-dipole-induced-dipole attraction is proportional to r^{-6} [52]. However, once the molecules approach too closely a repulsive force is felt that forces them apart. To calculate various properties, a potential function is needed that

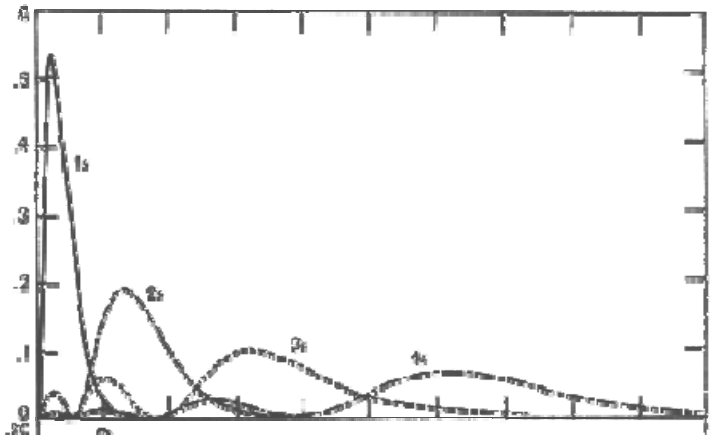

Figure 3.2: The typical schematic for the probability of finding an electron a distance between r and r + dr from the nucleus

describes these interactions [52]. Figure 3.3 shows common potential functions that are often used for atomic interactions.

In many derivations, the hard sphere potential is used due to its simplicity. This potential was used for the hole formation term used in calculating solubility in section 3.2. The atom is assumed to be a hard spherical ball. The radius of the atom is then defined as the point at which the potential first equals zero. However, the Lennard-Jones Potential models the interaction of the nonpolar atoms more realistically [52]. It includes a repulsion as well as attraction term. This potential is usually used as a later correction to the hard sphere potential assumption.

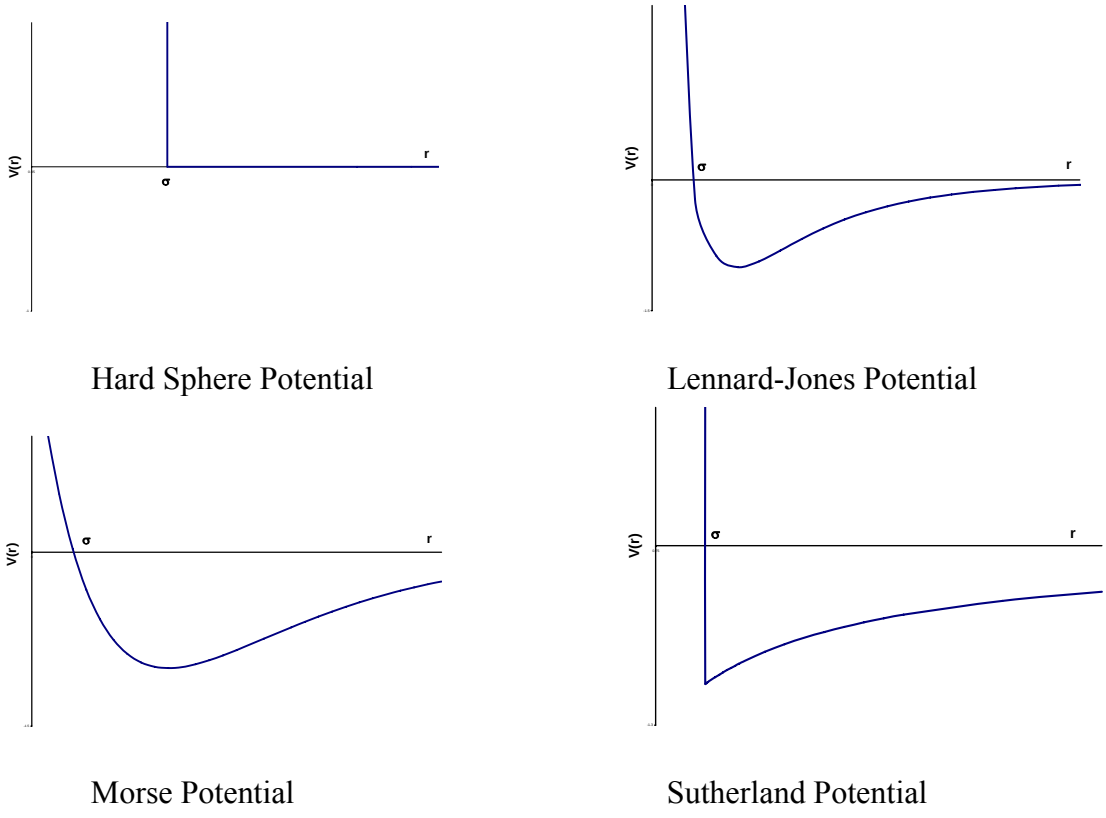

Figure 3.2: Various common atomic interaction potentials.

Using the potential function definition for atomic interactions, we obtain a radius on the order of 120 pm for helium [96]. Since the models derived in this dissertation arrive from an initial hard sphere radius with an interaction correction term, the hard sphere or van der Waals radius definition is the one that should be used in these models.

4. Experimental Determination of Solubility

4.1 Previous Experimental Methods

Just as a variety of theories have been implemented for the solubility of noble gases in liquid metals, so too has been the variety of experimental methods. Due to the inactivity of noble gases, the experimental methods must be physical in nature rather than chemical. In physical measuring methods, an initially gas-free solvent is brought into contact with a set amount of gas. The physical method often takes advantage of changes in volume, weight or pressure of the system. However, many have attempted to measure solubility using radioactive isotope detection, as well.

Mitra et al. [24, 25, 28] proposed various methods for measuring radioactive xenon in liquid metals. In one method, a small amount of liquid metal—about 5 grams of bismuth in their case—is held in a Pyrex capsule at the desired temperature under one atmosphere pressure of radioactive xenon until it is saturated with xenon. The metal sample in the capsule is quickly removed from a furnace. At room temperature, the sample freezes within a few seconds. The solid bismuth sample is then dissolved in nitric acid in a controlled environment. The melting of the sample causes the dissolved xenon to be released. The released xenon is transmitted to a counting device where solubility values can be inferred. However, this method has been noted to have numerous sources of error. Measuring technique errors inherent in using the counting system as well as systematic errors like counting gas not coming out of solution but adsorbed on the surface or enclosed in bubbles cause one to doubt the reliability of this method. Due to the large number of sources of error, the measurement results are not reproducible, and, therefore, the method can be considered unsuccessful. Raseman et al., Eshaya et al., and Watson all

used very similar methods to determine the solubility of xenon or helium in bismuth. Nevertheless, they all obtained very different results despite careful experimentation.

Another method that was first used by Mitra et al. [25] utilized two chambers. Mitra called his setup the Saturator-Desorber assembly. The experimental arrangement resembled a manometer. No valve separated the two chambers. Approximately 100 cm^3 of liquid metal—liquid bismuth or mercury for this setup—was placed in the assembly and filled the tube that connected the Saturator with the Desorber. Activated xenon was charged on the Saturator side while simultaneously nitrogen was charged on the Desorber side. The assumption is that xenon would go into solution. After assumed saturation, the nitrogen was evacuated on the Desorber side. The change in pressure would draw the liquid metal through the tube. Xenon was also supplied on the Saturator side to maintain the saturation pressure. Above the Desorber chamber was a counting chamber. Some of the same inherent errors in Mitra et al. other method can also be found in this method. Mitra is actually one of the few experimentalists who tried to find solubility of a noble gas in mercury. However, Mitra emphasizes that the results are preliminary and could be very erroneous. He estimates that the logarithm of the atom fraction solubility could be off by at least a factor of two.

Hewitt et al. [33] also adopted the freezing method proposed by Mitra et al. and applied it to the determination of both radioactive xenon and neutral xenon in bismuth. After thorough enrichment with xenon in each case, the saturated bismuth is again very rapidly cooled and frozen. The surface of the solid bismuth samples are then freed of adsorbed xenon by scratching the uppermost layer. The bismuth sample saturated with radioactive xenon is crushed and ground to a powder. The xenon released in the process

is determined by measurement of the activity. The bismuth sample saturated with neutral xenon is melted on a sintered plate under vacuum while gradually stripped of xenon by hydrogen bubbling through the sample. The resulting hydrogen-xenon mixture is passed through an activated carbon cold trap. When all the xenon from the bismuth sample has finally reached the cold trap, the cold trap is heated, and the xenon is carried away by a certain amount of pure hydrogen. The quantitative ratio of hydrogen and xenon is determined by a mass spectrometer. Hewitt et al. obtained very different values with the two measuring methods.

Johnson and Shuttleworth [34, 35] also utilized a freezing method. A 4 cm metal sample and krypton-85 gas were sealed in a silica tube. The tube was placed in a furnace where it was stirred at a steady two revolutions per minute by an electric motor. The stirring lasted for two days. On the third day, the stirring was stopped and the tube was placed in a vertical position to allow any gas bubbles to rise to the surface. The next day the tube was removed and the liquid metal solidified. After solidification, the surface was machined-off and the bulk material was rolled into thin foils about 0.005 cm thick. Each specimen was placed under a Geiger-Muller counter, and the count rate was related to a solubility value.

Adapting a method by Grimes et al. [66] where they determined the solubility of noble gases in fused salts, Slotnick et al. [36] determined the solubility of helium in liquid lithium and liquid potassium. In this method, helium is bubbled through approximately 1.0×10^{-3} cm^3 (1.0 L) of liquid metal at a set temperature and pressure until saturation is achieved. The system was allowed to sit for several hours so that undissolved gas bubbles could rise to the surface. About one half of the helium-liquid

metal solution was transferred to another vessel filled with a set amount of argon. The argon was bubbled through the liquid metal and repumped back to the bubbler. This cycle continued as argon would remove helium from the liquid metal. The ratio of argon atoms to helium atoms was determined by a mass spectrometer. To increase the sensitivity, the argon-helium mixture could be passed through a carbon cold trap which removed the argon.

Dhar [37, 38, 39] carried out a very similar experiment to determine the solubility of argon and krypton in liquid sodium. However, Dhar used helium as the stripping gas. The argon and krypton would be removed through a carbon cold trap as well. The concentration of argon would be determined using a mass spectrometer, and the concentration of radioactive krypton would be determined using a radiation detector.

However, Dhar and Veleckis [40] eventually determined that the stripping method was found to be inefficient. Almost 40% of the argon was never accounted for. Therefore, to improve the method, the carbon in the cold trap was replaced with a molecular sieve. And the mass spectrometer was replaced by a gas chromatograph due to its greater sensitivity.

Due to all the inherent errors in the freezing and activity measurements, Thormeier [21, 22] devised a novel method that is based on the dissolution of the inert gas in the liquid metal under pressure and degassing under vacuum. The pressure increase during degassing corresponds to the amount of gas coming out of solution. Thormeier believed this method could account for any solubility in the wide range between 1.0×10^{-10} to 3.0×10^{-5} mole fraction. His setup consisted of three large tanks (approximately 20 L each). Two of the tanks can be in continuous connection by means

of an electromagnetic pump. These tanks are pressurized with the desirable solute gas and mixing takes place by the continuous pumping. However, the pump is turned off and the tanks sit for about 10 hours to allow gas bubbles to rise out of the liquid metal—sodium in his experiment. One tank is eventually brought to vacuum causing a pressure difference that pulls the saturated sodium into a degassing tank. By measuring the pressure and the pressure differences, Thormeier could determine the solubility relationship by means of Henry's Law.

4.2 Empirical Method to find Solubility

As mentioned earlier, Hildebrand [57] arrived at a term he called the solubility parameter [see equation (3-75)]. While the full theory of Hildebrand might be considered a little too simplistic, a comparison of known solubility parameters might be of good use in predicting the solubility of helium in mercury. According to Hildebrand, the solubility parameter is a function of temperature. Therefore, a plot of apparently credible experimental solubility values as a function of the associated solubility parameters of the liquid metals at the same temperature might show a trend that could be beneficial in predicting solubility of helium in mercury.

From the discussion in section 4.1, credible Henry coefficients and solubility parameters from past experiments have been reported in Table 4.1. The values have also been plotted in Figure 4.1, where a clear trend can be seen. As an aside, the cadmium and krypton data appears to be an outlier. However, Thormeier [21] notes that this data point is very questionable anyway because of the method of extrapolation to 500°C.

Table 4.1: Experimental Henry Coefficients and solubility parameters from various reliable experiments

Reference	System	$(K_H)_{500°C}$ (Pa-molMetal-molGas)	$(\delta)_{500°C}$ $(10^4\ J^{1/2}\cdot m^{-3/2})$
Dhar	Na/Kr	$6.54x10^{13}$	5.90
Johnson and Shuttleworth	Pb/Kr	$4.09x10^{18}$	9.79
	Sn/Kr	$1.36x10^{21}$	12.66
	Cd/Kr	$9.81x10^{22}$	8.12
	In/Kr	$2.88x10^{21}$	11.76
Foust	Na/Kr	$8.00x10^{13}$	5.90
Slotnick	Li/He	$3.06x10^{13}$	9.77
	K/He	$2.58x10^{10}$	3.76
Watson	Bi/He	$1.00x10^{14}$	9.17
Thormeier	Na/He	$9.81x10^{11}$	5.90
Veleckis	Na/He	$7.20x10^{11}$	5.90

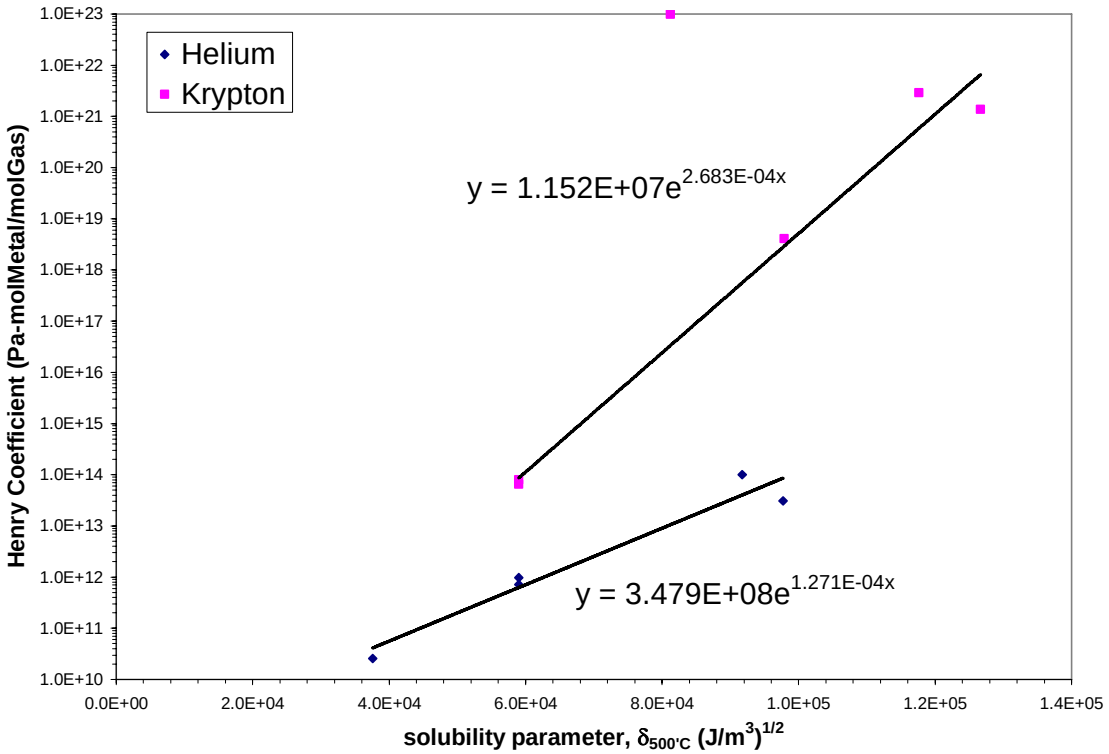

Figure 4.1: Henry Coefficient verses solubility parameter for helium and krypton in various liquid metals

Examining equation (3-75), we see that the solubility parameter is related to the enthalpy of vaporization as well as the molar volume of the liquid. Both terms are a function of temperature. According to the Clausius-Clapeyron equation [67], the enthalpy of vaporization is related to the vapor pressure as

$$\Delta\overline{H}_v = -R\frac{d\ln p_v}{d(\frac{1}{T})}, \tag{4-1}$$

where p_v is the vapor pressure and is reported in mercury in Appendix A.8. Using this relationship, an enthalpy of vaporization can be calculated. The natural logarithm of the vapor pressure as a function of inverse temperature can be seen in Figure 4.2 below. The slope of this curve is equal to -7332.3 for all values of the inverse temperature. The molar volume is a function of temperature because it is related to the density of mercury. Therefore, the solubility parameter for mercury, given by equation 3-75, is plotted as a function of temperature in Figure 4.3 below.

To use the results from Table 4.1 and Figure 4.1, we must extrapolate the solubility parameter for mercury out to 500°C. The major concern with this extrapolation is that mercury boils at 357°C. Therefore, the extrapolated value is not physical. Nevertheless, the value is estimated to be $5.8\text{x}10^4$ $J^{1/2}\cdot m^{-3/2}$. Inserting this value into the best fit curve of the helium data in Figure 4.1, one obtains a Henry coefficient of $5.5\text{x}10^{11}$ Pa-molHg/molHe. Figure 4.4 shows the theoretical Henry coefficients calculated for mercury that are reported in Table 3.5. The insert plot of Figure 4.4 includes the empirical value obtained from other solubility systems. From this, we confirm that the solubility of helium in mercury is once again confirmed to be quite low.

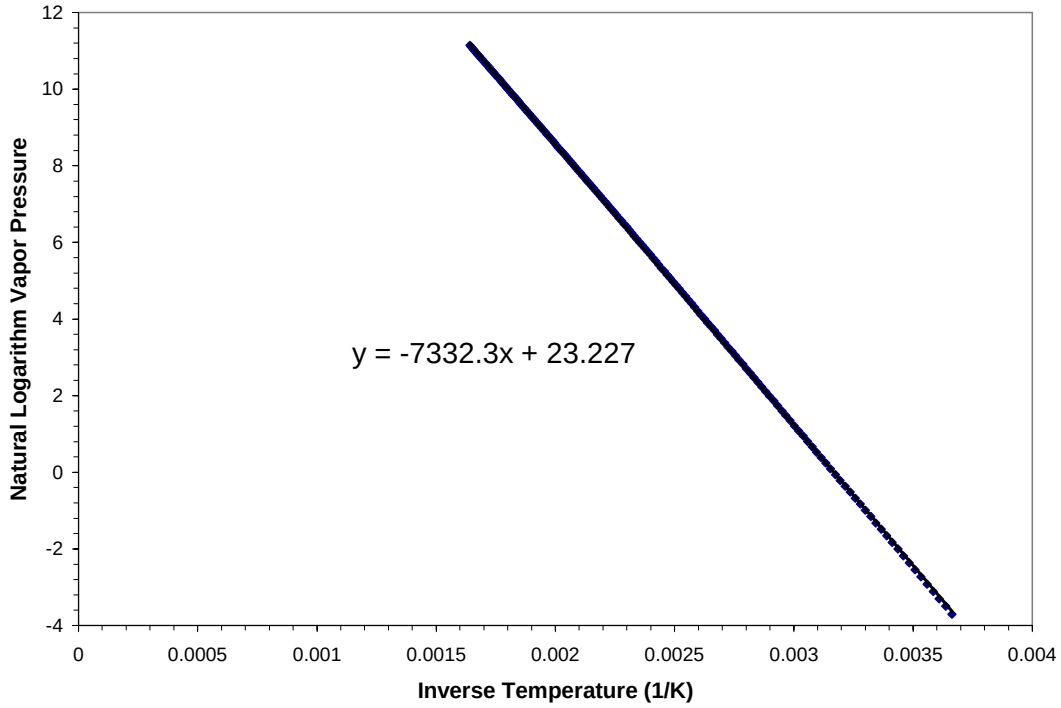

Figure 4.2: Mercury's natural logarithm vapor pressure as a function of inverse temperature used in equation (4-1)

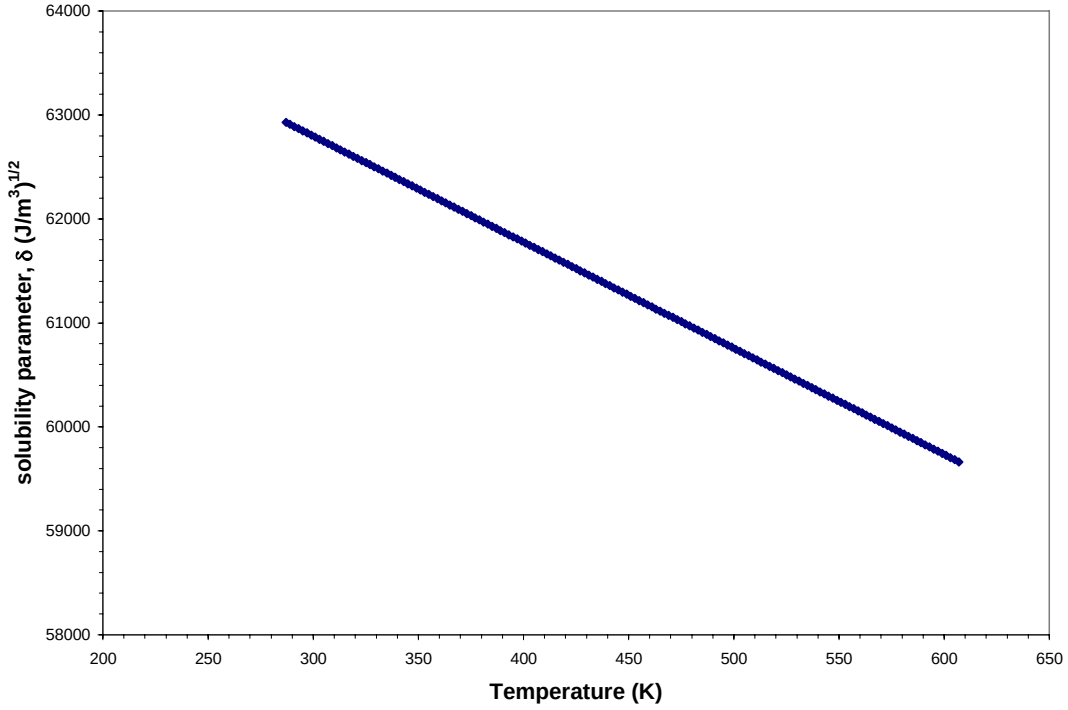

Figure 4.3: Mercury's Solubility Parameter as a function of temperature based on equation (3-75)

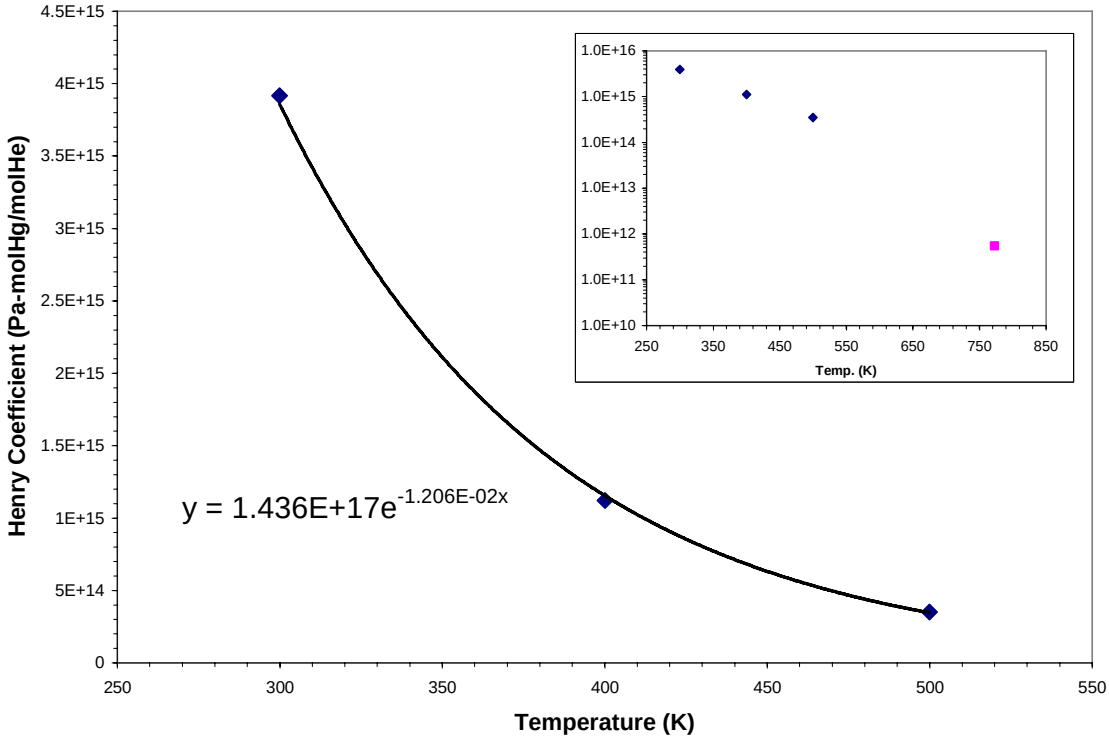

Figure 4.4: Theoretical Henry coefficient values from Table 3.5 [insert: log of scale Henry coefficient with extrapolated value using mercury solubility parameter and Figure 4.1]

4.3 Hg/He Experimental Method

Solubility experiments for mercury are almost non-existent. Noted above, Mitra's results [28] for xenon in mercury are emphasized as preliminary. Gas solubility in mercury has always been acknowledged to be very low. Therefore, mercury has been used in ASTM standard methods as a blocking media for gas solubility studies in organic fluids and water. Other than Mitra's preliminary work, the only other experiment found that dealt with gas solubility in mercury was work by Moss [68]. In his report titled *The Solubility of Helium in Certain Typical Lubricants and Mercury*, the only mention of mercury in the whole report is when Moss writes, "In the case of Mercury there was no indication of helium in the samples after four days of soaking at 400 lb/in^2 and periodic

shaking. The temperature was about 20°C." Therefore, we found it necessary to develop an experiment to measure the solubility of helium in mercury. Our experiment was based on the approach of Thormeier [21]. However, we charged the mercury with helium and recorded the pressure change. Any change was attributed to gas going into solution.

The mercury was transferred to our lab after quadruple distillation in a glove box under nitrogen cover gas and packaged in glass bottles by Bethlehem Apparatus [69]. A small volume of nitrogen remained in each bottle to allow for thermal expansion during shipment. While it is expected that the mercury may be saturated with nitrogen at one atmosphere upon arrival to the lab, the nitrogen dissolved in the mercury does not compromise any of the theoretical models used to predict the helium solubility. The nitrogen evolution from the mercury will elevate the cover gas pressure. However, the nitrogen solubility is expected to be much less than that of helium. Nevertheless, to insure minimum impurities, the mercury is degassed prior to each test sequence.

A 1.2 liter 316 stainless steel vessel with electro-polished internal surfaces from Eagle Stainless was filled with the quadruple distilled 99.999% mercury. After degassing, the small evacuated volume above the mercury is charged with helium to a gage pressure of 483 kPa (70 psig). The mercury fill volume for the vessel is confirmed with a mass measurement to a precision of 0.1 cc, allowing the gas head space volume to be known within 1 cc. The gas volume is controlled carefully since this volume determines the pressure sensitivity of the system to gas solution in the mercury. Furthermore, experience revealed that bellows valves should be used over ball valves to prevent the helium gas from leaving the vessel.

As seen in Figure 4.5, the stainless steel vessel is surrounded by three close fitting copper coils. The top coil surrounds the top third of the vessel, the second coil surrounds the middle third, and the bottom coil surrounds the bottom third. During standard operation, water maintained at a constant temperature flows through all three coils. However, to aid diffusion of helium solute into the mercury solvent, slightly hotter water is pumped periodically through the middle coil. A temperature gradient then occurs across the vessel which causes thermal stirring due to natural convection within the mercury [70]. The setup can be seen in Figure 4.6 below. The two operation modes can be seen schematically in Figure 4.7 below. Rayleigh numbers near 6.0×10^8 are created during the stir, which correspond to turbulent natural convection in the enclosure. This technique for thermal stirring causes a perturbation of the system pressure due to the mercury bulk temperature change and related thermal expansion, but this effect is limited to 1.0 psia by perturbing the temperature of only one zone of the temperature control coils. The stirring sequence is performed every 50 hours for 5 hours during the test period.

The whole setup is surrounded by 10 cm (3.9 in) of Styrofoam insulation and various thermocouples are placed around the vessel. A pressure sensor is then used to measure any deviation in pressure. Since the setup is well insulated, during standard operation, any long term pressure change is attributed to helium gas passing into the mercury solvent. A schematic of the vessel, insulation, and pressure transducer can be seen in Figure 4.8.

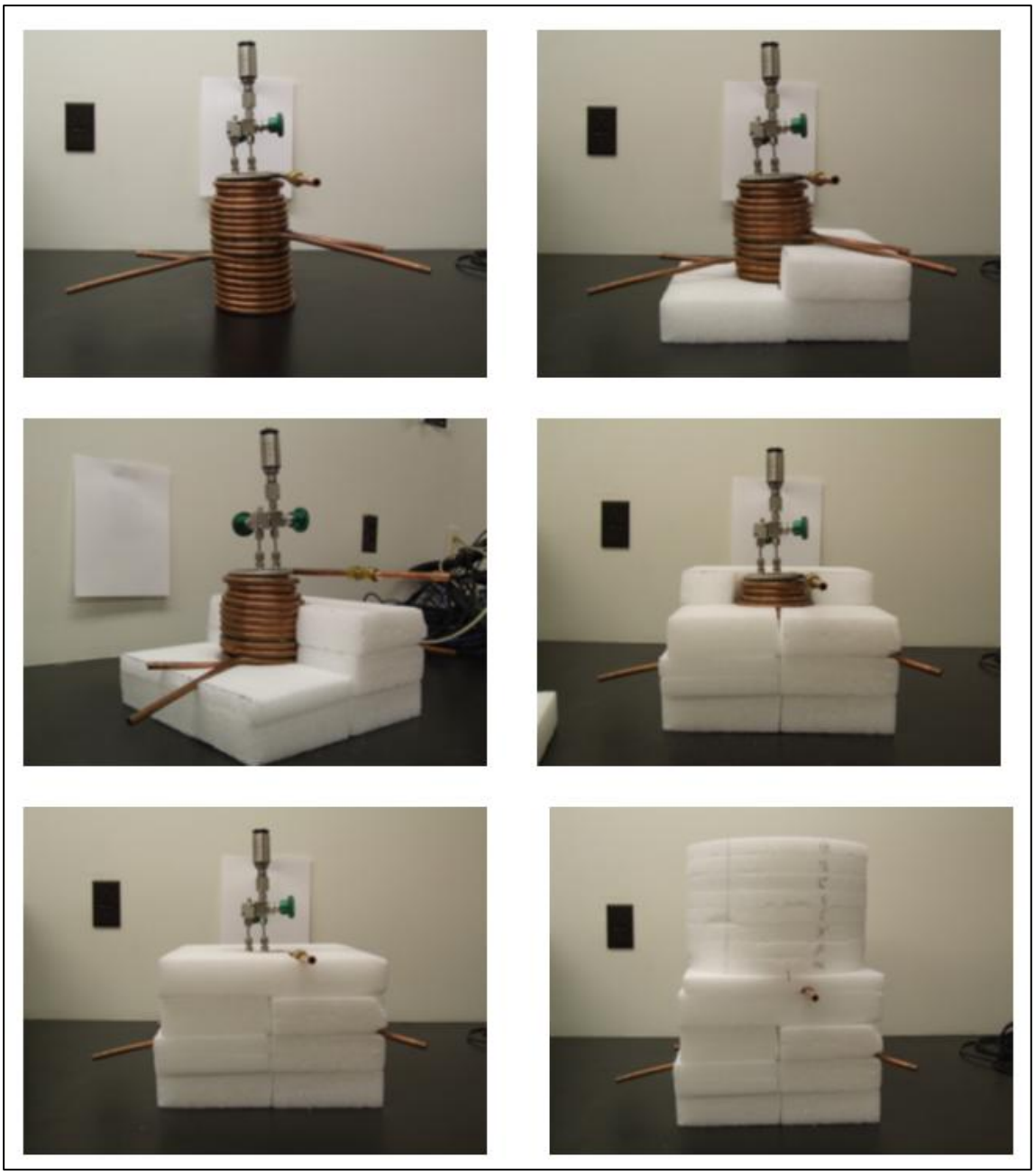

Figure 4.5: Eagle Stainless Vessel with Styrofoam insulation

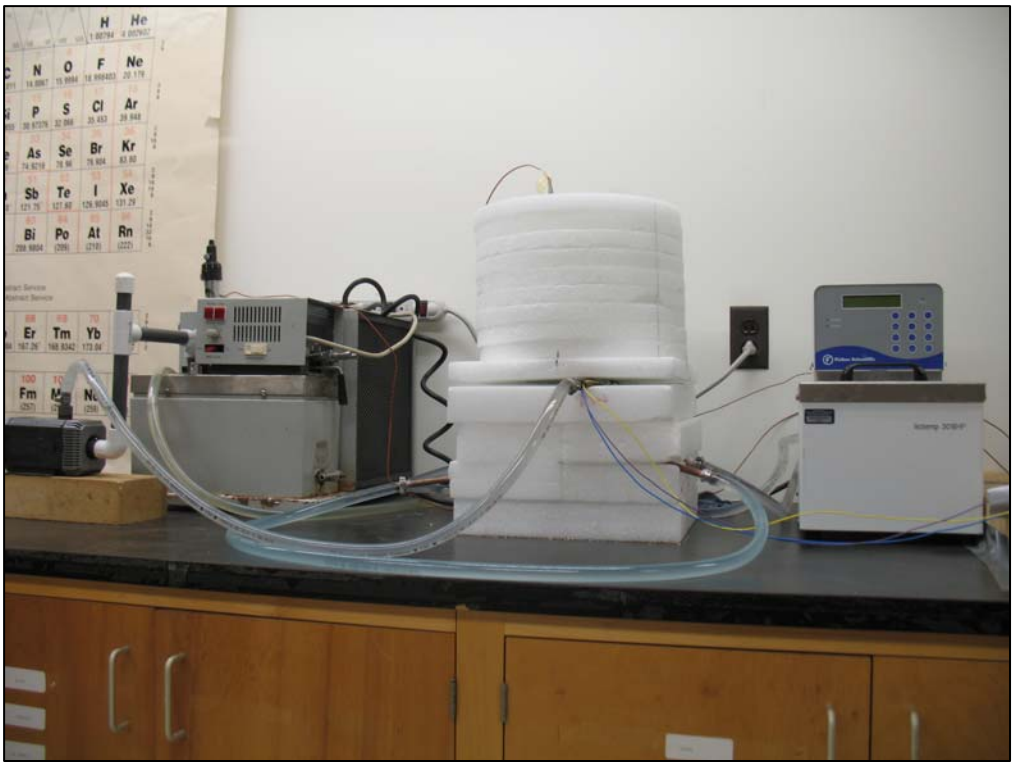

Figure 4.6: Final Gas Charge Setup with duel temperature control

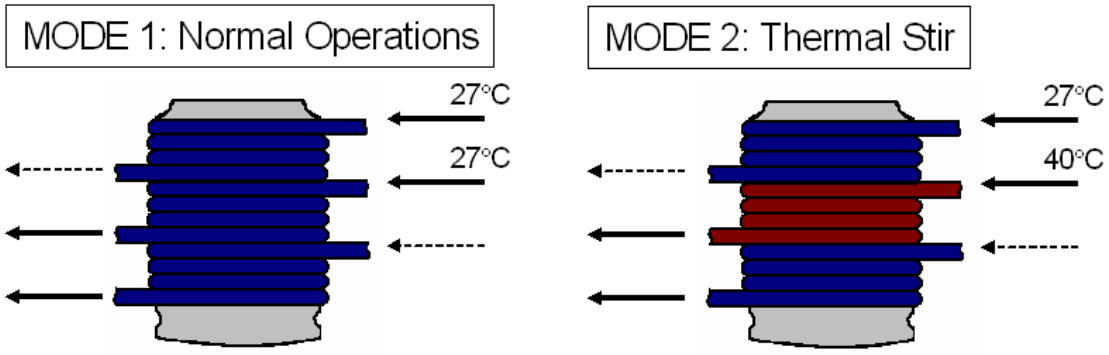

Figure 4.7: Schematic of temperature control models during Gas Charge Experiment

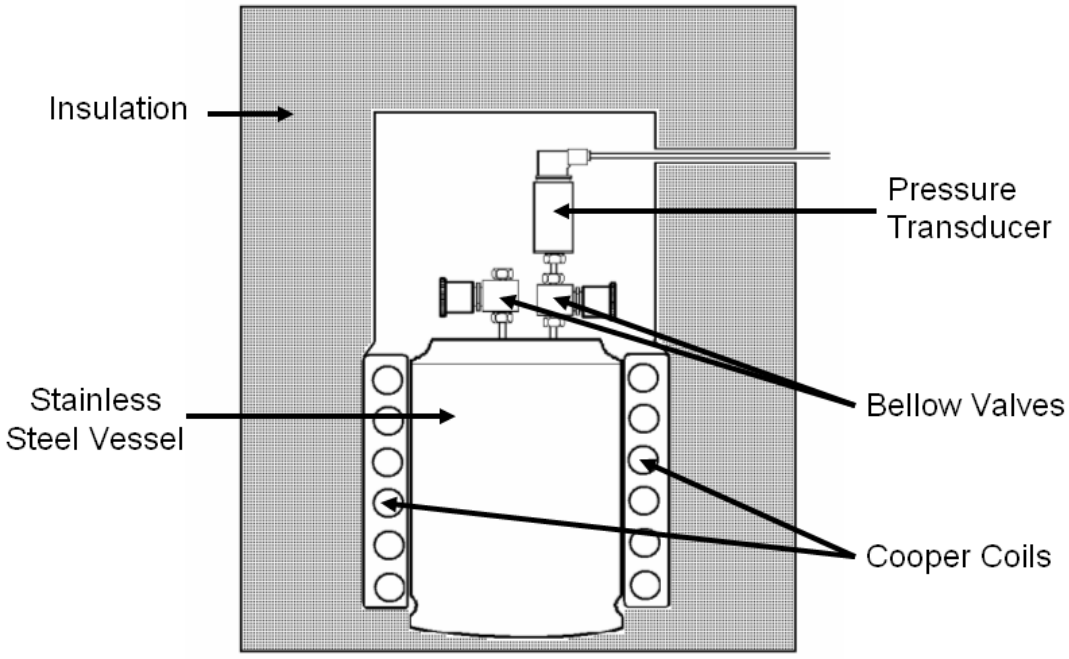

Figure 4.8: Schematic of Vessel Setup for Gas Charge Experiment

Assuming helium is an ideal gas, the solubility of helium in mercury, equation (3-1), can be written:

$$x_{He} \approx \frac{\Delta P V_{He} / RT}{\rho_{Hg} V_{Hg} / M_{Hg}}. \qquad (4\text{-}2)$$

where M_{Hg} is the atomic mass for mercury and ΔP is the change in pressure in the cover gas due to helium diffusing into the mercury.

After 10 days no pressure change was detected. The steady pressure trend as a function of time can be seen in Figure 4.9. The gaps in the plot correspond to the thermal stirring mode. With no detectable pressure change, a lower limit can be placed on the

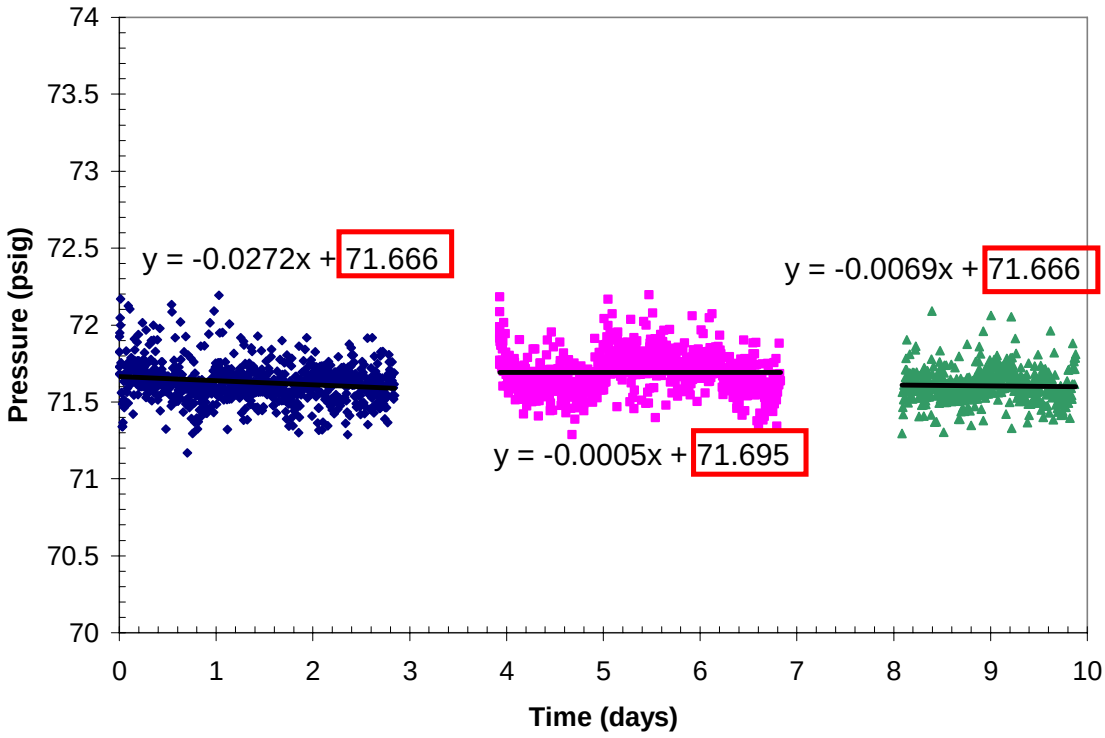

Figure 4.9: Pressure as a function of time for Gas Charge Experiment

Henry coefficient. Due to the sensitivity of the pressure sensor and the uncertainty in the regulated temperature, the smallest detectable pressure change with this system is assumed to equal 3 kPa (approx. 0.5 psi). In other words, we would expect to notice a pressure change as small as 3 kPa; however, since we did not notice this change, we can use this value as a lower limit on the Henry coefficient. This small change corresponds to a Henry coefficient which must be greater than 9.0×10^{12} Pa-molHg/molHe. Therefore, the upper limit for solubility of helium in mercury is 1.0×10^{-8} molHe/molHg at 101.3 kPa (14.7 psi) and room temperature.

The experimental Henry coefficient lower limit is below the theoretical Henry coefficient of 3.9×10^{15} Pa-molHg/molHe calculated . The theoretical Henry coefficient

corresponds to a solubility of 2.6×10^{-11} molHe/molHg at 101.3 kPa and room temperature. All theoretical values were calculated using the data from Tables 3.1 and 3.2.

While experimentally we were not able to find the exact solubility of helium in mercury, we were able to confirm that the solubility is low enough to allow stable bubble populations in the SNS. This confirmation of the theory is necessary because solubility values for various experiments range several orders of magnitude as seen in Table 3.2. This confirmed measured low solubility value for helium in mercury will be helpful to other scientific and engineering applications.

5. Oak Ridge National Lab Blow-down Experiment

An experience held by individuals at ORNL [72], where assumed audible indications of bubbling after a rapid depressurization over mercury, gave reason to duplicate a rapid depressurization with a more controlled environment. The reported low solubility seemed at variance with these observations, so there was a need to investigate the nature of this bubbling phenomenon.

The test was performed at ORNL's Target Test Facility (TTF). The TTF is a full scale, prototype of the SNS Hg flow loop initially used to test remote tooling for target change out. The TTF was also designed to duplicate flow characteristics within the SNS flow loop; therefore, it contains approximately 1,400 L of Hg [73]. A 60 L tank was placed underneath the front section of the loop. The tank was then filled to approximately ¾ full, valved-off from the rest of the loop, and charged with helium to about 4.8 bar (~70 psig). After a length of time, the valve between the tank and the loop was opened, and the pressure within the tank quickly dropped to the loop pressure. Several experiments were performed. The length of time that the mercury was pressurized ranged from 10 minutes to as long as 24 hours. Furthermore, the loop was pressurized at 1 atmosphere for a few of the experiments and vacuum for the other experiments. The setup can be seen in Figure 5.1 below.

Near the end of the tank a microphone was mounted. After every degassing, the sound signal was amplified and recorded. A noticeable churning sound was heard with every experiment. It appeared that the sound was more intense with the experiments that depressurized to vacuum compared to those that depressurized to atmospheric pressure.

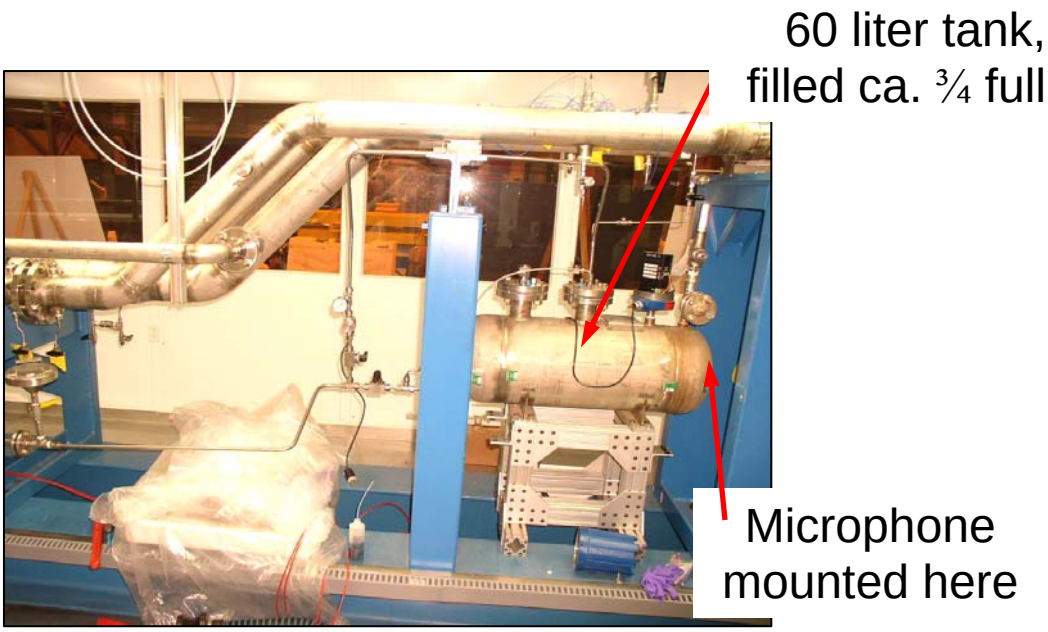

Figure 5.1: Initial 60 L tank used in ORNL Blow Down Experiment

After duplicating the audible sounds that had been attested to by earlier experience, a decision was made to duplicate the experiment with a window to obtain a visual. This decision was also made because of the inability to draw any definite conclusions from the recorded signals. The second setup can be seen in Figure 5.2. Instead of mounting a microphone, a camera was used to watch for any noticeable changes. The vessel was once again pressurized; this time to about 50 psig. The tank was depressurized after 24 hours to approximately 30 Torr. The pressure trace can be seen in Figure 5.3.

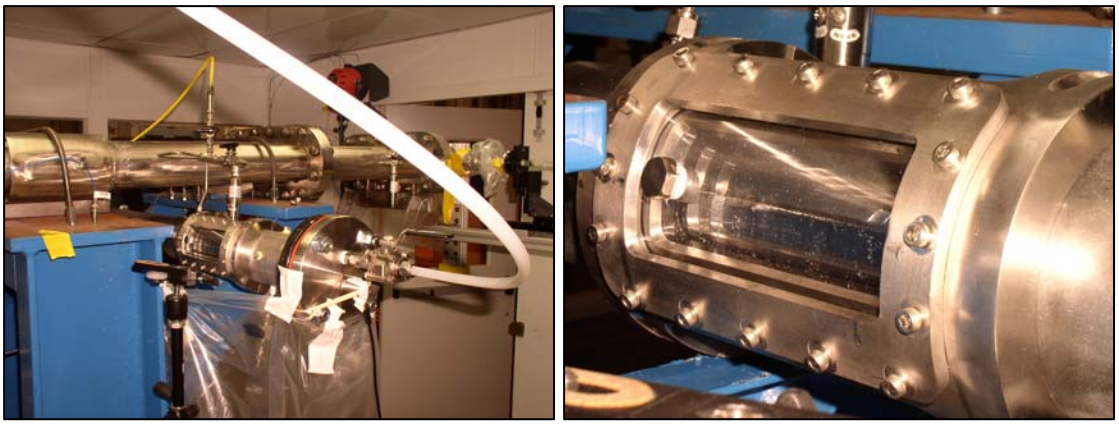

Figure 5.2: Final tank with portal used in ORNL Blow Down Experiment

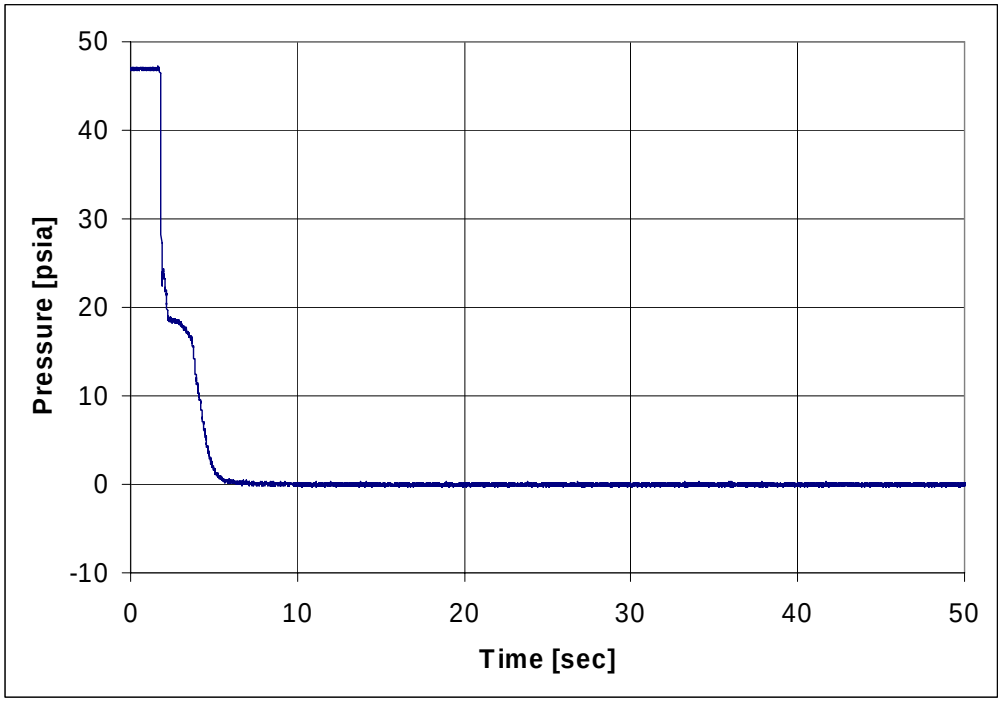

Figure 5.3: Pressure trace for final ORNL Blow Down Experiment

From the digital movie, bubbles were obviously seen. Figure 5.4 is a still shot at the beginning of the experiment. The light gray horizontal line near the very top is the mercury free surface. Figure 5.5 is a still shot 5 seconds after the start of the depressurization. From Figure 5.3 above, we see time corresponds to approximately when the system is near vacuum. However, it should be noted that the bubbles only developed on the wall. No noticeable bubbles developed within the bulk of the mercury and rose to the free surface.

If we assume that the gas trapped on the wall acts as an ideal gas, we can see that the radius of the trapped bubble is related to the pressure by

$$r \propto \sqrt[3]{\frac{1}{P}} . \tag{5-1}$$

Therefore, as the pressure, P, approaches zero, the radius approaches infinity. The pressure trace, Figure 5.3, was used to determine the bubble radius trend. Figure 5.6 shows how a unit sized bubble would grow with our pressure trace. The error of the pressure transducer used in our experiment did not allow for meaningful results after 5 seconds. However, as seen in Figure 5.6, if the localized pressure was near 30 Torr, the initially trapped gas would have grown by a factor of 4. However, if the localized pressure was near 1 Torr, the initially trapped gas would have grown by a factor of 14.

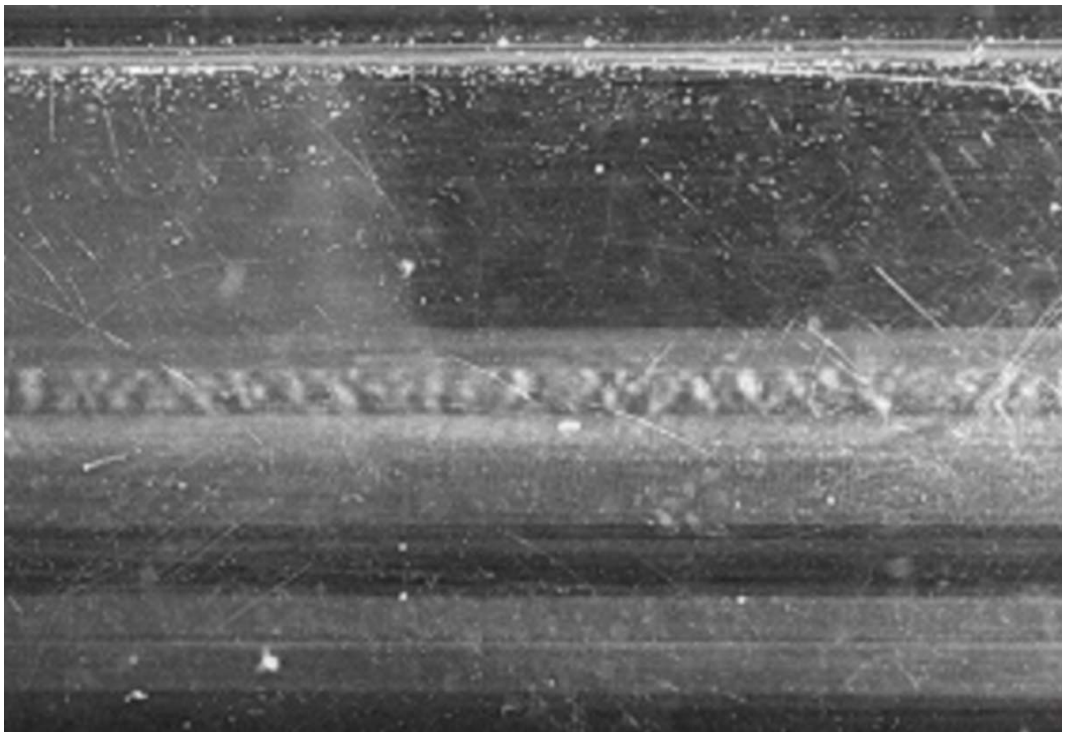

Figure 5.4: Initial mercury profile in final tank during ORNL Blow Down Experiment

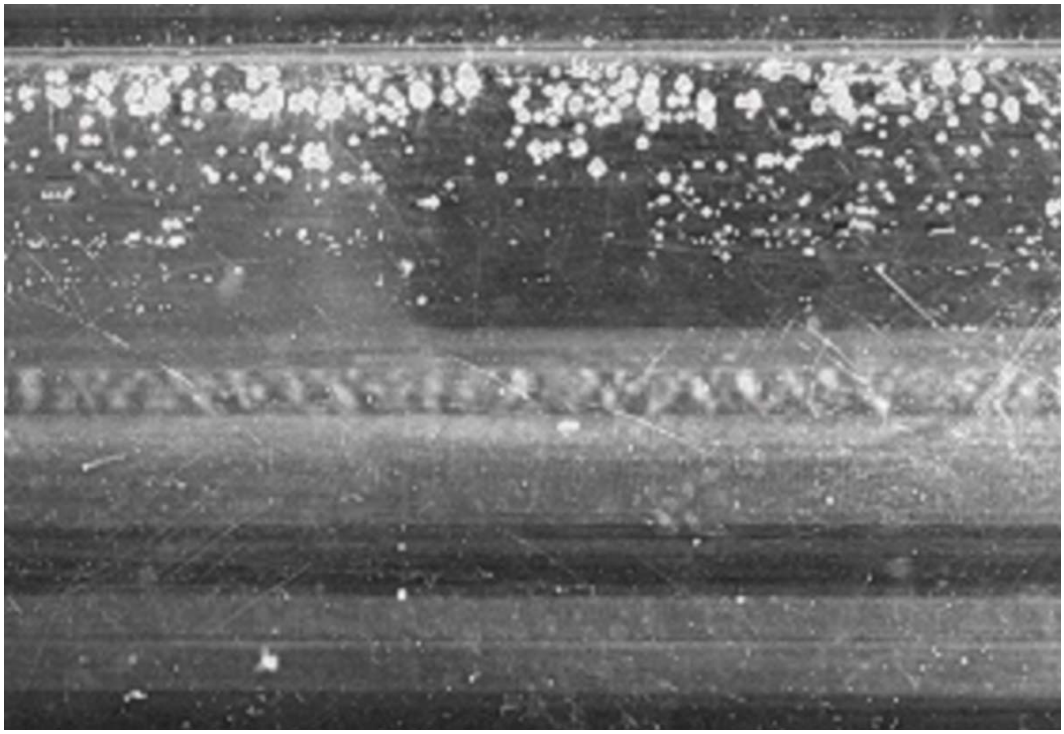

Figure 5.5: Mercury profile 5.0 sec after the release of pressure during ORNL Blow Down Experiment

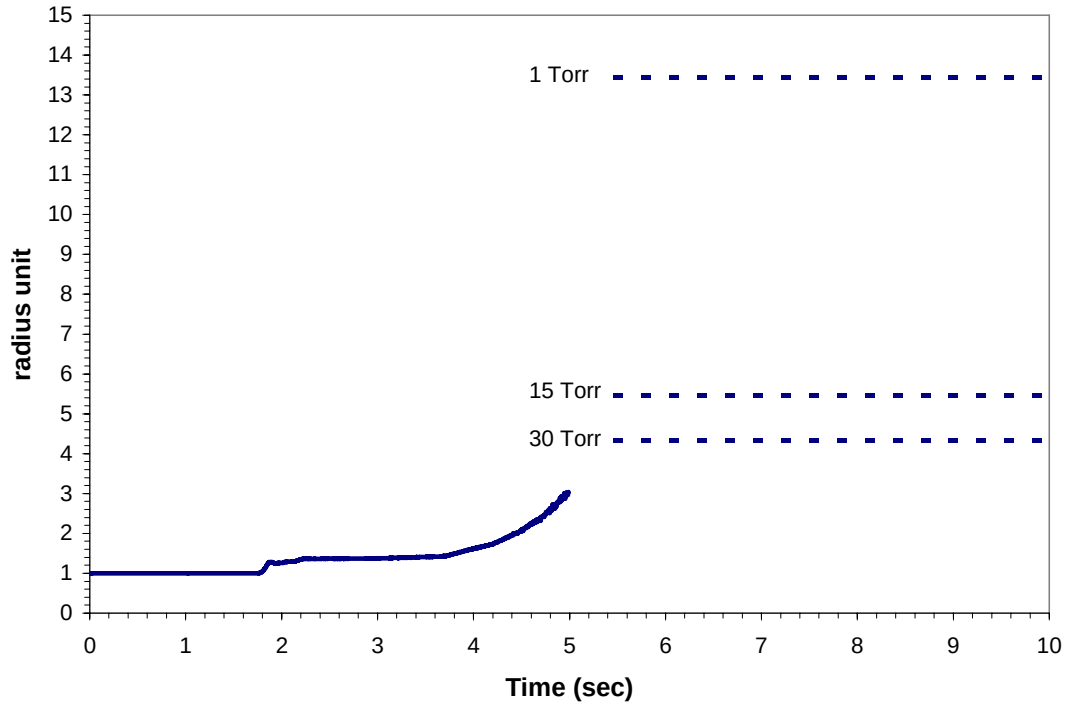

Figure 5.6: Predicted bubble growth with depressurization based on pressure trace

Not only is the bubble growing due to the pressure change, but the solubility of helium in the Lexan (polycarbonate or PC) window is very large. According to Koros et al. [74], the Henry coefficient for helium in polycarbonate is 6.99×10^{6} Pa-cm^3 polymer/cm^3 (STP) He. A typical density of polycarbonate is on the order of 1.21 g/cm^3, and a typical molar mass is 35,800 g/mol. Therefore, the Henry coefficient can be written as 5.29×10^{6} Pa-molPC/molHe. This Henry coefficient corresponds to a solubility of 7.5×10^{-4} molHe/molPC at 101.3 kPa. Hence, helium has a much stronger tendency to enter the Lexan rather than the mercury. We concluded that the bubble growth was a combination of helium trapped in scratches and growing with the depressurization as well as helium coming out of the Lexan.

6. Helium Bubble Trapped on Wall Experiment

6.1 Theory of Bubble Shrinkage

P.S. Epstein and M. S. Plesset [20] derived an approximate expression for the rate of solution by diffusion of a gas bubble in an undersaturated liquid-gas solution. They began with Fick's second law,

$$\frac{\partial C}{\partial t} = D\frac{\partial^2 C}{\partial r^2}, \tag{6-1}$$

where D is the diffusion coefficient and C is the concentration of the diffusing substance. To solve this partial differential equation an initial concentration and two boundary concentrations are required. For a spherical symmetric solution, the following conditions can be assumed

$$C(r,0) = C_\infty, r > R, \tag{6-2}$$

$$\begin{matrix} \lim_{r\to\infty} C(r,t) = C_\infty \\ C(R,t) = C_s \end{matrix}, \text{ t} > 0 \tag{6-3}$$

where C_∞ is the uniform gas concentration in the bulk of the solvent and C_s is the saturated concentration. Solving the above initial, bounded, partial differential equation, Epstein and Plesset arrived at the following solution

$$\frac{dR}{dt} = \frac{D(C_\infty - C_s)}{\rho_G + 2\sigma/3R}\left\{\frac{1}{R} + \frac{1}{\sqrt{\pi Dt}}\right\}, \tag{6-4}$$

where σ is the surface tension and ρ_G is the density of the gas. For our scenario, we can assume that C_∞ is initially zero. Also, using Henry's Law [see equation (2-6)], equation (6-4) can be written as

$$\frac{dR}{dt} = -\frac{p_s}{\rho_G + 2\sigma/3R}\left\{\frac{1}{R} + \frac{1}{\sqrt{\pi Dt}}\right\}\frac{D}{K_H}, \tag{6-5}$$

where K_H is going to have units of Pa-m^3/kg. Using this solution, Epstein and Plesset also obtained the time that an initial sized, R_o, bubble would collapse in an undersaturated solution.

$$t_{collapse} = \frac{\rho_G R_o^2}{2p_s}\frac{K_H}{D} \tag{6-6}$$

A second model was derived by Takemura and Yabe [75] starting with the following equation considering the mass flux and the change of mass inside the bubble.

$$\frac{d}{dt}\left(\frac{4}{3}\pi R^3 \rho_G\right) = 2\pi R^2 \rho_L D\int_0^{\pi}\left(\frac{dC}{dr}\right)_s \sin\theta\, d\theta = -4\pi R^2 (C_s - C_\infty)\alpha \tag{6-7}$$

where α is the mass transfer coefficient. The above relationships can be written in terms of the Sherwood number, $Sh = 2\alpha R/D$, and be represented as

$$Sh = -\frac{2R\dot{R}p_G}{D(p_G - p_\infty)}\frac{K_H}{\rho_G \Re T} \tag{6-8}$$

where $\Re$ is temporarily adopted as the gas constant so not to confuse it with the radius of the bubble, R. If the Reynolds number is small enough, the concentration gradient can be considered constant. Therefore, it can be shown that the Sh number is constant and is equal to 2. Therefore, utilizing this fact and the surface tension relationship, $p_G - p_\infty = 2\sigma/R$, equation (6-8) can be written in terms of the change in bubble radius with time [12],

$$\dot{R} = \frac{dR}{dt} = -\frac{2\sigma\rho_L \Re T}{R(p_\infty R + 2\sigma)}\frac{D}{K_H}. \tag{6-9}$$

6.2 Diffusion Coefficient for Noble Gases in Mercury

The theoretical value for helium solubility in mercury has already been established. In other words, K_H has already been derived. Since no experimental value exists for the diffusion of helium in mercury, this value must also be determined theoretically before the theories of section 6.1 can be useful.

Solute diffusion in liquid metals is not well understood. The study of diffusion in gases as well as in solid metals has seen a larger development. However, large disagreements exist in the science community on how impurities diffuse through liquids—specifically liquid metals. The three theories that are most recognized are the fluctuation theory, the "hole" model, and the hard sphere theory [76, 77]. However, the lack of very little consistent or reliable diffusion data exists in liquid metals to confirm either theory.

The theory of diffusion considers that the diffusion coefficient, D, can be written in the form of the Arrhenius equation [76],

$$D = D_o \exp(-\frac{Q}{RT}), \tag{6-10}$$

where D_o is the frequency factor, Q is the activation energy, and we have returned back to the standard R-notation for the gas constant [see section 6.1 for different notation]. The crux of the various theories is to obtain a value for the frequency factor and the activation energy.

In the fluctuation theory, any diffusion in liquid metals results from local density fluctuations that cause the formation of voids. Swalin [78] derived the following relationship for the self-diffusion coefficient,

$$D_{self} = 1.29x10^{-8} \frac{T^2}{\Delta H_v \alpha^2} \text{ (cm}^2\text{/s)}, \tag{6-11}$$

where ΔH_v is the heat of vaporization in units of kcal/mol and α is related to the curvature of the potential with units of reciprocal angstroms. According to Swalin, ΔH_v for mercury is equal to 14.7 kcal and α is equal to 2.1 $\overset{o}{A}^{-1}$. Assuming that the self-diffusion of mercury is also related to equation (6-10), from Swalin's theory, the frequency factor, D_o, is equal to $1.8x10^{-8}$ m^2/s and the activation energy, Q, is equal to 1.3 kcal/mol.

The "hole" model of diffusivity in liquid metals resembles the vacancy mechanism in solids [79]. The activation energy for a solute diffusion, Q_G, is given by

$$Q_G = Q - \frac{\alpha A V z_e e^2}{4.185x10^7 d} \exp(-qa), \tag{6-12}$$

Where Q is the activation energy for solvent self-diffusion, A is Avogadro's number, α is the screening potential factor, V is the solvent valence, z_e is the relative valence of the solute, d is the atom separation distance, e is the electron charge, and q is the screening parameter. The frequency factor for diffusion is given by

$$D_o = \gamma f J^2 \nu \exp(\Delta S / R), \tag{6-13}$$

where γ is a geometrical factor, f is the correlation coefficient, J is the atom "jump" distance, ν is the vibrational frequency, and ΔS is the entropy change associated with the thermally activated process. However, Cahoon [94] showed that using the "hole" model, the entropy change comes out negative. Yet, he argues that for a hole mechanism, the

entropy must be positive. Therefore, he concludes that the hole mechanism for liquid diffusion is implausible.

Nevertheless, Cahoon [76] at an early date had derived a modified "hole" theory for solute impurity diffusion in liquid metals. In doing so, he assumed that the solute in liquid metals diffusion coefficient is given by the form of equation (6-9) and the activation energy is given by equation (6-12) where Q is given by

$$Q = 0.17RT_m(16 + z_o), \tag{6-14}$$

where T_m is the melting point of the liquid metal and z_o is the atomic valence.

Chhabra et al. [80] studied the diffusion of oxygen and nitrogen in liquid metals. Their work is based on the "hard sphere" theory. They derived the following relationship for the diffusion coefficient for a solute impurity in a solvent:

$$D_{LG} = 0.2\frac{BRa_L^3}{a_G}\left[\frac{T}{V}\left(\frac{V - V_o}{V_o}\right)\right], \tag{6-15}$$

where a_L is the solvent diameter, a_G is the solute diameter, B is a characteristic constant of the liquid metal appearing in the Hilderand's fluidity equation [81]. The "hole" model and "hard sphere" theory are similar in principle. However, the difference between the two theories lies in the fact that the "hole" model assumes atoms to be point charges with no volume or mass. On the other hand, the "hard sphere" theory assumes atoms to be neutral hard spheres having a specified mass and volume [79]. Therefore, the "hole" model does not involve atomic diameters, and the "hard sphere" model does not include atomic valences.

In 2006 Liu et al. [79] attempted to somehow combine the concept of the work of Cahoon [80, 94] and the work of Chhabra [80]. In the end, they obtained the following relationship from the earlier theories:

$$D_{LG} = D_o \frac{a_L}{a_G} \exp[-0.17 T_m (16 + K_o)/T]. \tag{6-16}$$

Overall, with the lack of reliable experimental results, no theory can be shown to be valid. However, all the theories give values in similar magnitudes. The current experiments with self-diffusion in mercury give a frequency factor on the order of 1.0×10^{-8} to 1.8×10^{-8} m^2/s [82, 83, 95]. Therefore, if one uses equation (6-16) and a frequency factor of 1.5×10^{-5} m^2/s, we obtain a diffusion coefficient of helium in mercury as 5×10^{-9} m^2/s.

We should not forget the infamous Stokes-Einstein [52] equation for the diffusion coefficient. Their equation took the form:

$$D_{LG} = \frac{k_B T}{6\pi \eta_L r_G}, \tag{6-17}$$

where where η_L is the viscosity of the liquid metal. Using this expression, one obtains a value of 7×10^{-9} m^2/s, which is very similar with the value obtained above. Interestingly, while the Henry coefficient of various systems ranges several orders of magnitude, the solute impurity diffusion coefficient is very similar in magnitude from system to system. The experimental helium diffusion coefficient in water was found to be 9.2×10^{-9} m^2/s [84].

In reality, the diffusion of a solute atom into and through a solvent is not just related to molecular diffusion. All the models given above are molecular diffusion

theories. The effective diffusion coefficient is a combination of numerous effects, like diffusion based on molecular diffusion, convective or buoyancy diffusion, and diffusion by the Soret effect [77]. The effective diffusion coefficient is just the sum of the diffusion coefficient for each effect. This fact has been a large contributor in the lack of repeatable diffusion experiments. Therefore, to eliminate convective diffusion, low gravity experiments have been derived.

6.3 Applying the Bubble Shrinkage Theory

Using a theoretical diffusion coefficient of $5x10^{-9}$ m^2/s and the theoretical Henry coefficient derived in section 3 of $1.44x10^{13}$ $Pa\text{-}m^3/kg$ [note the unit change], one can calculate the radius as a function of time for a collapsing bubble. The results of using the Epstein [20] and Takemura [75] models with a cover pressure of 300 kPa and a temperature of 300 K can be seen in Figure 6.1. The initial bubble radius was chosen to be 30 microns. The theories give slightly different collapse times. The Epstein and Plesset model predicts a lifetime around 215 hours (~9 days); while the Takemura et al. model predicts a lifetime around 77 hours (~3 days). The different value is quite large. However, in terms of engineering a bubble injection method at the SNS, 3 days and 9 days can both be considered infinitely long.

Alluded to before, the diffusion process is not just driven by molecular diffusion. For comparison, we can make a comparison plot where we assume the effective diffusion coefficient is as high as $5x10^{-7}$ m^2/s. This value was selected just because it is two decades greater than the molecular diffusion coefficient. Figure 6.2 shows a comparison

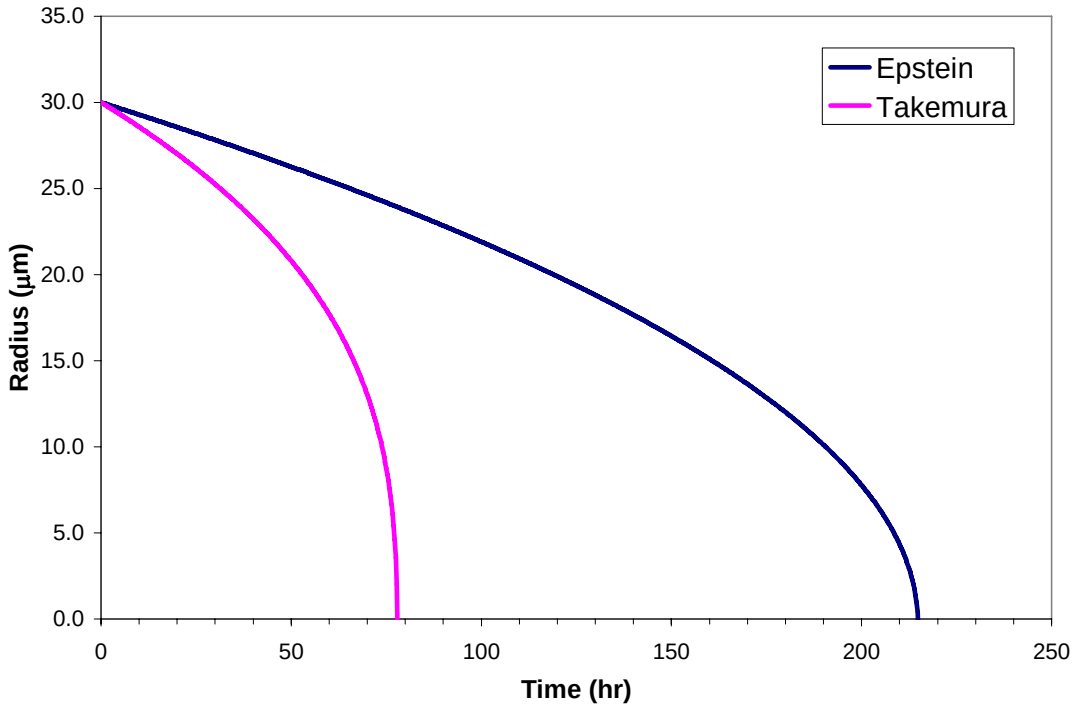

Figure 6.1: Theoretical Helium Bubble Shrinkage based on the models of Epstein and Takemura using D = $5x10^{-9}$ m^2/s

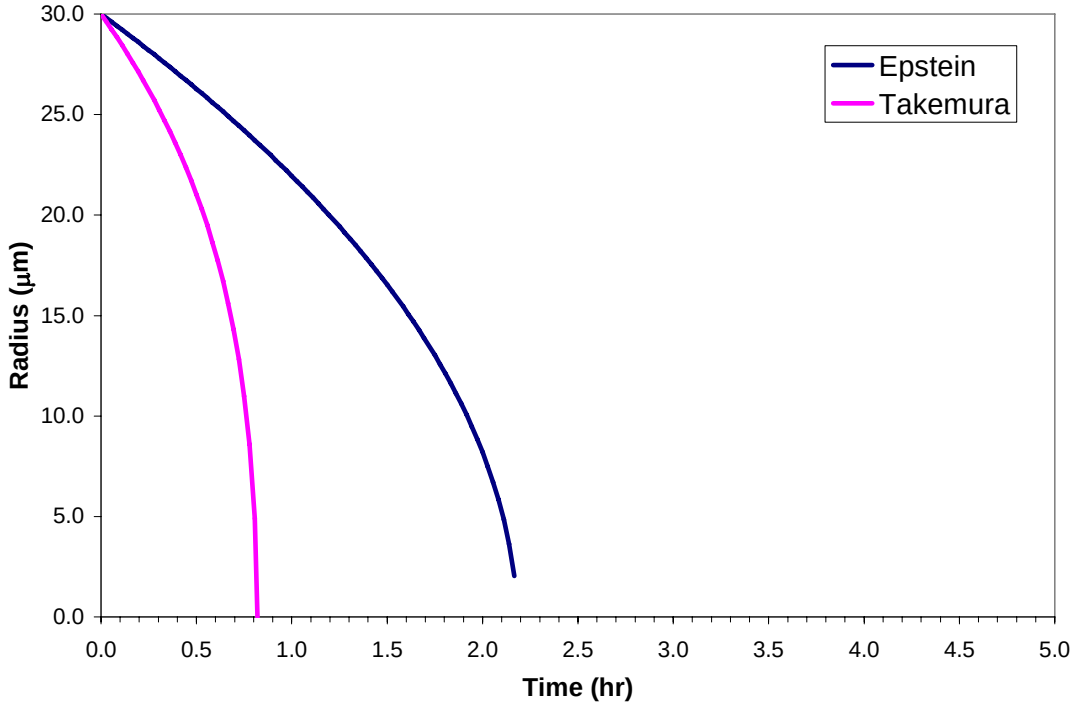

Figure 6.2: Theoretical Helium Bubble Shrinkage based on the models of Epstein and Takemura using D = $5x10^{-7}$ m^2/s

of the models with this arbitrary diffusion coefficient. While the bubble lifetime is much less, we are still talking about a bubble lifetime of hours.

6.4 Experimental Setup and Results

Experiments at the JSNS under the direction of Hasegawa attempted to find the ratio D/K_H by capturing small helium bubbles on the surface of a transparent lid [85]. They watched individual bubbles shrink and fit an altered Takemura's model [75] to their results. Because the bubble on the surface is not spherical, the altered model is given by

$$\dot{R} = \frac{dR}{dt} = -\frac{\sigma(1+\cos\theta)\rho_L \Re T}{R(p_\infty R + \sigma(1+\cos\theta))}\frac{D}{K_H}, \tag{6-18}$$

where θ is the contact angle between the bubble surface and the horizontal wall and is a correction to the surface tension. Currently, they claim their results are preliminary. As of January 2008, Hasegawa reported an experimental D/K_H ratio of $7.0\text{x}10^{-20}$ $m^2\text{-}s^{-1}/Pa\text{-}m^3\text{-}kg^{-1}$ [85]. Unfortunately, using our theoretical diffusion coefficient of $5\text{x}10^{-9}$ m^2/s and our theoretical Henry coefficient of $1.44\text{x}10^{13}$ $Pa\text{-}m^3/kg$, we obtain a theoretical D/K_H ratio of $3.5\text{x}10^{-22}$ $m^2\text{-}s^{-1}/Pa\text{-}m^3\text{-}kg^{-1}$. However, as mentioned before, the diffusion process is not just driven by molecular diffusion. Therefore, if we use the arbitrary $5\text{x}10^{-7}$ m^2/s, we obtain a D/K_H ratio of $3.5\text{x}10^{-20}$ $m^2\text{-}s^{-1}/Pa\text{-}m^3\text{-}kg^{-1}$.

We decided to perform our own bubble capture experiment. A 490 mL vessel was constructed out of Lexan. A special lid with an intruded bottom allowed for a horizontal surface to be submerged 2-cm into the mercury. At the bottom of the vessel was a needle injector tip where gas could be supplied. Helium was initially blown through the lines. After a few seconds, the line was closed off. Using a mallet, we

lightly tapped the side of the vessel which caused small gas bubbles to detach from the injector tip. The bubbles rose and were trapped on the lid. We zoomed in on one of the bubbles using a lab microscope and recorded the radius as a function of time. The setup can be seen in Figure 6.3.

Before using mercury, we performed the experiment in water. Figure 6.4 shows a sample of pictures that reveal the helium bubble shrinking in the liquid water. The results are plotted and show in Figure 6.5. The solid line is a best fit curve using the altered Takemura model [75] with a contact angel of 90°. Using the experimental, molecular diffusion coefficient of helium in water, 9.2×10^{-9} m^2/s, and the experimental Henry coefficient of helium in water, 6.5×10^{7} $Pa\text{-}m^3/kg$, we obtain a D/K_H ratio of 1.5×10^{-16} $m^2\text{-}s^{-1}/Pa\text{-}m^3\text{-}kg^{-1}$. This value corresponds very well with our experimental ratio of 1.4×10^{-16} $m^2\text{-}s^{-1}/Pa\text{-}m^3\text{-}kg^{-1}$ from our best fit curve.

An experiment with mercury and helium was also performed in a similar fashion. However, a new lid was constructed for this experiment. Unfortunately, as can be seen in comparing Figure 6.4 with Figure 6.6, the new lid obtained a lot of scratches in production. Also, a different trend was observed with the bubble radius as a function of time. As seen in Figure 6.7, the radius dropped quickly and leveled off to a constant value. The first few data points were fit with the altered Takemura model and a speculative contact angle of 45°. However, the experimental D/K_H ratio of 4.9×10^{-18} $m^2\text{-}s^{-1}/Pa\text{-}m^3\text{-}kg^{-1}$ obtained from the best fit curve is too large. Furthermore, the leveling off of the radius would not make sense with a D/K_H ratio so high. One large source of error might be that the momentum of the injected bubble caused the initial measurement to give a larger radius because it has *pancaked* on the top surface. The quick decrease in

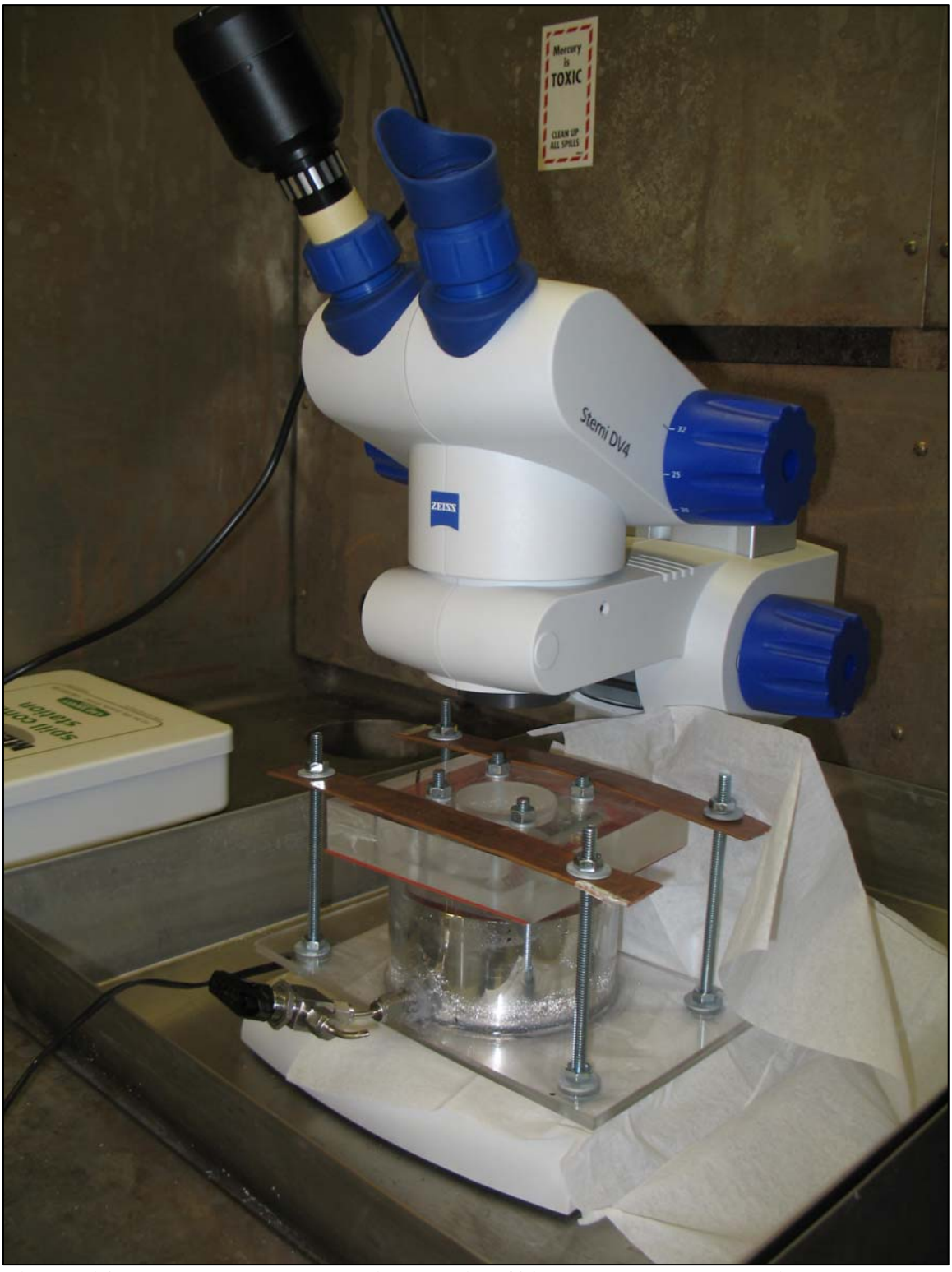

Figure 6.3: Bubble capture experiment with 490 mL vessel and lab microscope

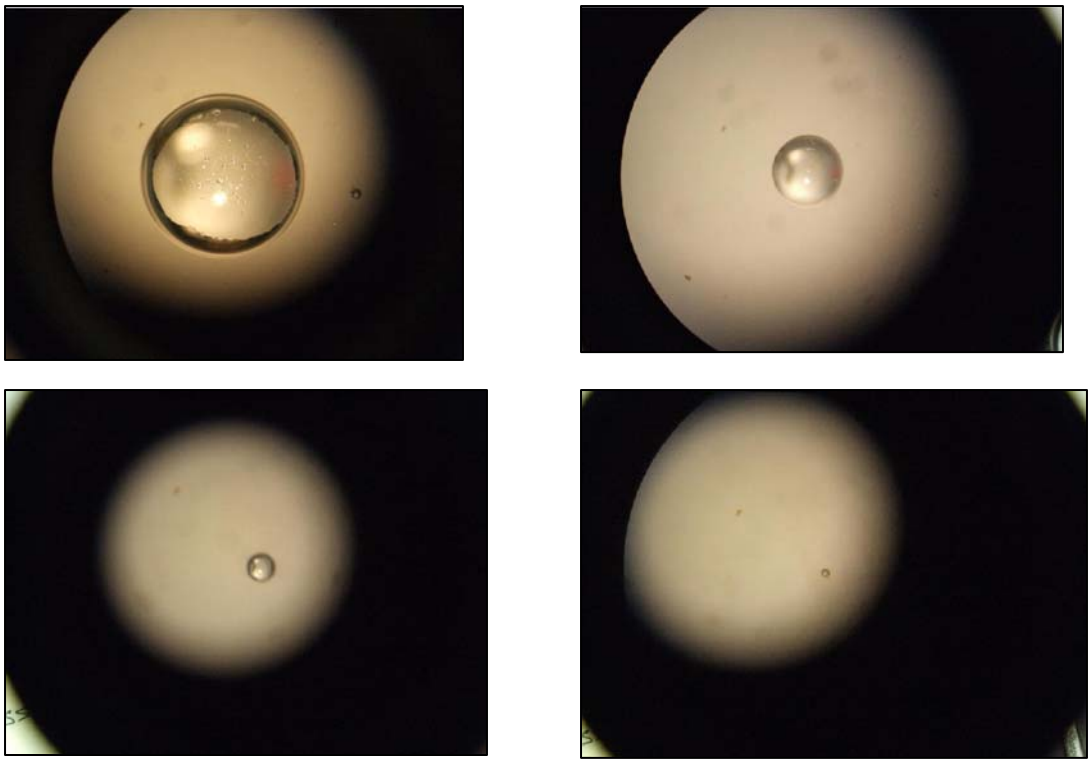

Figure 6.4: Helium Bubble pictures trapped on surface in Water

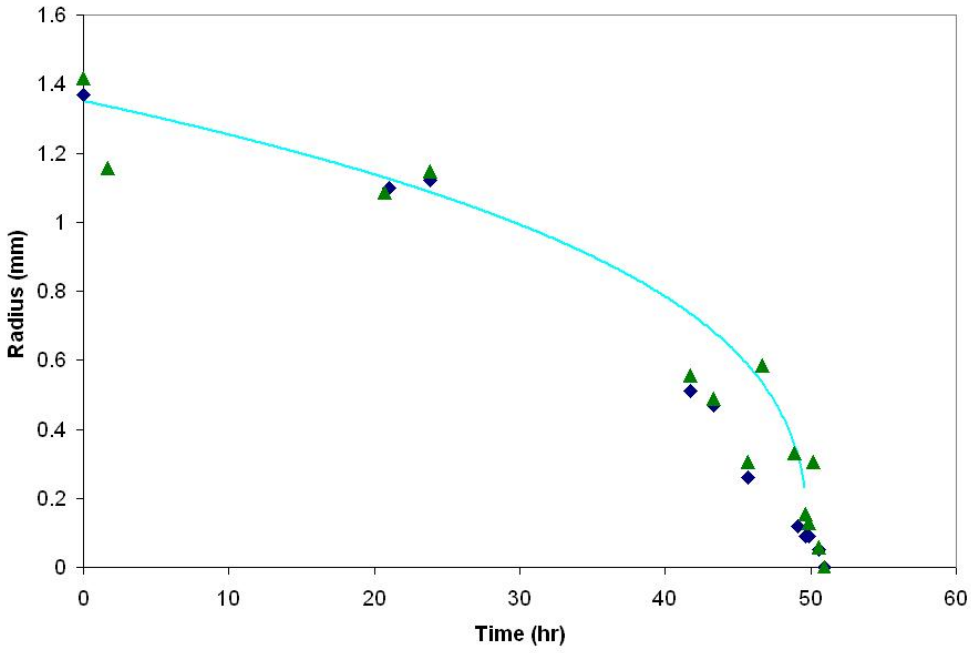

Figure 6.5: Helium Bubble in Water radius as a function of time in Bubble Trap Experiment

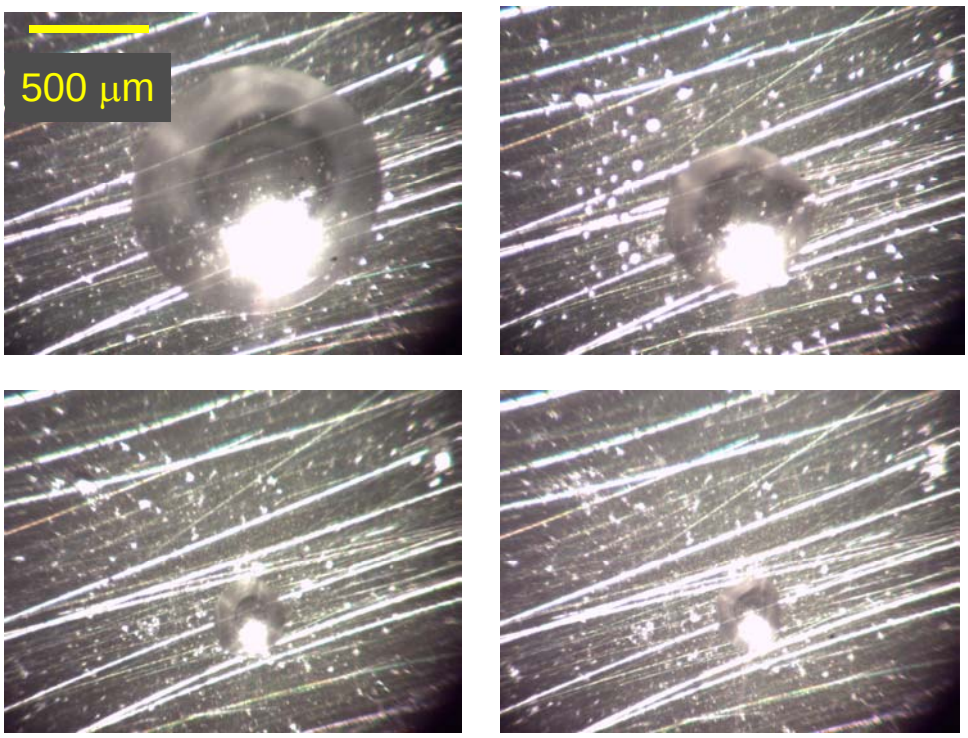

Figure 6.6: Helium Bubble pictures trapped on surface in Mercury

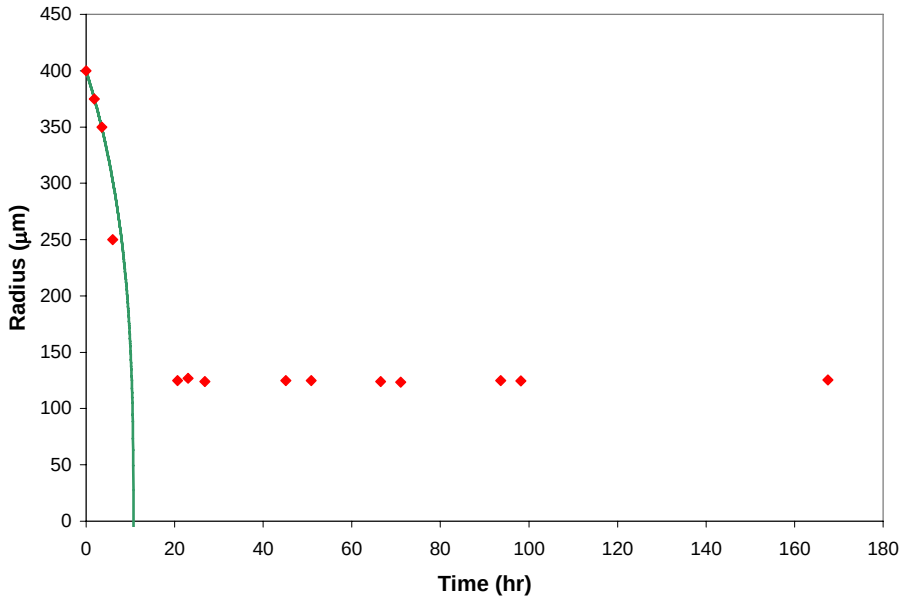

Figure 6.7: Helium Bubble in Water radius as a function of time in Bubble Trap Experiment

visual radius could be due to the bubble taking shape and developing a contact angle based on the surface tension of the mercury. A second source of error might be that helium escaped from the bubble into the surface scratches. The high helium solubility in Lexan as mentioned in section 5 could be a third source of error, as well. Nevertheless, note that in Figure 6.6 that the small bubble population around the large bubble changes very little. This trend is consistent with some of the findings of Hasegawa [85] where he noted that some small bubbles would disappear while others would not.

Even though no quantitative results can be extracted from the bubble shrinkage model, the fact that the bubble did not completely disappear in mercury does confirm that the solubility of helium in mercury is very small. For example, a back of the envelope calculation shows that for our vessel volume, 490 mL, and the experimental solubility of helium in water, 7.2×10^{-6} molHe/molH_2O at 101.3 kPa, we would expect a helium bubble trapped on the surface with at most a radius of 12 millimeters to disappear. Our initial bubble had a radius of about 1.4 mm and disappeared. However, with our vessel volume and the theoretical solubility of helium in mercury, 2.6×10^{-11} molHe/molHg at 101.3 kPa, we would expect that the bubble radius of 0.4 millimeters (400 microns) would change very little—on the order of 10 microns. Furthermore, with our volume of mercury, the smallest bubble that would disappear assuming the theoretical solubility value was correct would have a radius around 0.180 millimeters (180 microns). Nevertheless, from the trends of Figure 6.1 and Figure 6.2, we would expect the bubble lifetime to be very large.

In section 4.3 we arrived at an upper limit on solubility—1.0×10^{-8} molHe/molHg at 101.3 kPa. However, with this solubility, we would have expected the bubble to keep

shrinking and eventually disappear with our setup. But since it appeared to level off, we can expect that the solubility is much less than this upper limit we have established. This outcome strengthens the conclusion that the theoretical solubility of helium in mercury may be valid.

7. Bubble Rise in Mercury

Now that it has been shown that noble gas bubbles in mercury will not disappear in any considerable amount of time, one may be interested in how the bubbles will perform in the mercury. One issue that might be of importance and needed to be addressed is the terminal rise velocity of a bubble in stagnant mercury. The inability to visually see bubbles in the bulk of mercury has hindered the number of rise velocity experiments in mercury. However, an *archeological* literature survey dug up a few experiments with corresponding theory.

In 1967 Davenport et al. [86] injected spherical cap nitrogen bubbles into mercury. A cup attached to a shaft was placed near the bottom of a 60 cm high, 7.6 cm inner diameter cylinder. Nitrogen gas was injected below the cup. Once the cup had collected a set amount of gas, the operator would manually rotate the shaft, and the gas bubble would exit the cup and rise to the top. Davenport was able to generate bubbles with equivalent radii ranging from 0.4 cm to 2.4 cm. The bubble shape was measured using electrical probes. Once a bubble passed by a probe, the circuit was broken and the corresponding lamp was extinguished. Terminal rise velocities for the various bubbles sizes were also calculated using a stop watch method. The stop watch was started when the cup was turned to a 45° angle and was stopped when a disturbance was recognized on the mercury surface. Davenport compared his results to theory by Davies and Taylor [87]. Davies and Taylor derived the following equation for potential flow, around a sphere in the region close to the forward stagnation point combined with Bernoulli's equation:

$$U_{\infty} = 1.02\sqrt{gr_e}\ , \tag{7-1}$$

where U_∞ is the terminal rise velocity for a bubble with an equivalent radius, r_e. Davenport [86] credits the difference in the theory of Davies and Taylor to his experimental results because of the constricting effects of the wall of the cylinder. Further error might be accredited to the possible inaccuracies in the measuring method.

In 1968 Schwerdtfeger [88] injected argon bubbles into mercury using a glass injector tip at the bottom of a 50 cm high column. The measurements were taken using an ultrasonic pulse-echo instrument. Furthermore, Schwerdtfeger placed a 10 cm thick layer of distilled water above the mercury for observation of the bubbles after emersion from the mercury. Schwerdtfeger was able to generate bubbles with equivalent radii ranging from 0.1 cm to 0.75 cm. He compared his experimental results to a model for air bubbles in water by Haberman and Morton [89].

In 1977 Mori et al. [90] injected nitrogen bubbles into mercury using a similar approach as Schwerdtfeger [88]. The bubbles were detected using an ingenious electrical triple probe. The radius as well as the shape could be measured due to the staggered nature of each probe. They were able to generate bubbles ranging from 0.05 cm to 0.3 cm (0.5 mm to 3 mm). For the smaller bubbles they compared their experimental results to the theory of Sawi [91] and to the theory of Moore [92]. Both theorists generated mathematical functions $G_1(\chi)$ and $G_2(\chi)$, where χ is the aspect ratio for the bubble. These gentlemen reported the following relationships for the drag coefficient, C_D, and the Weber number, We:

$$\begin{aligned} C_D &= \frac{48}{\mathrm{Re}} G_1(\chi), \\ We &= G_2(\chi) \end{aligned} \tag{7-2}$$

where Re is the Reynolds number. For the larger bubbles, Mori [90] compared his results to the theory of Mendelson [93]:

$$U_\infty = \sqrt{\frac{\sigma}{r_e \rho_\infty} + g r_e} \tag{7-3}$$

Interestingly, Mendelson is given credit for this relationship. However, it is the same relationship given by Haberman and Morton for air bubbles in water [89].

All the above experimental results and theoretical trends are plotted in Figure 7.1. The decrease in velocity (as seen in the theory of Sawi) is due to a symmetric deformation of the bubble, i.e., χ differs substantially from unity. A spiral motion is induced by the asymmetric flow. However, the spiral motion begins to lessen with larger bubbles with a further deformation of the bubble. Finally, the bubble develops a spherical cap shape and the drag coefficient becomes nearly constant. Therefore, the terminal velocity increases is proportional to the square root of r_e.

The micro-bubbles desired for the SNS fall below the experimental results shown here. However, an ongoing challenge for the SNS is the ability to inject small bubbles into the mercury. The inability to wet mercury causes the injected gas bubble to grow down the injector tip. Further work is currently going on at the University of Tennessee as well as ORNL to tackle this issue.

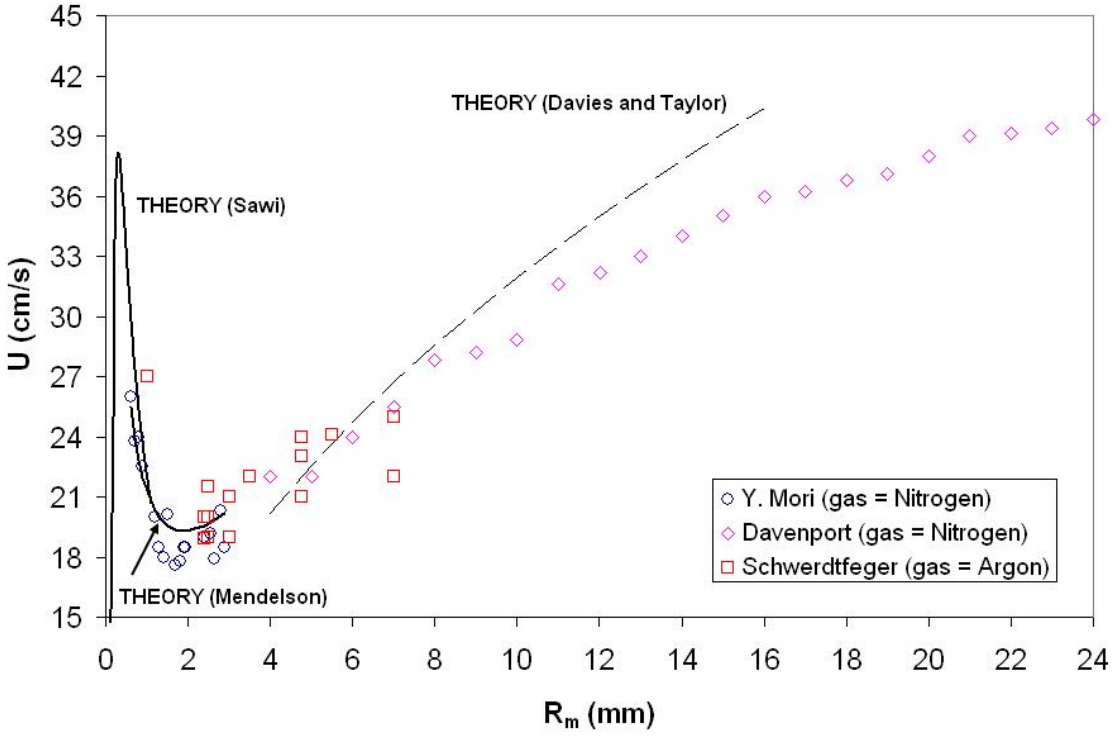

Figure 7.1: Terminal bubble velocity versus equivalent bubble radius

8. Summary of Conclusions and Suggestions for Future Work

The gas charge experiment established a lower limit on the Henry coefficient for helium in mercury as $9x10^{12}$ Pa-molHg/molHe. This value corresponds to an upper limit on solubility at $1.1x10^{-8}$ molHe/molHg at 101.3 kPa. These values help validate the theoretically predicted Henry coefficient of $3.9x10^{15}$ Pa-molHg/molHe based on Thormeier's model. Furthermore, the helium bubble trap experiment also helped validate the predicted solubility due to the fact that the bubble did not complete disappear as would be expected if the helium dissolved into the mercury.

The results are in agreement with past solubility experiments performed in various liquid metals. While it has been shown that the experimental values as well as the theoretical predictions in liquid metals vary several orders of magnitude, all the results confirm low solubility of inert gases in liquid metals.

The work shown here confirms that the micro-bubble population should be stable within the Spallation Neutron Source mercury flow loop. It is not expected for the bubbles to disappear in any considerable amount of time due to the inert gas going into solution. Therefore, one big step has been accomplished in assisting the current SNS as well as future spallation sources in mitigating cavitation damage.

Due to the low solubility of helium in mercury, in the future, a strategy will need to be implemented that removes the injected helium gas. Current preliminary work is being done at the University of Tennessee that utilizes a hydrocyclone setup to separate the gas from the liquid mercury.

The solubility limit obtained in this dissertation is adequate to support high power target gas injection design work. A solubility value with modest uncertainty is desired. Theories considered herein are based on static or semi-static mechanistic models. A return to the theoretical solubility models in dynamic fluids is needed. Overall, the physical knowledge in fluids at the microscopic level is limited. Progress in understanding the solubility physics in liquid metals was shown in this dissertation; however, a greater understanding of the basic physics in liquids is still needed.

References

List of References

[1.] Bauer, Günter S. "Target Design and Technology for Research Spallation Neutron Sources." Technology and Applications of Accelerator Driven Systems (ADS). October 17-28 2005. Miramare, Trieste, Italy.

[2.] Yaws, C.L., ed. *Chemical Properties Handbook.* McGraw-Hill: 1999.

[3.] *ORNL Neutron Sciences*. http://neutrons.ornl.gov/aboutsns/aboutsns.shtml

[4.] J-PARC: Materials and Life Science Facility. http://j-parc.jp/MatLife/en/index.html

[5.] European Spallation Source Initiative. http://essi.neutron-eu.net/essi

[6.] Futakawa, M. et al., *Inter. J. Impact Eng*., 2003, Vol. 28, no. 2, p 123.

[7.] Soyama, H. et al., *Tribol. Lett*., 2006, Vol. 23, no. 1, p 23.

[8.] Haines, J., "Status of the SNS Target Systems." 2nd International High-Power Targetry Workshop. October 10, 2005.

[9.] Riemer, B., "Benchmarking Dynamic Strain Predictions of Pulsed Mercury Spallation Target Vessels." High-power Targetry for Future Accelerators Worskshop. September 8-12, 2003.

[10.] Riemer, B., "Brief Review of the Cavitation Issue; Key areas for workshop discussion." Mitigation of Cavitation Damage in Liquid Metal Spallation Targets Workshop. January 24, 2008.

[11.] Riemer, B., "Small Gas Bubble Experiments with a Mercury Test Loop in Proton Beam." Mitigation of Cavitation Damage in Liquid Metal Spallation Targets Workshop. January 24, 2008.

[12.] Futakawa, M.; Naoe, T.; Kogawa, H; Hasegawa, S.; Fujiwara, A.; Okita, K.; Matsumoto, Y.; Tanaka, T. "Bubbling Mitigation Technology R&D activity in JSNS." Mitigation of Cavitation Damage in Liquid Metal Spallation Targets Workshop. January 24, 2008.

[13.] Wendel, M.W., *June 2005 Gas Bubble/Mercury In-beam Tests at WNR*. 2nd International High-Power Targetry Worshop. October 13, 2005.

[14.] Riemer, B., *Proton radiography experiment to visualize gas bubbles in mercury*. The Eighteenth Meeting of the International Collaboration on Advanced Neutron Sources. April 2007.

[15.] Wendel, M.W. "Progress in Creating Stabilized Gas Layers in Flowing Liquid Mercury." Mitigation of Cavitation Damage in Liquid Metal Spallation Targets Workshop. January 25, 2008.

[16.] Manzi, N.J.; Geary, S.; Squires, A.; Chitnis, P.V.; Cleveland, R.O.; Holt, R.G.; Roy, R.A., "Fighting bubbles with bubbles: A sparse, foam-anchored bubble layer for wall damage mitigation." Mitigation of Cavitation Damage in Liquid Metal Spallation Targets Workshop. January 26, 2008.

[17.] Berry, R.S.; Rice, S.A.; Ross, J., Physical Chemistry. 2nd Edition. Oxford University Press: New York. 2000.

[18.] Fowler, R.H. and Guggenheim, E.A., *Statistical Thermodynamics*, Cambridge: Cambridge Univ. Press, 1939.

[19.] Lu, Bo. *Theoretical Study of Noble Gas Bubble Behavior in Mercury.* Masters thesis, The University of Tennessee, TN, (May 2006)

[20.] Epstein, P. and Plesset, M, *On the Stability of Gas Bubbles in Liquid-Gas Solutions,* Journal of Chemical Physics, 1950, Vol.18, No.11, p.1505.

[21.] Thormeier, K., Die *Loslichkeit von Edelgasen im Reaktorkuhmittel Natrium and sich daraus ergebende Sicherheitsaspekte*, Report KFK 1166, Karlsruhe: Kernforschungszentrum Karlsruhe, 1970. [Translated into English]

[22.] Thormeier, K., *Solubility of the Noble Gases in Liquid Sodium.* Nuclear Engineering Design, 1970, Vol. 14, No. 1, p 69.

[23.] Barrer, R.M. *Diffusion in and through solids*. Cambridge 1951, pg. 146.

[24.] Bonilla, C.F. Proceedings of the First International Conference on the Peaceful Uses of Atomic Energy, Geneva, 1955. P/122 Vol. 9, p. 331. United Nations, New York

[25.] Mitra, C.R. and Boniall, C.F. Solubility and Stripping of Rare Gases in Molten Metals, BNL-3337 (March 1956)

[26.] (a.) Raseman, C.J.; Susskind, H.; and Waide, C.H. Liquid Metal Fuel Reactor In-Pile Fuel Processing Loop (Loop B): Construction, Operation, Experimental Results BNL-403 (Jan. 1957), p. 14-1
(b.) … Chemical Engineering Progress, 1957, Vol. 53, p. 86.

[27.] Watson, G.M. (1958) referenced in [33].

[28.] Mitra, C.R., Solubility of Xenon in Liquid Metals, Ph.D. thesis, Columbia University, N.Y., (1958)

[29.] Eshaya, A.M.; Hoffmann, F., Removal of Volatile Fission Products, BNL-4097 (Dec. 1958), p. 27-31.

[30.] Eshaya, A.M.; Hoffmann, F., Fission Product Volative Removal, BNL-4355 (Feb. 1959), p. 29-32.

[31.] Eshaya, A.M.; Kenney, W.F., Solubility of Xenon in Liquid Bismuth, BNL-617 (Jan. 1959)

[32.] Eshaya, A.M.; Wiewall, R.H., The Chemistry of Fission Products in a Molten Metal Nuclear Fuel, Transactions of the New York Academy of Sciences, 1959, Vol. 21, p. 668.

[33.] Hewitt, G.F.; Lacey, J.A.; Lyall, E., The Determination of Xenon in Liquid Bismuth, Journal of Nuclear Energy, Pt. B: Reactor Technology, 1960, Vol 1, No. 3, p. 167.

[34.] Johnson, G.W.; Shuttleworth, R., The Solubility of Krypton in Liquid Lead, Tin and Silver. The Philosophy Magazine, 1959, Vol. 4, No. 44, p. 957.

[35.] Johnson, G.W.; Shuttleworth, R., The Solubility of Krypton in Liquid Cadmium and Indium, The Philosophy Magazine, 1961, Vol. 6, No. 67, p. 943.

[36.] Slotnick, H.; Kapelner, S.M.; Cleary, R.E., The Solubility of Helium in Lithium and Potassium, PWAC-380 (Feb. 1965)

[37.] Dhar, S.K., Solubility of Argon in Liquid Sodium, ANL-6800 (1963), p. 183-187

[38.] Dhar, S.K., Solubility of Krypton in Liquid Sodium, ANL-6900 (1964), p. 125-127.

[39.] Dhar, S.K., Solubility of Argon in Liquid Sodium, ANL-7350 (1967), p. 59-60.

[40.] Veleckis, E.; Dhar, S.K.; Cafassor, F.A.; Feder, H.M., Solubility of Helium and Argon in Liquid Sodium, The Journal of Physical Chemistry, 1971, Vol. 75, No. 18, p. 2832

[41.] Foust, O.J., 1972 Sodium—Nak Engineering Handbook vol. 1 New York: Gordon and Breach)

[42.] Reed, E.L.; Droher, J.J., Solubility and Diffusivity of Inert Gases in Liquid Sodium, Potassium, and NaK LMEC-69-36. (Jan. 1970)

[43.] Debu, Majumdar. "Advanced Reactors Around the World." Nuclear Plant Journal, 2003, Vol. 21, Issue 5, p. 51.

[44.] Reiss, H.; Frisch, H.L.; Lebowitz, J.L., "Aspects of the Statistical Thermodynamics of Read Fluids." The Journal of Chemical Physics, 1960, Vol. 32, No. 1, p 119.

[45.] Reiss, H.; Frisch, H.L.; Helfand, E.; Lebowitz, J.L., "Statistical Mechanics of Rigid Spheres." The Journal of Chemical Physics, 1959, Vol. 31, No.2, p 369.

[46.] Pierotti, R.A., "The Solubility of Gases in Liquids." The Journal of Chemical Physics., 1963, Vol. 67, No. 1, p 1840.

[47.] Young, D.M and Crowell, A.D., *Physical absorption of gases*. London: 1962.

[48.] Lösch, F., Tabellen zur Berechnung thermodynamischer Funktionen beim Vorliegen innermolekularer Schwingungen, eds. H. Landolt and R. Börnstein, Zahlenwerte und Funktionen aus Physik, Chemie, Astronomie, Geophysik und Technik, Vol. II, Part 4. Bernlin, Götteingen, Heidelberg: 1961. p 736.

[49.] Shpil'rain, E.E.; Skovorod'ko, S.N.; Mozgovoi, A.G., "The Solubility of Inert Gases in Liquid-Metal Heat-Transfer Agents." High Temperature, 2000, Vol. 38, No. 3, p 384.

[50.] Dawber, P.G. and Elliott, R.J., "The Vibration of an Atom of Different Mass in a Cubic Crystal." Proceeding of the Royal Society of London A, 1963, Vol. 273, No. 1352, p. 222.

[51.] Neff, R.O.; McQuarrie, D.A., 1973 Journal of Physical Chemistry. 1973, Vol. 77, p. 413.

[52.] Hirschfelder, J.O; Curtiss, C.F.; Bird, R.B., *Molecular theory of gases and liquids*. New York: 1965.

[53.] Lide, D.R., ed. *CRC Handbook of Chemistry and Physics. 87th Edition*, 2006-2007.

[54.] Goldschmidt, V.M., *Geochemistry*. Oxford: 1954.

[55.] Smithells, C.J., *Metals: Reference Book:* Edition 4. London: 1967.

[56.] Perry, R.H. and Green, D.W., eds. *Perry's Chemical Engineers' Handbook (7th Edition)*. McGraw-Hill: 1997.

[57.] Hildebrand, J.H., Journal of Physical Chemistry, 1954, Vol. 58, p. 671

[58.] Epstein, L.F. The Solubility of Helium Gas in Liquid Sodium, KAPL-M-LFE-10 (Jan. 1952)

[59.] Mandel, H. (March 1966) referenced in [21]

[60.] Uhlig, H.H., Journal of Physical Chemistry 1937, Vol. 41, p. 1215.

[61.] McMillan, W.G., Estimates of the Solubility and Diffusion Constant of Xenon in Liquid Bismuth, BNL-3337 (March 1955)

[62.] Kubaschewski, O., (1958) referenced in [33]

[63.] Fukase, S.; Satoh, T., Solubilities of rare gases in liquid sodium and Faber's formula for vacancy formation energies. Journal of Physics F: Metal Phys., 1976, Vol. 6, No. 7, p 1233.

[64.] Faber, T.E., 1972 An Introduction to the Theory of Liquid Metals (Cambridge: Cambridge University Press)

[65.] Shpil'rain, E.E.; Skovorod'ko, S.N.; Mozgovoi, A.G., New Data on the Solubility of Inert Gases in Liquid Alkali Metals at High Temperature. High Temperature, 2002, Vol. 40, No. 6, p. 825.

[66.] Grimes, W.R.; Smith, N.V.; Watson, G.M., Solubility of Noble Gases in Molten Fluorides, Pt. I. The Journal of Physical Chemistry, 1958, Vol. 62, No. 7, p. 862.

[67.] McQuarrie, Donald Allan and John Douglas Simon. Molecular Thermodynamics. University Science Books, 1999.

[68.] Moss, T.R., The Solubility of Helium in Certain Typical Lubricants and Mercury, AERE E/R 754 (1958)

[69.] Bethlehem Apparatus Company, Inc. Certificate of Analysis Guaranteed Purity: Better than 99.99995% P.O.# E26578, Job# S07P1423, Shiva ID: S070221076. Inspector: Todd Rizzuto. Jan. 16, 2008.

[70.] Selver, R; Kamotani, Y.; Ostrach, S., "Natural Convection of a Liquid Metal in Vertical Circular Cylinders Heated Locally From the Side." Journal of Heat Transfer, 1998, Vol. 120, p. 108.

[71.] Markham, A.E. and Kobe, K.A., "The Solubility of Gases in Liquids." Chemical Reviews, 1941, Vol. 28, No. 3, p 519.

[72.] Personal conversation with Bernie Remier (Jan. 2008)

[73.] Clementi, E.; D.L. Raimondi; and W.P. Reinhardt. The Journal of Chemical Physics. 1967, Vol 47, No. 4, p. 1300.

[74.] Koros, W.J.; Chan, A.H.; and Paul, D.R., Sorption and Transport of Various Gases in Poly-Carbonate. Journal of Membrane Science. 1977, Vol. 2, p. 165.

[75.] Takemura, Fumio and Akira Yabe. "Gas dissolution process of spherical rising gas bubbles." Chemical Engineering Science, 1998, Vol. 53, No. 15, p. 2691.

[76.] Cahoon, J.R., A Modified "Hole" Theory for Solute Impurity Diffusion in Liquid Metals. Metallurgical and Materials Transactions A, March 1997, Vol. 28A, p. 583.

[77.] Smith, R.W.; Zhu, X.; Tunnicliffe, M.C.; Smith, T.J.N.; Misener, L.; Adamson, J., Ann.. New York Academy of Science. 2002, Vol. 974, p. 57.

[78.] Swalin, R.A., On the Theory of Self-Diffusion in Liquid Metals. Acta Metallurgica, 1959, Vol. 7, p. 736.

[79.] Liu, Yong; Long, Zhengyi; Wang, Haibing; Du, Yong; Huang, Baiyun. A predictive equation for solute diffusivity in liquid metals. Scripta Materialia. 2006, Vol. 55, p. 367.

[80.] Chhabra, R.P.; Roy, A.K., Diffusivity of Oxygen and Nitrogen in Liquid Metals: An Explicit Formulation. Zeitschrift fur Metallkunkde, 1988, Vol. 64, p. 79.

[81.] Hildebrand, J.H., Viscosity and Diffusivity: A Predictive Treatment. John Wiley & Sons, New York, 1977.

[82.] Nachtrieb, N.H., Petit, J., Self-Diffusion in Liquid Mercury. The Journal of Chemical Physics April 1956, Vol 24, No. 4, p. 746

[83.] Hoffman, R.E., The Self-Diffusion of Liquid Mercury. The Journal of Chemical Physics October 1952, Vol. 20, No. 10, p. 1567.

[84.] Weiss, Ray F., Solubility of Helium and Neon in Water and Seawater. Journal of Chemical and Engineering Data, 1971, Vol. 16, No. 2.

[85.] Personal conversation with S. Hasegawa (Jan. 2008)

[86.] Davenport W.G.; Bradshaw, A.V.; Richardson, F.D., "Behaviour of Spherical Cap Bubbles in Liquid Metals." The Journal of Iron and Steel Institute. 1967, Vol 205, pg 1034.

[87.] Davies, R.M.; Taylor, G.I., Proceedings of the Royal Society, 1950, Vol. 200, No. 1061, p. 375.

[88.] Schwerdtfeger, K. "Velocity of rise of argon bubbles in mercury." Chemical. Engineering Science. 1968, Vol. 23, p. 937.

[89.] Haberman, W.L.; Morton, R.K.: David Taylor Model Basin Report No. 802, 1953.

[90.] Mori, Y.; Hijikata, K.; Kuriyama, I.; "Experimental Study of Bubble Motion in Mercury With and Without a Magnetic Field." Journal of Heat Transfer. 1977, Vol 99, p. 404.

[91.] Sawi, M.E. Distorted Gas Bubbles at Large Reynolds Number. Journal of Fluid Mechanics, 1974, Vol. 62, p. 163.

[92.] Moore, D.W., The Velocity of Rise of Distorted Gas Bubbles in a Liquid of Small Viscosity. Journal of Fluid Mechanics, 1965, Vol. 23, p. 749.

[93.] Mendelson, H.Dl, The Prediction of Bubble Terminal Velocities From Wave Theory. AIChE Journal, 1967, Vol. 13, p. 250.

[94.] Cahoon, J.R., The Entropy Factor in Liquid Diffusion. Metallurgical and Materials Transactions A. March 2003, Vol. 34A, p. 882.

[95.] Meyer, R. E., The Journal of Physical Chemistry. 1961, Vol. 65, No. 3, p. 567.

[96.] Bondi, A., The Journal of Physical Chemistry. 1964, Vol 68, No. 3, p. 441.

[97.] Yaws, C.L., ed., *Chemical Properties Handbook*. McGraw-Hill: 1999.

[98.] Dean, J.A., ed., *Lange's Handbook of Chemistry (15 Edition)*. McGraw-Hill: 1999.

Appendix

APPENDIX A: Physical Properties of Mercury

A.1 General Properties [53, 56, 97, 98]

	Isotope	Atomic mass (u)	Abundance (%)
80	^{196}Hg	195.965833(3)	0.15(1)
	^{197}Hg	196.967213(3)	
	^{198}Hg	197.9667690(4)	9.97(20)
	^{199}Hg	198.9682799(4)	16.87(22)
	^{200}Hg	199.9683260(4)	23.10(19)
	^{201}Hg	200.9703023(6)	13.18(9)
	^{202}Hg	201.9706430(6)	29.86(26)
	^{203}Hg	202.9728725(18)	
	^{204}Hg	203.9734939(4)	6.87(15)

Atomic mass	=	200.59(2) g/mol
Atomic radius	=	150 pm
Atomic radius (calc.)	=	171 pm
Covalent radius	=	149 pm
Van der Waals radius	=	155 pm
Triple point, T_{tp}	=	234.313 K (-38.837°C)
Melting point, T_m	=	234.321 K (-38.829°C)
Boiling point, T_b	=	629.77 K (356.62°C)
Critical point, T_c/P_c	=	1750 K (1477°C) / 172.0 MPa
Debye Temp., T_{Debye}	=	70 K
$\Delta_{fus}H(T_m)$	=	2.295 kJ/mol
$\Delta_{vap}H(T_b)$	=	59.11 kJ/mol
Magnetic Susceptibility	=	-24.1×10^{-6} cm^3/mol
Entropy, S°(298.15 K)	=	75.90 J mol^{-1} K^{-1}
Polarizability	=	5.02×10^{-30} m^3

A.2 Heat Capacity

C_P =	28.00	J mol^{-1} K^{-1}	@ 20°C	[97]
	27.983	J mol^{-1} K^{-1}	@ 25°C	[53]
	27.8821	J mol^{-1} K^{-1}	@ 27°C	[56]

$$C_P = 30.388 + (-1.0980E-02)T + (9.4412E-06)T^2 + (6.7418E-10)T^3 \quad [97]$$

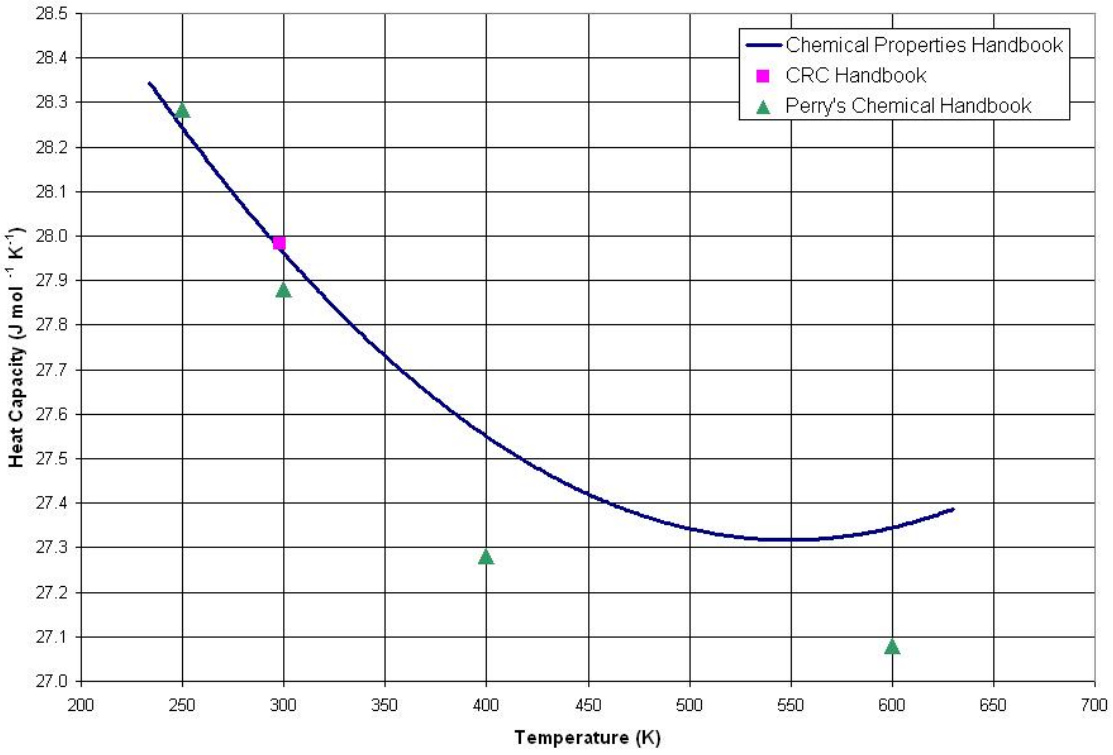

A.3 Density

ρ =	13.4989	g cm^{-3}	@ 20°C	[97]
	13.5459	g cm^{-3}	@ 20°C	[53]

$$\rho \approx -0.00241T + 14.25241 \qquad [53]$$

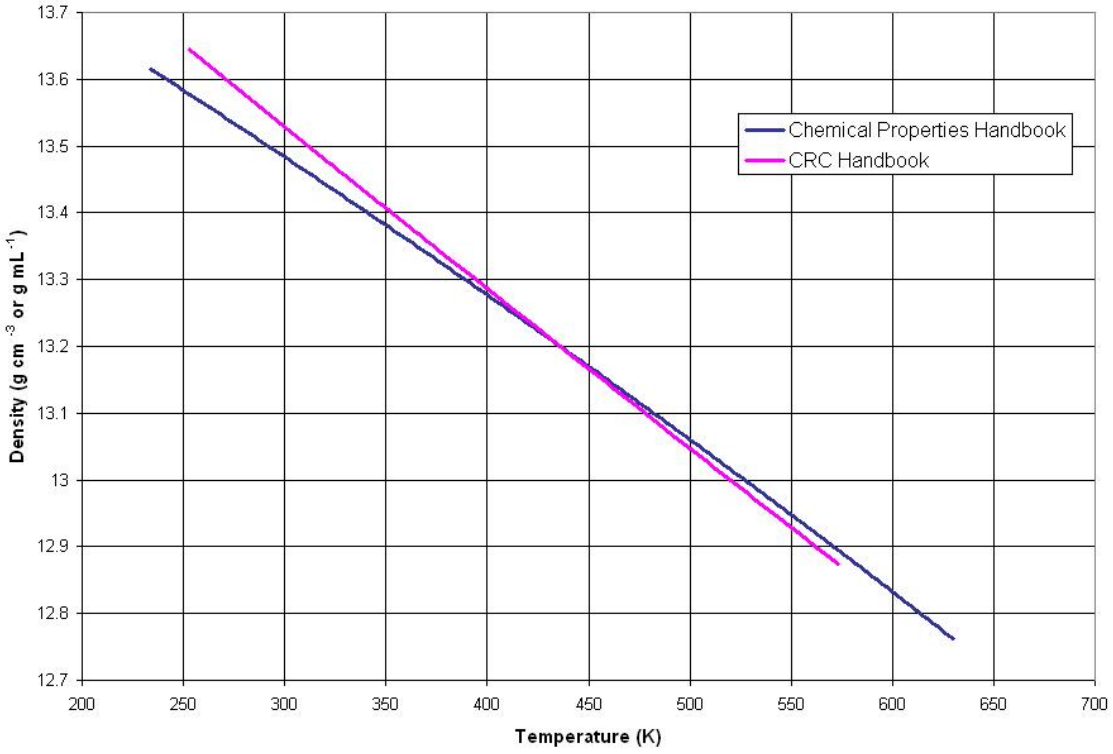

A.4 Surface Tension

σ =	492.955	mN/m	@ 20°C	[97]
	485.48	mN/m	@ 25°C	[53]

$$\sigma = -0.2049T + 546.54 \qquad [98]$$

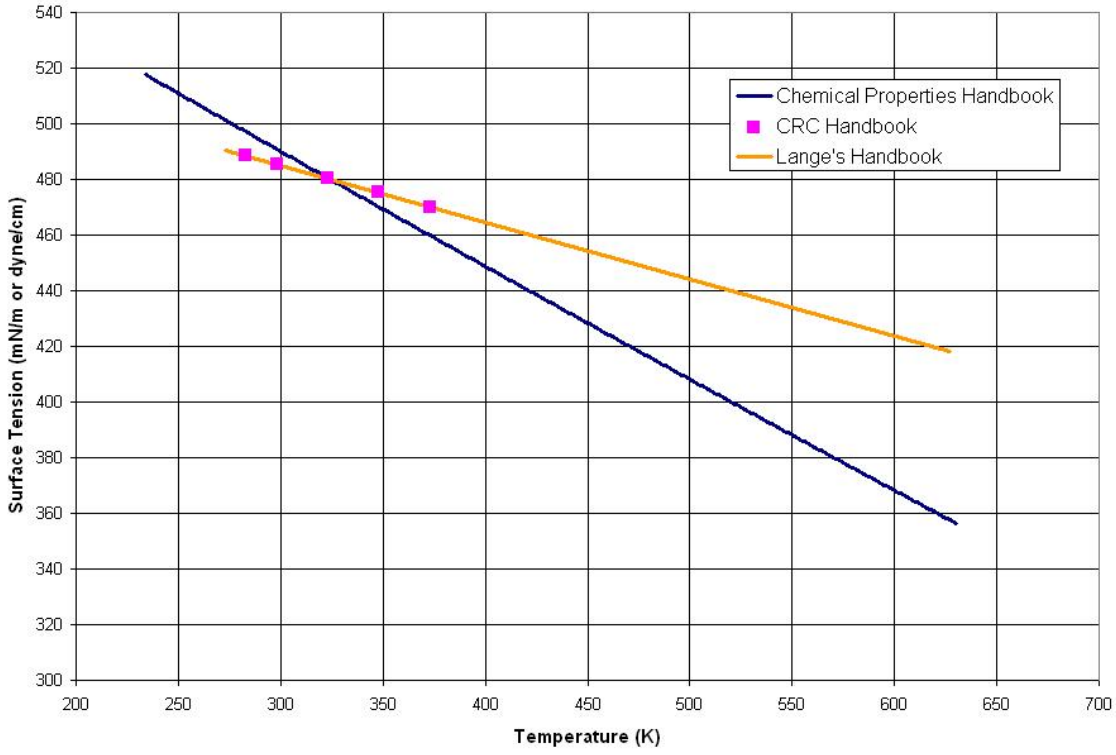

A.5 Dynamic Viscosity

η =	1.5624 mPa-s	@ 20°C	[97]
	1.526 mPa-s	@ 25°C	[53]

$$\log \eta = -0.2748 + 1.3697E02/T + (4.1785E-06)T - (1.995E-09)T^2 \quad [97]$$

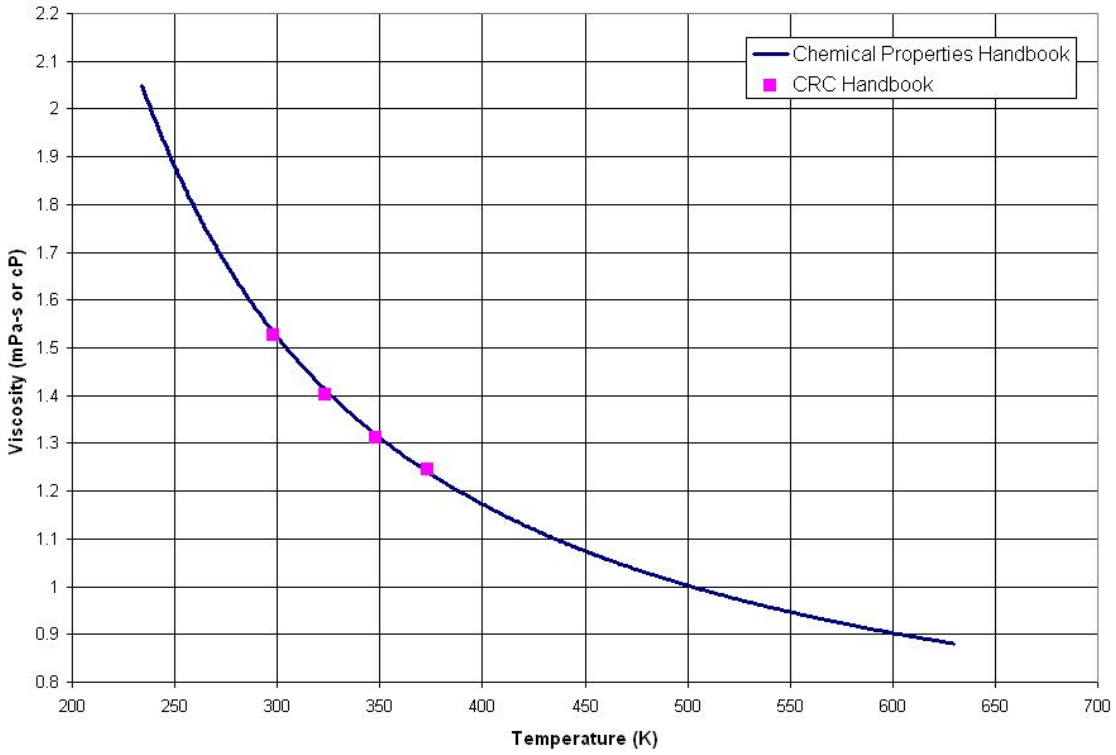

A.6 Thermal Conductivity

k =	8.056	$W\ m^{-1}\ K^{-1}$	@ 20°C	[97]
	8.514	$W\ m^{-1}\ K^{-1}$	@ 25°C	[53]
	8.000	$W\ m^{-1}\ K^{-1}$	@ 27°C	[56]
	8.25	$W\ m^{-1}\ K^{-1}$	@ 25°C	[98]

$$k = 0.9230 + (2.8887E\text{-}02)T - (1.5499E\text{-}05)T^2 \quad [97]$$

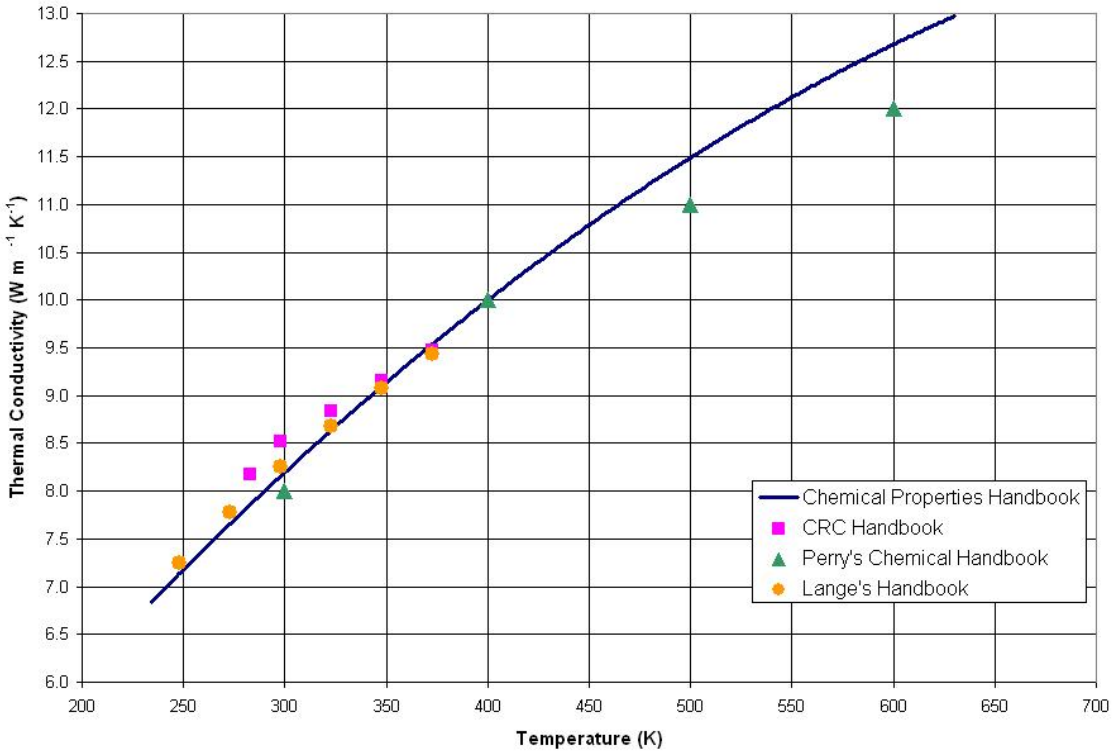

A.7 Coefficient of Thermal Expansion

α =	0.0001811	K^{-1}	@ 20°C	[53]
	0.00018182	K^{-1}	0.0 to 100°C	[56]

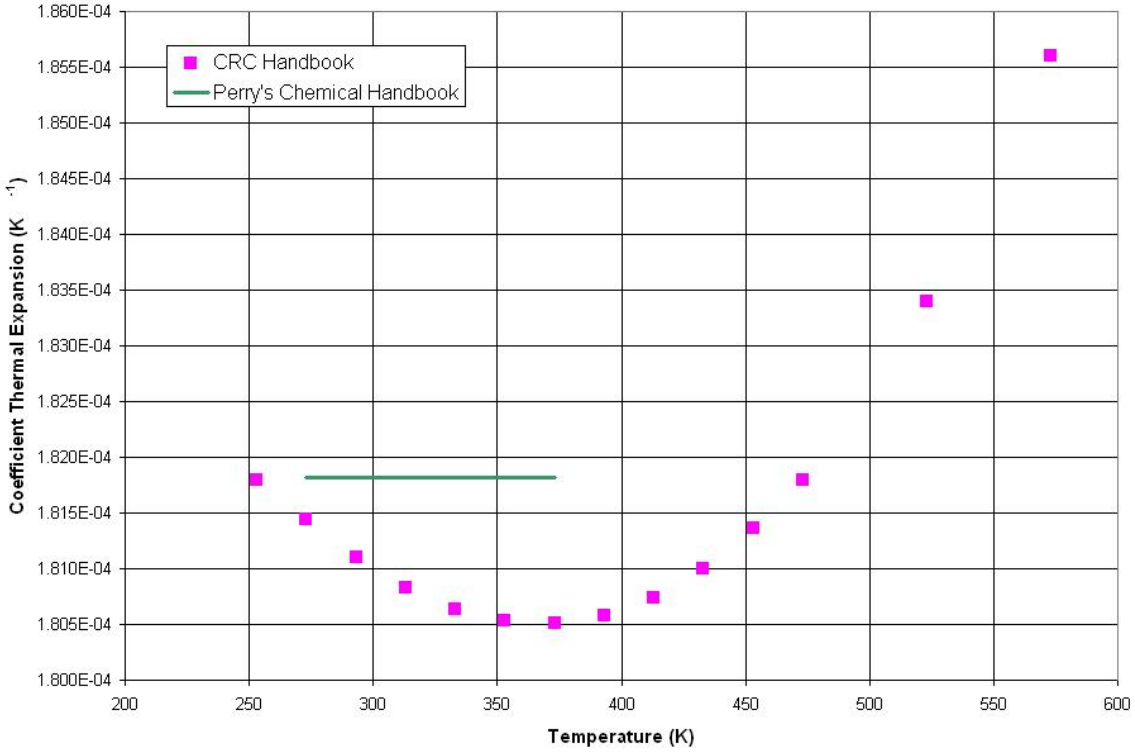

A.8 Vapor Pressure

p_{vapor} = 0.2614 Pa	@ 25°C	[53]
133.32 Pa	@ 126°C	[56]
0.1601 Pa	@ 20°C	[98]

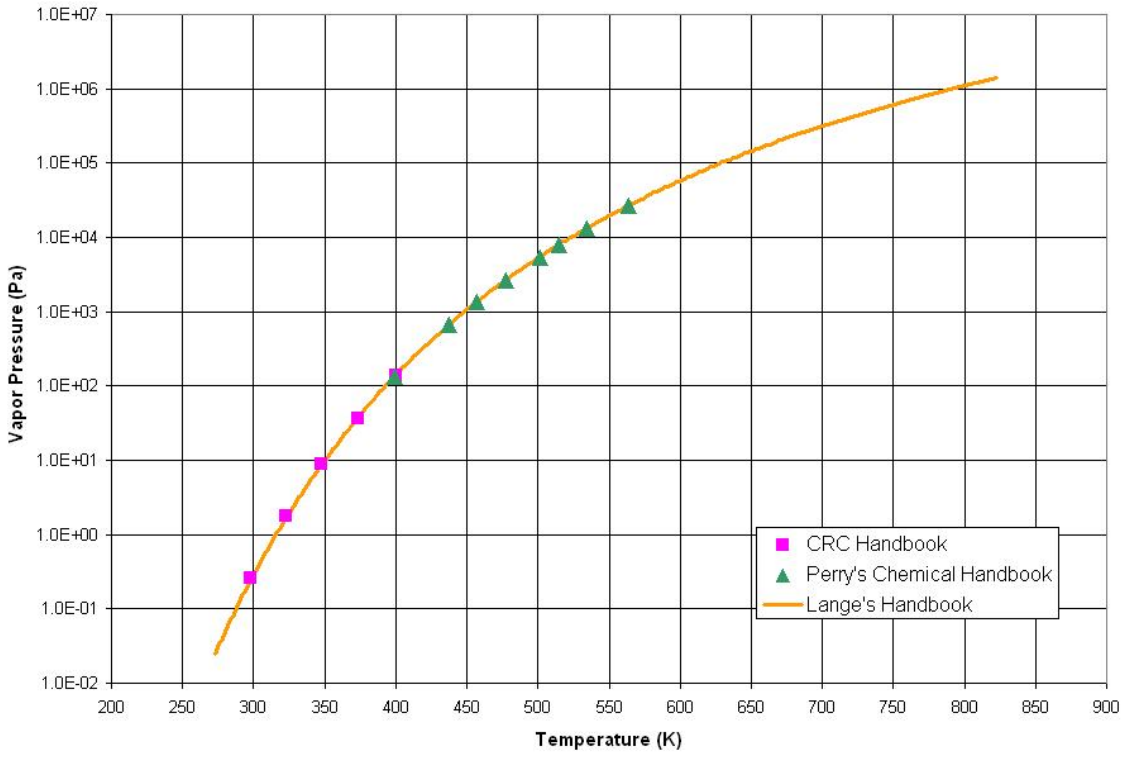

A.9 Sound Speed

$c_{sound} = 1451.4$ m/s @ 20°C [53]

$$c_{sound} = -0.4666T + 1588.1 \quad [53]$$

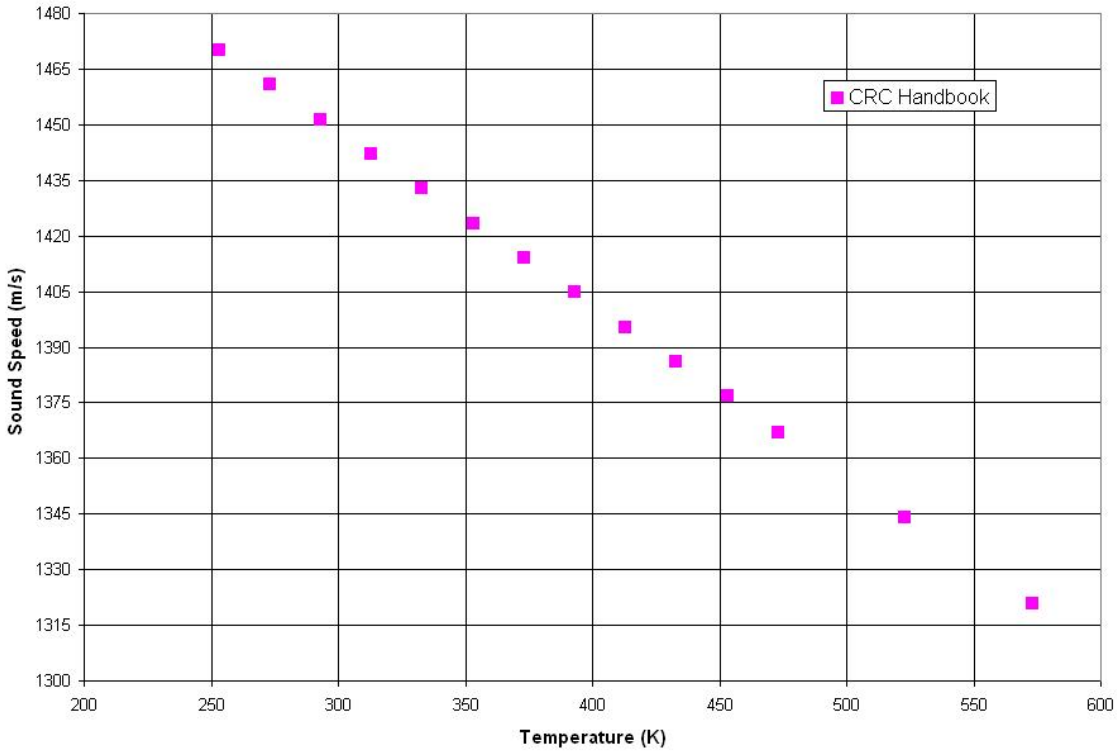

A.10 Isothermal Compressablility [98]

Temperature (°C)	Isothermal Compressability (Pa^{-1}) [2]	
	1E5 Pa	1E8 Pa
-20	3.83E-11	
0	3.918E-11	3.78E-11
20	4.013E-11	3.87E-11
40	4.109E-11	3.96E-11
60	4.207E-11	
80	4.308E-11	4.14E-11
100	4.41E-11	
120	4.513E-11	4.33E-11
140	4.622E-11	
160	4.731E-11	4.53E-11
180	4.844E-11	
200	4.96E-11	
250	5.26E-11	
300	5.59E-11	

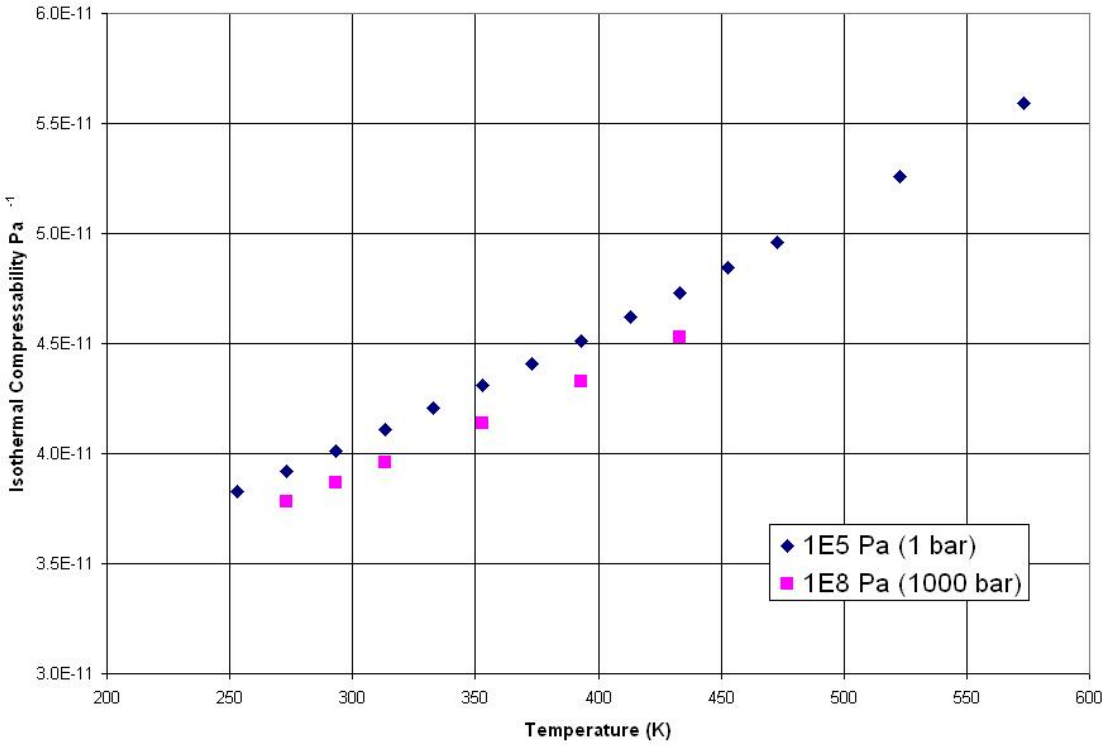

APPENDIX B: MATLAB code utilizing solubility model

```
% MATLAB script to compute the solubility of noble gases in mercury
% based on the method by Shpilrain, E.E., et.al, High Temperature, 38(3),
% 407-411, 2000
% sub- & super- script 1 means mercury(solvent)
% sub- & super- script 2 means gas phase(solute)
% output: x21 (molar fraction of component 2 in component 1, dimensionless);
% kh: Henry's law constants; D: gas diffusion coefficient

clear all;

% ************************common constants************************
% universal gas constant (J/mol*K)
R = 8.31441;
% electron charge(C)
e = -1.60221892e-19;
% electron mass(kg);
me = 9.109534e-31;
% planck's constant (J*s)
h = 6.626176e-34;
% Avogadro's Constant (1/mol)
A = 6.022045e+23;
% atomic mass unit (kg)
amu = 1.6605655e-27;
% Boltzmann's constant (J/K)
k = 1.3800662e-23;

% ********************common variable************************
% system temperature(K), can use more values
Ts = 300.0:50.0:600.0;
% gas cover pressure(bar), can use more values
p2s = 1.0e5;
% mercury vapor pressure (pa): it varies with temperature,
% but it's small enough to be neglected. Typical value at room temperture
% adopted (From CRC Handbook of Chemistry and Physics, 85th version,
% pp.6-147, 2004-2005
p12 = 3.68e-4*1e3;
p2s = p2s-p12;

% ********* MERCURY (1) properties to be used ************
% From: Lange's Handbook of Chemistry (15th Edition), Table 4.6
% atomic radius and diameter (m)
r1 = 1.51e-10;
```

```
d1 = 2*r1;
% atomic mass
m1 = 200.59*amu;
% molar weight/mass (kg/mol)
M1 = m1*A;
% density (kg/m^3)
rho1 = 13.5336e+3;
% number density (1/m^3)
rho1a = rho1*A/M1;
% molar volume of mercury (m^3/mol)
v1 = M1/rho1;
% From CRC Handbook of Chemistry and Physics, 85th version,
% pp.6-134, pp.6-186, pp.10-167, 2004-2005
% thermal expansion coefficient 100^oC (1/K) TEMPERATURE DEPENDENT
alpha = 1.81e-4;
% isothermal compressibility 100^oC(/Pa) TEMPERATURE DEPENDENT
beta = 4.410e-11;
% dynamic viscosity (Pa*s) at 25^oC
mu1 = 1.526e-3;
% polarizability of mercury atom (m^3)
alpha1 = 5.02e-30;
% number of electrons in the outer shell of atoms of mercury
y1 = 41.76;
% eta in U^in
eta = pi*rho1a*d1^3/6;
% Debye temperature of mercury
deb1 = 3/4*mu1*h/k*((A/M1)^2/rho1)^(1/3);

% ******************gas(2) properties for calculation***************
% HELIUM
% initial values
% r2 = 0.49*1.0e-10;
% shpilrain
% r2 =1.35*1.0e-10;
% thormeier
r2 =1.30*1.0e-10;
% From chemicool.com
% r2 = 31*1.0e-12;
% From CRC Handbook of Chemistry and Physics, 85th version,
% pp.10-167, 2004-2005;
% polarizability of gass atom (m^3)
alpha2 = 0.204956e-30;
% number of electrons in the outer shell of gas atoms
y2 = 1.7;
% gas atomic mass
```

```
m2 = 4.002602;
% Gas molar mass
m2a = m2*1.0e-3;
% Gas atomic mass
m2 = m2*amu;

% use the loop to compute for each pressure and temperature
for i = 1:length(Ts)
T = Ts(i);
% gas partial pressure above the solution(Pa)
% internal presure
P1 = T*alpha/beta;
% dk = r1+r2 (m)
dk = r1+r2;

%********************U^in_12********************%
q0 = R*T*(-log(1-eta)+4.5*(eta/(1-eta))^2)-pi*A*d1^3*P1/6;
q1 = -R*T/d1*(6*eta/(1-eta)+18*(eta/(1-eta))^2)+pi*A*d1^2*P1;
q2 = R*T/d1^2*(12*eta/(1-eta)+18*(eta/(1-eta))^2)-2*pi*A*d1*P1;
q3 = 4*pi*A*P1/3;
Uin = q0+q1*dk+q2*dk.^2+q3*dk.^3;

%********************U^p_12 ********************%
C = 3*e*h/4/pi/sqrt(me)*alpha1*alpha2;
C = C./(sqrt(alpha1/y1)+sqrt(alpha2./y2));
Up = -8*pi*rho1a*A/9*C./dk.^3;

%********************U^os_12********************%
% Debye temperature of gases
deb2 = deb1.*sqrt(m1./m2);
Uos = R*deb2./(exp(deb2/T)-1);

%********************U12************************%
U12 = Uin+Up+Uos;

%********************S12 entropy********************%
S12 = deb2/T./(exp(deb2/T)-1)-log(1-exp(-deb2/T));

%****x21(molar fraction): output for each pressure and temperature****%
x21(i,:) = p2s*v1/R/T*exp(-U12/R/T+S12);
kh(i,:) = 1.0e5*v1./(x21(i,:).*m2a);
D(i,:) = k*T/6/pi/mu1./r2;
end

disp('!!********************compuatation finished**************************!!');
```

```
disp(['Temperature from ',num2str(300),'K ','to ',num2str(600),'K ',...
'with step of ', num2str(50),'K']);
x21
kh
D
save sol.mat
```

APPENDIX C: Atomic Radius Sensitivity Study of Thormeier's Model

From the early work of Guggenheim and Fowler, Thormeier arrived at the following relationship for Henry's coefficient:

$$K_H^{-1} = \frac{\overline{V}_L}{RT} \exp\left(\frac{-\Delta \overline{F}_{LG}}{RT} \right). \tag{3-37}$$

where

$$\Delta \overline{F}_{LG} = \overline{F}_{LG}^{hole} + \overline{U}_{LG}^{\text{int}} + \overline{F}_{LG}^{vib}, \tag{3-67}$$

and each term in equation (3-67) is defined by equation (3-47), equation (3-56), and equation (3-66), respectively. As noted in the text and can be seen in Table 3.5, the primary term in equation (3-67) is the hole-formation molar energy. This term is a function of the solute hard sphere radius as well as the hard sphere radius of the solvent. Contained here is a sensitivity study on the solubility of helium in mercury with slight changes in atomic radii.

A large difference exists between the actual helium radius of 31 pm and the hard sphere radius or van der Waals radius of 130 pm. In Lu's masters thesis, he used the actual radius; however, the models are based on the hard sphere radius and used here in this work. The model derived by Thormeier is based on the hard sphere radius for both the solute and solvent. Using the hard sphere radius of 151 pm for mercury, Figure C.1 shows the relationship of the theoretical Henry coefficient to the atomic hard sphere radius of helium. Mimicking the format of Table 3.5, the break down for each term in equation (3-67) can be seen in Table C.1.

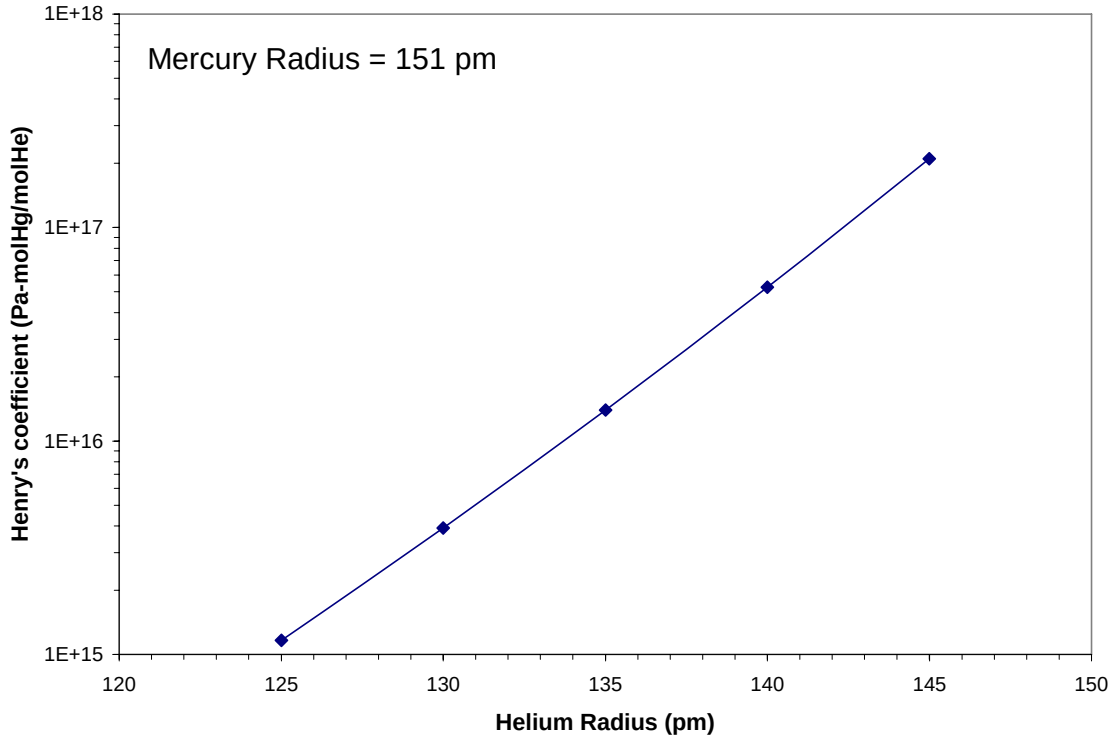

Figure C.1: Theoretical Henry Coefficient for Hg/He as a function of helium hard sphere radius based on Thormeier's model

Table C.1: Theoretical parameters for Henry Coefficient assuming Hg radius equals 151 pm

Helium Radius (pm)	$\overline{F}_{LG}^{hole}$ (J/mol)	$\overline{U}_{LG}^{\text{int}}$ (J/mol)	$\overline{F}_{LG}^{vib}$ (J/mol)	Temperature (K)	Theoretical K_H (Pa-molMetal/molHe)
125	4.03×10^{4}	0.128	-970.7	300	1.16×10^{15}
130	4.33×10^{4}	0.121	-970.7	300	3.92×10^{15}
135	4.65×10^{4}	0.115	-970.7	300	1.39×10^{16}
140	4.98×10^{4}	0.109	-970.7	300	5.26×10^{16}
145	5.32×10^{4}	0.104	-970.7	300	2.10×10^{17}

The actual atomic radius for mercury is reported to be approximately 150 pm. This value is slightly larger than the covalent radius of 149 pm predicted for mercury. However, the van der Waals radius for mercury is on the order of 155 pm. The Thormeier model is very sensitive to the solute radius as can be seen in Figure C.2 and Table C.2 below.

As can bee seen in Figures C.1 and C.2, the validity of the model hinges on the certainty of helium's and mercury's van der Waals radius.

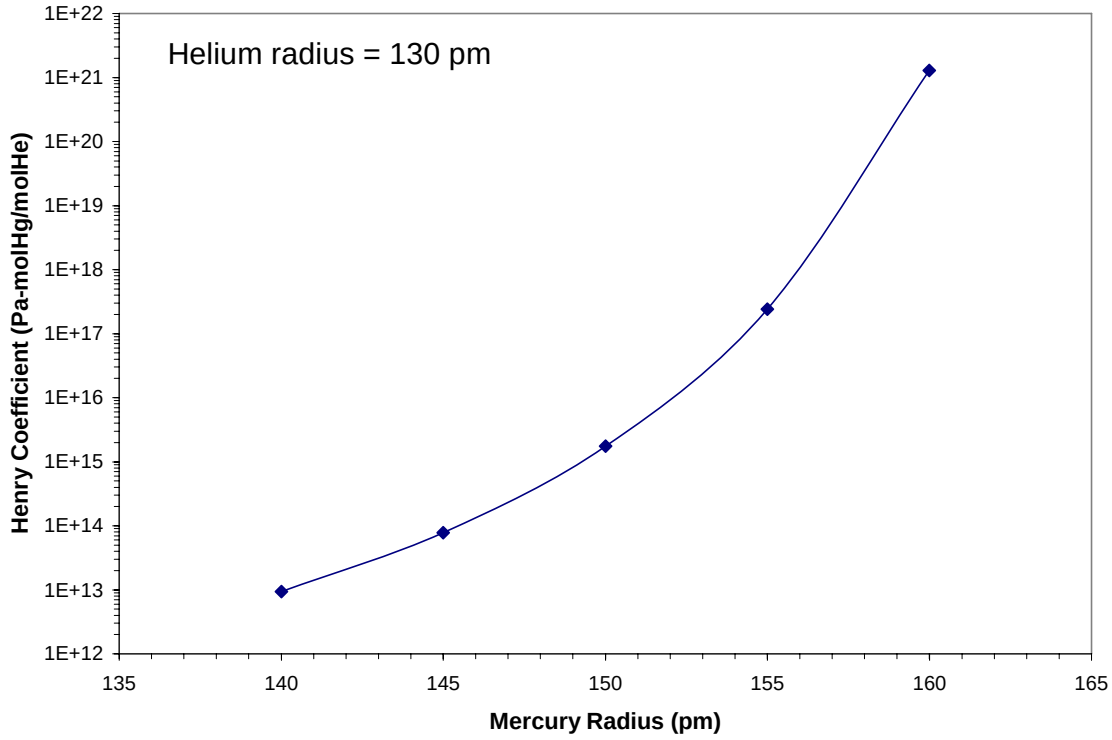

Figure C.2: Theoretical Henry Coefficient for Hg/He as a function of mercury hard sphere radius based on Thormeier's model

Table C.2: Theoretical parameters for Henry Coefficient assuming He radius equals 130 pm

Mercury Radius (pm)	$\overline{F}_{LG}^{hole}$ (J/mol)	$\overline{U}_{LG}^{\text{int}}$ (J/mol)	$\overline{F}_{LG}^{vib}$ (J/mol)	Temperature (K)	Theoretical K_H (Pa-molMetal/molHe)
140	2.82×10^4	0.137	-970.7	300	9.34×10^{12}
145	3.35×10^4	0.129	-970.7	300	7.78×10^{13}
150	4.13×10^4	0.123	-970.7	300	1.76×10^{15}
155	5.36×10^4	0.116	-970.7	300	2.40×10^{17}
160	7.50×10^4	0.110	-970.7	300	1.28×10^{21}

VITA

Matthew Wesley Francis was born in Knoxville, Tennessee, on February 21, 1983 to Christopher C. Francis and Linda B. Francis. From September 1988 to May 2001, he attended the public schools of Knox County. He started the University of Tennessee in the summer term in 2001. As an undergraduate in Nuclear Engineering, he co-oped four semesters in the Core Analysis Group in the Nuclear Fuel Department of Southern Nuclear. In August 2005, he graduated summa cum laude with a bachelor of science in Nuclear Engineering at the University of Tennessee. Two semesters later, Matthew graduated with a master of science in Nuclear Engineering at the University of Tennessee under the advisement of Dr. Mario Fontana. In June 2006, he joined the High Power Target Group as a graduate research assistant under the advisement of Dr. Arthur E. Ruggles. His research is a Department of Energy-funded project towards developing methods in understanding the inert gas bubble behavior in the mercury target of the Spallation Neutron Source at Oak Ridge National Laboratory.